A FLUID INCLUSION STUDY OF THE BUNKER HILL MINE, COEUR D'ALENE DISTRICT, IDAHO

By

Martin Kenneth Bijak

Submitted in partial fulfillment of
the requirements of the
degree of Master of Science

New Mexico Institute of Mining
and Technology
Soccoro, New Mexico 87801

October 1985

ACKNOWLEDGEMENTS

This thesis would have been impossible without the help and ideas of many individuals, especially my advisor- David Norman, and the Bunker Hill staff. This thesis would also have been equally impossible without the previous work of many individuals in the district, only some of whom are referenced in the appendix.

Persons who contributed in some way to this study: The staff of the Bunker Hill and Crescent mines (Gulf Resources and Chemical Corp.); Mine Geologists Robert Meyer, Norm Radford, Jim Duff, Paul Dirkson, Steve Levine and Dennis Dalton; the miners for helpful information and for tolerating a sometimes awkward graduate student; Dave Leach and Gary Landis of the U.S.Geological Survey; Rudy Kluiber, Carl Bernhardt, Scott Long, Mike Palin, Eric Bigelow, Ted Eggleston, Fred Kuellmer, Dave Johnson and Dan White; Carl Popp, Lynn Branvold and Charles Smith for help with the analyses; Dianne Meier, Jennifer Lee the operator, the muses- who shall remain anomalous, a lot of user consultants and others for help with word processing; SUNY at Buffalo for my undergraduate education. Special thanks to Clay T. Smith(for most careful editing and comments) and Carl Popp for being on my thesis advisory committee and again to Dave Norman.

This study would have been impossible without financial assistance through a HEW fellowship, VA benefits and state and federal aid in my undergraduate education and last, the NYSHSC loan program.

ABSTRACT

A FLUID INCLUSION STUDY OF THE BUNKER HILL MINE, COEUR D'ALENE DISTRICT, IDAHO

The Bunker Hill mine and neighboring Crescent mine are Pb-Zn-Ag replacement and fissure vein deposits of controversial origin. A generalized paragenesis is siderite/sphalerite-quartz/quartz-galena-chalcopyrite/quartz-sulfosalts.

Fluid inclusions in quartz have homogenization temperatures of 320-250 ^{o}C and those in sphalerite, 350-320 ^{o}C. The bulk of the homogenizations in quartz are centered about 265-250 ^{o}C and form the most reliable minimum temperature of formation. In inclusions from both minerals, salinities are 13-10 eq. wt.% NaCl, boiling or liquid immiscibility is indicated. Gas analyses of inclusions in quartz indicate a minimum of 2.5 wt.% gases with roughly equal amounts of N_2 and CO_2, and lesser H_2, CH_4, C_nH_n and Ar. Hydrogen sulfide is 10^{-2} to 10^{-3} m. Leachate analysis of inclusion fluids in quartz indicates that $CaCl_2$ is the salt present in greatest concentration, roughly twice that of NaCl and three times that of KCl (wt.%). Sulfate is present only in trace quantities and Cl is the dominant anion.

A trend of increasing CO_2::N_2 is observed in the analyses of the aqueous fluid inclusions present in quartz within the sequence pre-mineralization, Bluebird(Zn), Link(Pb) and Crescent(Ag) quartz. This trend may be related to progressive basin metamorphism and may indicate paragenesis.

High nitrogen fluids suggest derivation from a sedimentary environment. It is suggested that the mineralizing fluids were derived through metamorphism of the Belt Supergroup and mineralization was at a minimum depth of 1.5 to over 5 km. True depths of formation may be greater.

A FLUID INCLUSION STUDY OF THE BUNKER HILL MINE, COEUR D'ALENE DISTRICT, IDAHO

By

Martin Kenneth Bijak

Submitted in partial fulfillment of
the requirements of the
degree of Master of Science

New Mexico Institute of Mining
and Technology
Soccoro, New Mexico 87801

October 1985

ABSTRACT

A FLUID INCLUSION STUDY OF THE BUNKER HILL MINE, COEUR D'ALENE DISTRICT, IDAHO

The Bunker Hill mine and neighboring Crescent mine are Pb-Zn-Ag replacement and fissure vein deposits of controversial origin. A generalized paragenesis is siderite/sphalerite-quartz/quartz-galena-chalcopyrite/quartz-sulfosalts.

Fluid inclusions in quartz have homogenization temperatures of 320-250 ^{o}C and those in sphalerite, 350-320 ^{o}C. The bulk of the homogenizations in quartz are centered about 265-250 ^{o}C and form the most reliable minimum temperature of formation. In inclusions from both minerals, salinities are 13-10 eq. wt.% NaCl, boiling or liquid immiscibility is indicated. Gas analyses of inclusions in quartz indicate a minimum of 2.5 wt.% gases with roughly equal amounts of N_2 and CO_2, and lesser H_2, CH_4, C_nH_n and Ar. Hydrogen sulfide is 10^{-2} to 10^{-3} m. Leachate analysis of inclusion fluids in quartz indicates that $CaCl_2$ is the salt present in greatest concentration, roughly twice that of NaCl and three times that of KCl (wt.%). Sulfate is present only in trace quantities and Cl is the dominant anion.

A trend of increasing CO_2::N_2 is observed in the analyses of the aqueous fluid inclusions present in quartz within the sequence pre-mineralization, Bluebird(Zn), Link(Pb) and Crescent(Ag) quartz. This trend may be related to progressive basin metamorphism and may indicate paragenesis.

High nitrogen fluids suggest derivation from a sedimentary environment. It is suggested that the mineralizing fluids were derived through metamorphism of the Belt Supergroup and mineralization was at a minimum depth of 1.5 to over 5 km. True depths of formation may be greater.

TABLE OF CONTENTS

LIST OF ILLUSTRATIONS

List of symbols and abbreviations used:

Hexagon....Pre-mineralization, pre-reverse shear (milky quartz),

Circle.....Bluebird vein sample (quartz, sphalerite or galena),

Triangle...Link vein sample (quartz),

Square.....Crescent vein sample (quartz or siderite).

Colors:

red.....T_d of 750 to 550°C (high temperature)

blue.....T_d less than 500°C (low temperature)

colorless...intermediate T_d, gennerally 550°C

T .....temperature in degrees C unless otherwise stated

T_d ....decrepitation temperature

T_h ....homogenization temperature

L .....liquid phase

V .....vapor phase

Cal ...calcite	Ser ...sericite
Cpy ...chalcopyrite	Sid ...siderite
Gal ...galena	Sph ...sphalerite
Py ....pyrite	Tet ...tetrahedrite
Qtz ...quartz	

INTRODUCTION

The Bunker Hill mine is a Pb-Zn-Ag replacement and fissure vein deposit located in the Coeur d'Alene District of northern Idaho (fig. 1). It is located southwest of the town of Kellogg and in the near-western end of the "Page-Galena" mineral belt. The neighboring mine to the east is the Crescent mine and is also included in this study.

The origin of the Bunker Hill deposits is uncertain; district geologists favor many models. Recently, most favor has been given to "metamorphic-hydrothermal" explanations of the mineral deposits (Walker, 1977, Reid, et al., 1977?). This hypothesis suggests that Pb-Zn-Ag were either syngenetic or diagenetic with Belt sedimentation along the Lewis and Clark lineament and that there was Mid-Proterozoic remobilization of the deposits. Their suggestion concerns metallogenesis only and does not imply the existence of syn- or diagenetic orebodies, although some studies have suggested that this may have been the case (i.e.- Ramalingaswany, 1975). Whatever the ultimate origin of the metals, one continuous period of mineralization has been assumed to account for all of the major characteristics of the orebodies as they exist today (Juras, 1977).

Figure 1. Location of the Bunker Hill mine. Shown in outline are the outcrop limits of the Belt supergroup.

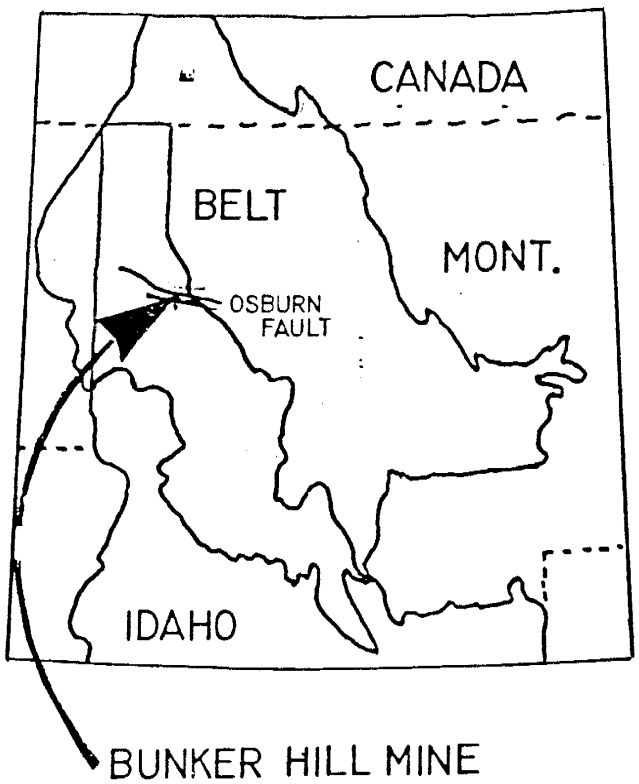

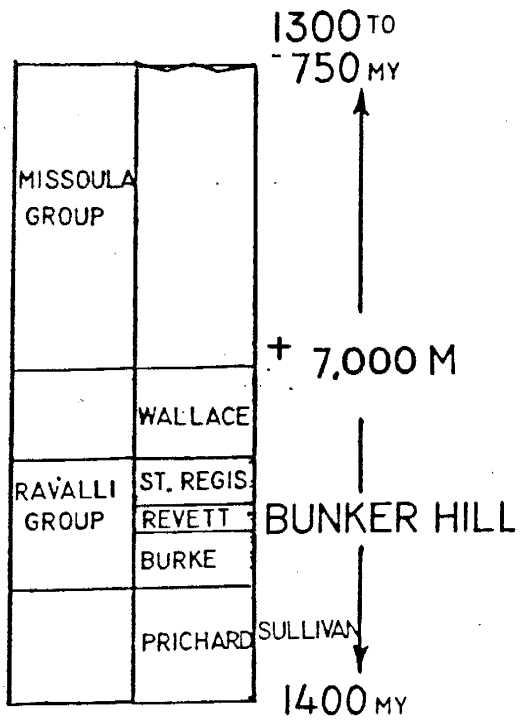

(AFTER HARRISON, 1972)

STATEMENT OF PURPOSE

The major problem with the current genetic models is that very little information is known about the geochemical environment of deposition. It is the principal aim of this thesis to characterize the ore-forming fluids of the various orebodies and use this information to constrain possible genetic models. Another aim of this thesis is to present the information in a critical manner in which the reader may perceive the problems encountered during the study of this mineral deposit and the probability that the information presented is accurate and reliable. It is hoped that the methods used to convey the information will help to delineate areas where further research may yield important discoveries.

PREVIOUS WORK

The earliest district studies were published by Ransome and Calkins (1908), and Oscar Hershey in a series of papers a short time later (1912-1913). Later studies expanded upon this work: Umpley and Jones (1923), McConnel (1939), Shenon and McConnel (1939), Fryklund (1964), Hobbs, et al., (1965), and Sorenson (1972). Too large an amount of work concerning specific problems in the district exists for comprehensive listing so only the major works and specific references used in this study are given.

Previous ideas on the genesis of the Coeur d'Alene Deposits have been centered around three principal hypotheses: The modified magmatic hydrothermal hypothesis, the hypothesis of deep remobilization and the sedigenetic-partial remobilizatin (lateral secretion) hypothesis (as discussed by Sorenson, 1969). The modified magmatic hydrothermal hypothesis is attributed to Fryklund and consists of a "deep point source" for the sulfides which may lie in a sulfide-rich zone in the mantle. No mention of the presumably hydrothermal mechanism of transport is given. The hypothesis of deep remobilization is attributed to Silverman, (1960) and consists of ore deposition about 1,400 m.y. ago into their present positions, or alternatively, in a relatively confined volume in a deeper or more distant location. The ores were then subsequently remobilized through orogenic or igneous processes into their present positions. The sedigenetic-partial remobilization (lateral secretion) hypothesis was largely formulated by Oscar Hershey from 1912-1917. This theory suggests that the ores were present as syngenetic disseminations through certain horizons of the Belt formations. Subsequent deformation and soaking by solutions of a presumably magmatic source, leached the metals and redeposited them into their present positions.

Recent work in the district has led to the consideration of a number of genetic models, both syngenetic and epigenetic. Textural observations have led some researchers to favor a sedimentary origin for some of the ores (Ramalingaswamy, et al., 1982). However, most district geologists have recently come to favor "metamorphic-hydrothermal" explanations for the deposits. In studies carried out concurrently with this one, Landis, et al., (1984 and 1983) and Leach, et al., (1983) have provided evidence for "metamorphic-hydrothermal" models.

Previous work of a geochemical nature pertaining to the characterization of the mineralizing fluids has been very limited. A preliminary study of a number of Quill orebody quartz samples was conducted by Joe Mills (1980), which indicated aqueous and gaseous inclusions were present that did not homogenize at temperatures of below 350°C. Secondary inclusions had homogenization temperatures (T_h's) of 280 to 250°C. Primary inclusions in quartz from the Silver vein in the Galena mine had T_h's of 280 to 240°C. An interesting study of minor elements contained in sphalerite and pyrrhotite has yielded temperature of formation estimates ranging between 370 to 490°C (Arnold, et al., 1962). These temperatures may be reasonable in comparison with the results obtained by Leach, et al., (1983) and with the results obtained from this study.

GEOLOGY

The mines of the Coeur d'Alene District are located in the Precambrian Belt-Purcell supergroup which extends from Idaho to British Columbia; a 23 km thick sequence of homogeneous fine-grained clastics, dominantly siltstone and argillite with considerable interstitial carbonate (Windley, 1977). The Belt supergroup thickness within the Coeur d'Alene district is estimated to be at least 7000 m (Hobbs, et al., 1965). The geometry and sedimentation of the Belt basin indicates the depositional environment to be a stable platform in an epicratonic re-entrant of a sea. Deposition was in shallow water with sedimentation from different source areas, over a great period of time during slow, gentle downwarping (Harrison, 1972).

The age of the basal units of the Belt sediments is estimated to be greater than 1400 my on the basis of model ages from lead isotopic compositions (Long, et al., 1960). Other geochronological studies support the validity of this date, giving ages for post-sedimentation events of approximately 1200 my (Sorenson, 1969 and Armstrong, 1975?). The age of mineralization is controversial but may be related to the time of the East Kootany orogeny (hypothesized), about 850 my ago (Harrison, 1972). This is also a conservative limiting age for the end of Belt sedimentation, which may have occured over a large time span

according to Harrison and others (1972, 1974). The uncertainty over the end of Belt sedimentation arises from the lack of any non-disputed dates for post-sedimentary events in the Wallace Fm and Missoula group of greater age than 850 my.

The dominating structural feature of the district is the Lewis and Clark shear zone, a major intracontinental plate boundary active at various times throughout the history of the Belt basin (Bennett, et al., 1982). In the district it is represented by three, major, northwest-trending strike-slip faults.

Several major structural features dominate the local geology of the Bunker Hill and Crescent mines. To the north is the Osburn fault which is the major structure of the district with a right-lateral displacement of nearly 25 km (Hobbs, Fryklund, 1968). Movement on the Osburn fault is indicated to be post-ore (Juras, 1977). The bounding structure to the east of the area studied is the Alhambra fault which has reverse shear movement; and to the west and south is the Pine Creek anticline (Meyer, 1977 and Radford, 1973). The mine lies on the overturned north limb of the Pine Creek anticline which establishes a west-northwest to northwest trend for the bedding planes. The orebodies in the Bunker Hill mine are structurally controlled by the fold fabric of overturned, WNW-trending folds- belonging to the

second of two stages of folding. The Tyler Ridge flexure is a parasitic fold form of this type which controls the Bluebird veins in the Bunker Hill mine (fig. 2). The plunge of the WNW-trending folds is controlled by their position on older, NNW-trending folds, which are more pronounced north of the Osburn fault. It is deduced that metal bearing fluids were introduced through the intensely fractured zones during the second stage of folding (Juras, 1977).

Figure 2. Plan view showing the relation of Bluebird and Link veins to parasitic fold-forms. The dotted line is the axial trace of the Tyler Ridge flexure, which plunges WNW (After Bunker Hill files). STE-siltite, QTZT-quartzite

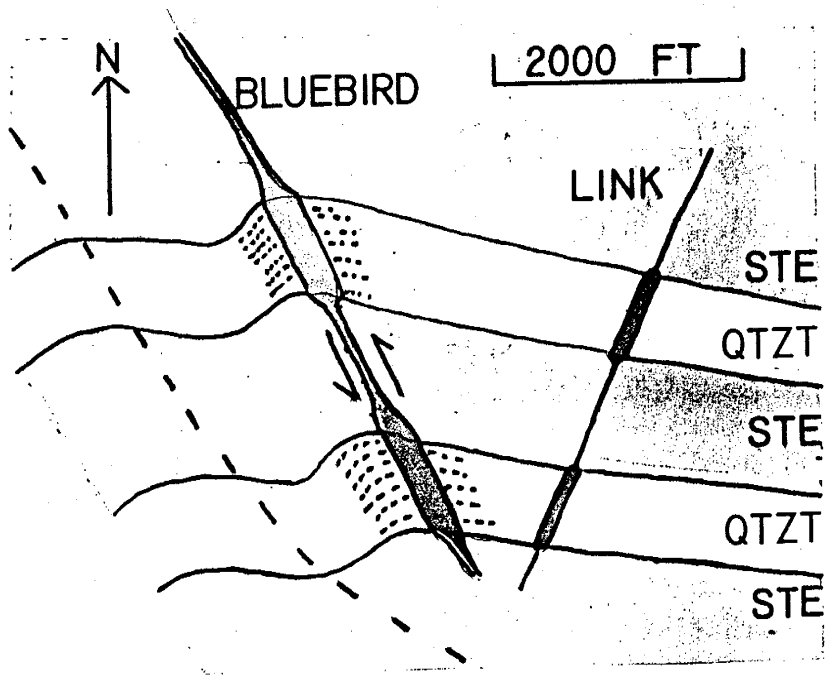

Most of the orebodies of the Bunker Hill and Crescent mines occur within the upper quartzite members of the Revett Formation (White, 1977), one of three preferentially mineralized horizons within the district (Bennett, et al., 1982). Two types of replacement-fissure veins are found within the Bunker Hill mine; they are the Bluebird and Link veins (fig. 2). The Bluebird veins strike northwest and dip to the southwest and were formed prior to the Link veins as evidenced by cross-cutting relationships, although both systems are related to the same deformational event (Juras, 1977). Bluebird veins contain sphalerite in excess of galena, with pyrite, quartz and siderite. The 14 Brown and Quill orebodies are examples of Bluebird veins. Link veins strike northeast to east and dip south from 40 to 70 degrees and mineralogically, they contain mostly galena with smaller amounts of sphalerite, chalcopyrite and tetrahedrite (Meyer, 1977). The 9 Jersey is an example of a Link vein. The 23 Francis and 19 'J' orebodies are not true Link veins because of different structural controls, but have the same type of mineralization as Link veins and are referred to as Link veins in this thesis. Mineralization in the Crescent mine consists largely of silver bearing tetrahedrite replacing siderite, with accessory quartz and chalcopyrite.

Another possible orebody-type is the March ore shoot, thought to represent a hybrid of the above types of mineralization with a different, more favorable structural

control. The caved and inaccessable March workings provided the richest ores in the history of the mine and a correlative deposit would be a most desirable exploration target.

The mineral parageneses of the Coeur d'Alene district which are based upon textural observations are capable of providing an unlimited source of interpretive confusion. Paragenetic relations between the major mineralization events will vary much less than the paragenetic relations within individual veins or samples, so a question of scale needs to be solved. A generalized paragenesis of the Bluebird and Link veins is given in figure 3. The earliest mineralization was probably barren milky quartz and possibly metamorphic sericitization. The earliest economic mineralization formed the sphalerite-galena Bluebird orebodies. In these veins an early siderite depositional stage was followed by a sphalerite stage with little or no galena deposited. Galena mineralization in the Bluebird veins is associated with a second stage of sphalerite mineralization. The principal stage of galena mineralization was probably associated with the Link vein formation, which may have overlapped with part of the final stage of Bluebird mineralization. The paragenetic relationship between the Crescent(Ag) mineralization and the Pb and Zn mineralization was uncertain at the time of this study.

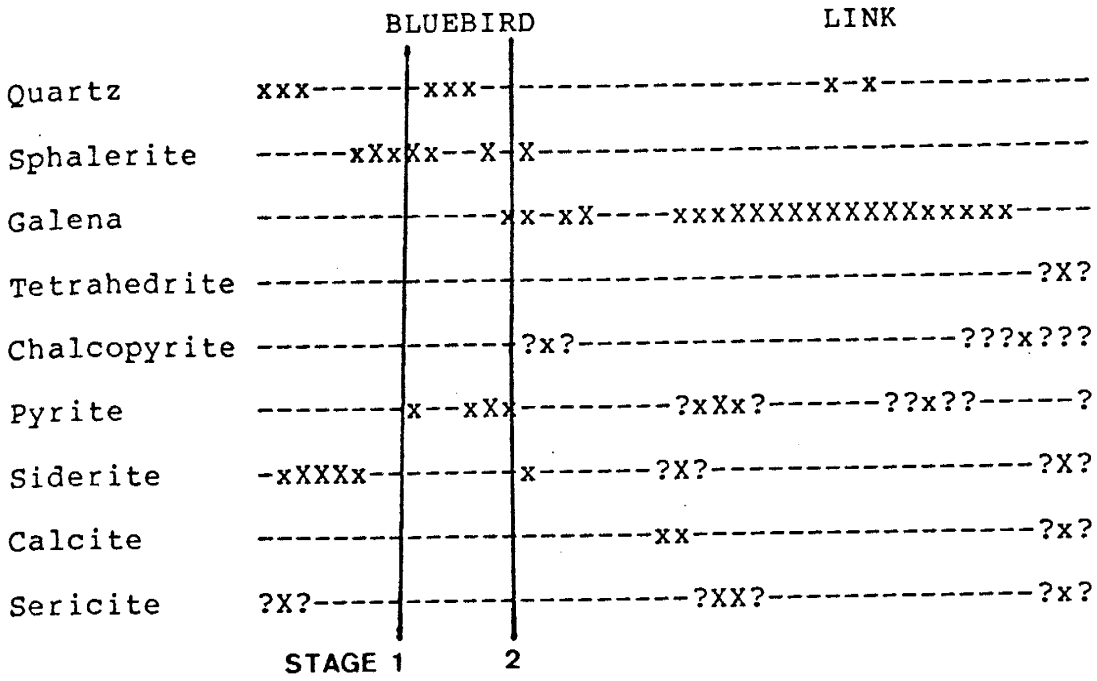

Figure 3. Generalized paragenesis of the Bluebird and Link veins (After Beck, 1980).

Large X; large amount deposited

Small x; minor amount deposited

?; uncertainty

-----> ; time towards right

Two types of disseminated ores are associated with the Bluebird vein type ores. "Crackle breccia" is a term used to describe the texturally-mottled disseminated-sulfides, predominately galena and sphalerite, following bedding in a quartzite host (fig. 4). The term is used in a purely descriptive sense by the Bunker Hill staff and does not imply any genetic conotations as in "crackle breccia" proper (Beck, 1980). The wetted slab in figure 4a shows an unusually well developed texture relative to the typical developement as shown in figure 4b. "Soaking" texture refers to ore characterized by the dissemination of very fine grained sphalerite and other sulfides throughout the host rock (fig. 5). Beck (1980) favors a replacement origin for both of the disseminated ore types on the basis of an ore microscopy study, but feels that the filling of open pore space was also very important.

Figure 4a. Mega-"crackle-breccia" (100-35-23).

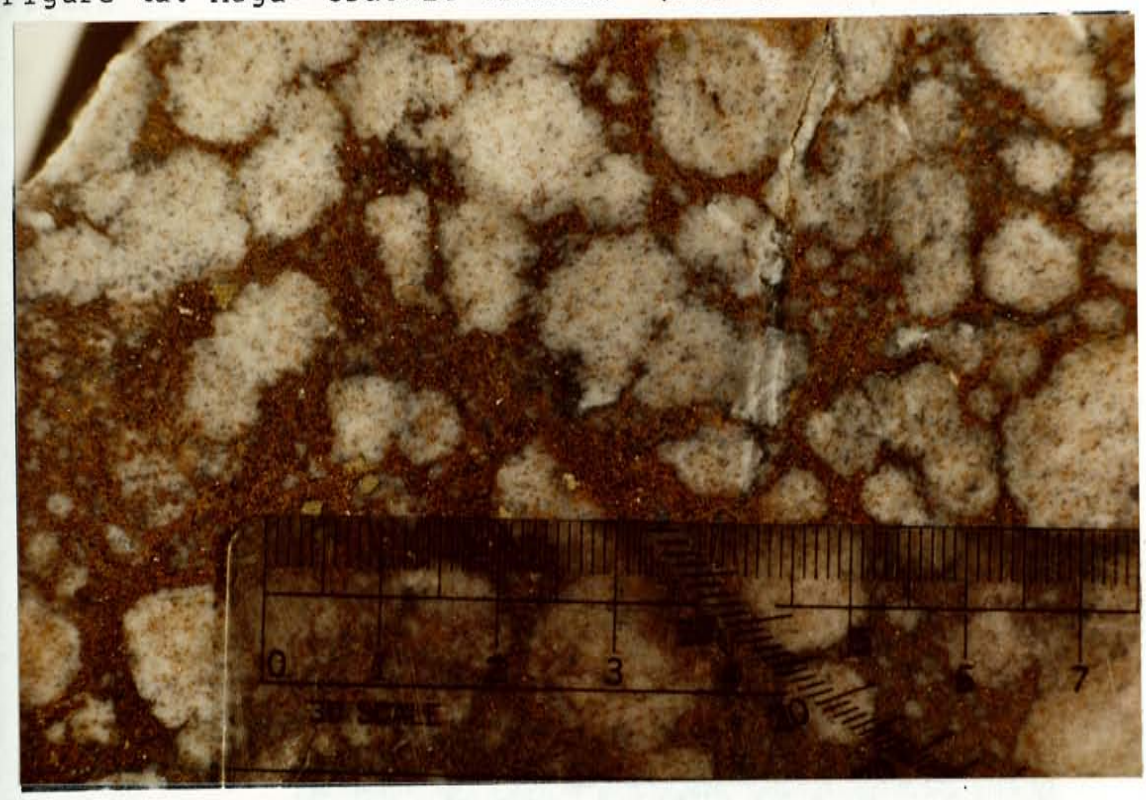

Figure 4b. Typical "crackle-breccia" texture.

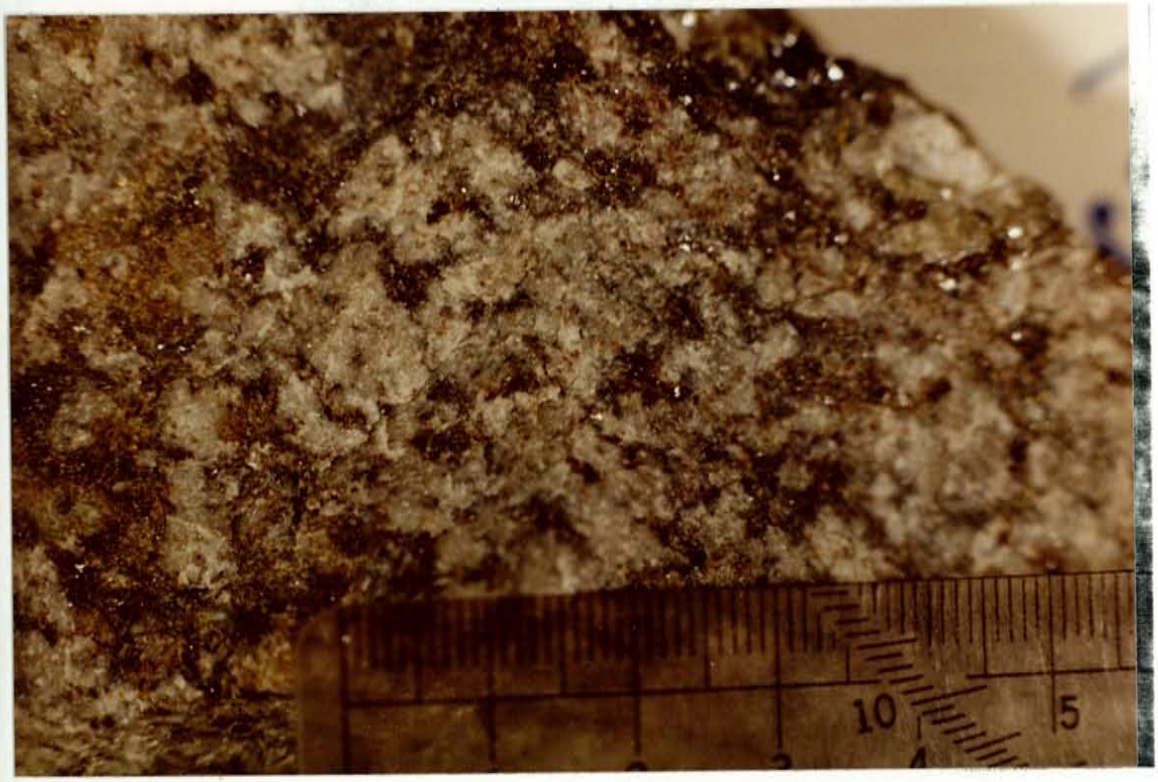

Figure 5. "Soaked" texture (130-35-23). Note the zone of sulfide remobilization adjacent to late Bluebird time micro-fractures (30 scale to an inch).

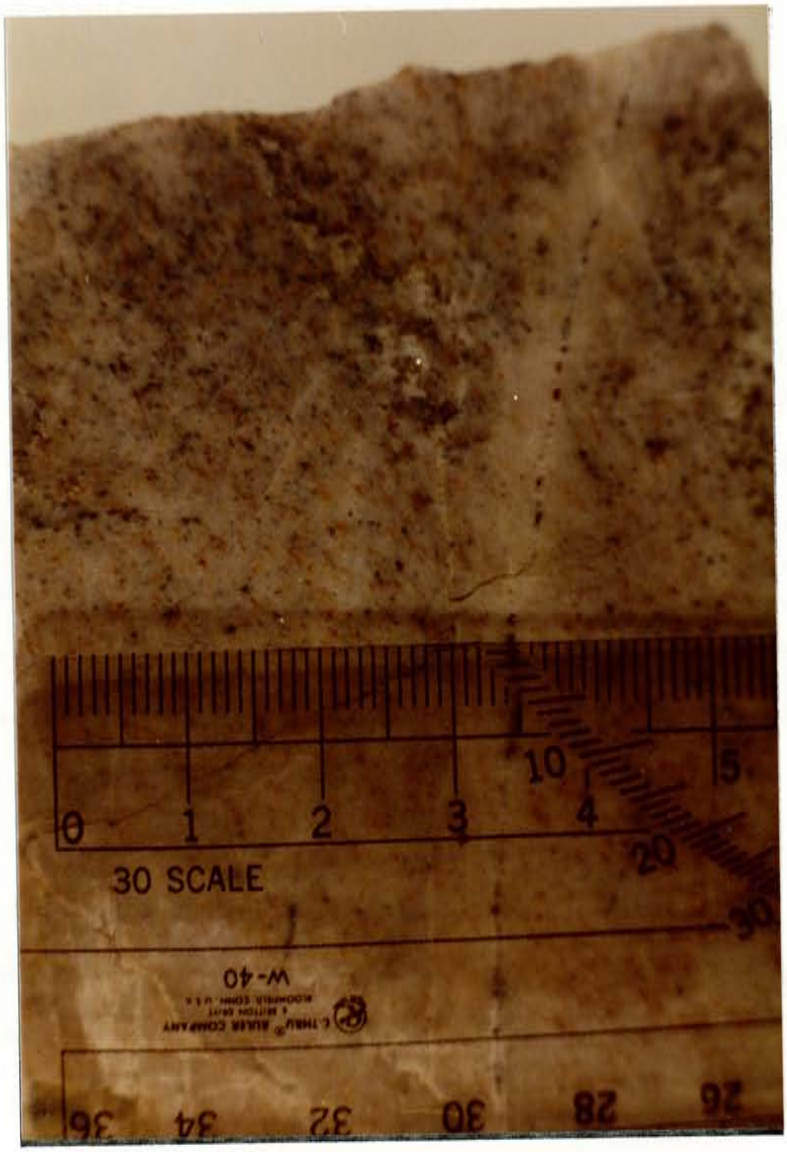

The term "Blue" rock has recently been used to describe disseminated ores (Landis, et al., 1983 and Landis, et al., 1984). The terms "Blue" and "Brown" ore are used in some photo descriptions in this thesis. Here they are used purely in a descriptive sense and do not imply a specific ore mineralogy. Both "Brown" and "Blue" ore may contain siderite and sphalerite. The presence of galena is uncertain. The terms are useful for delineating a paragenetic sequence of miscellaneous, different colored ores in outcrop scale. Technically, tone or color saturation of the ores, rather than color, is probably responsible for the easy distinction between the two mineralization stages. Whether or not there is a systematic variation in the Fe content and color of stage-1 and stage-2 sphalerite is uncertain. An investigation should be made to see if later sphalerite is darker in color than early sphalerite, the color difference being due to an increase in Fe content. The terms should be seriously considerred for descriptive use, especially if used with modifiers such as "soaking" (i.e. :"Blue"-"soaked ore"). No study has clearly delineated between these ore types and it is uncertain whether or not they correspond to the two stages of Bluebird mineralization indicated by Beck (1980). Whether or not these terms have value for district usage is questionable but they seem promising for local use.

Mineralized psuedo-stratiform fabrics are also present but appear to be permeability controlled epigenetic features which are localized to near vein areas in both Bluebird and Link veins.

Steel-galena texture is typical of Link mineralization (fig. 6). This texture consists of the development of a pervasive schistosity within the galena through shearing. This texture also occurs in much of the late-Bluebird galena mineralization. Note that the quartz in figure 6 is pre-mineralization, and milky white in color. Rounded quartz crystals which have been caught within the shearing are termed "pre-existing" crystals by the mine staff (fig. 7). The "pre-existing" crystals are clear, except for fracturing, rather than milky as in pre-mineralization quartz.

Figure 6. Steel-galena texture (25 Francis).

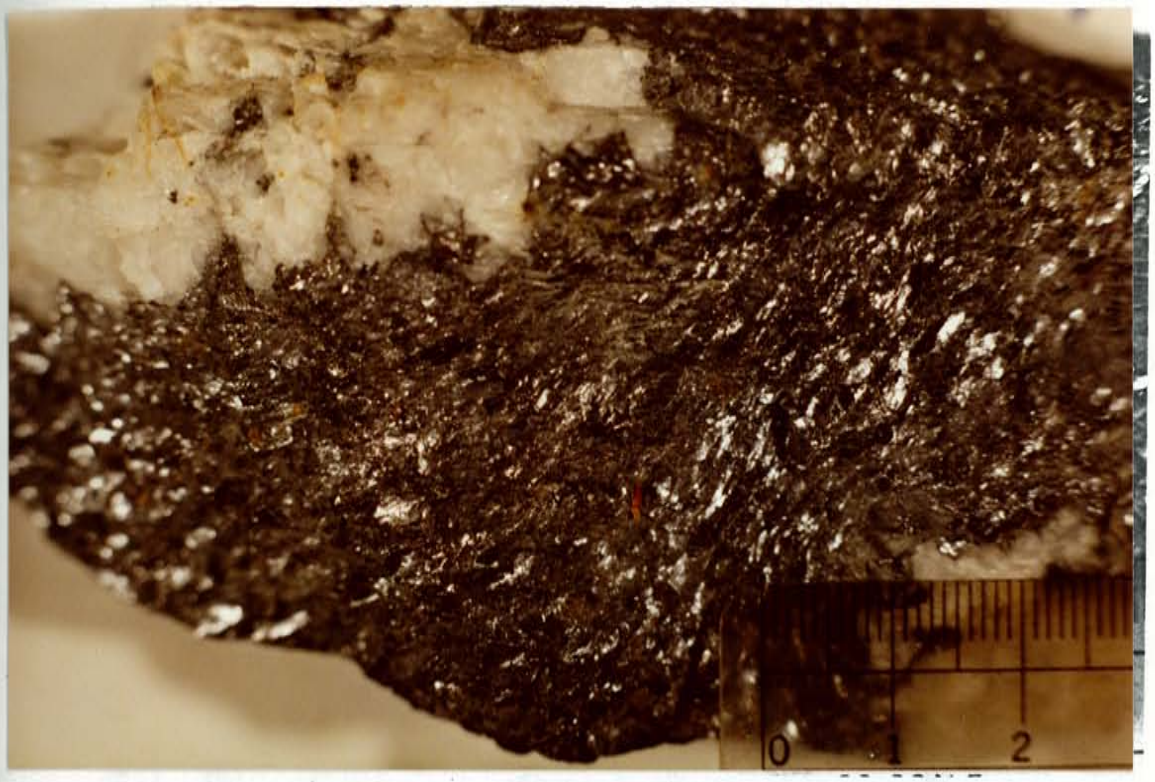

Figure 7. Pre-existing quartz crystal in steel-galena (110-35-21). Both textures are weakly developed.

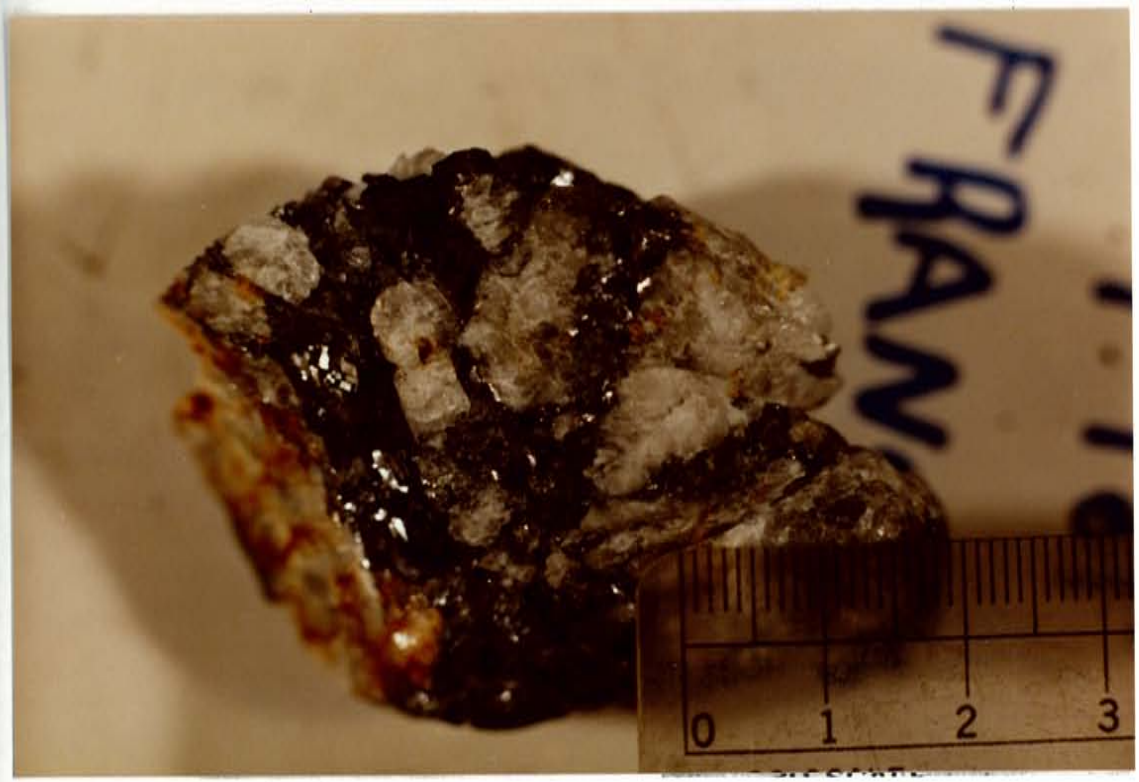

Typical Crescent mineralization within the Hook vein consists of argentiferous tetrahedrite replacing siderite (fig. 8). Minor chalcopyrite is also present.

Figure 8. Typical Crescent ore texture (37-11-9 East). Note that the siderite mineralization consists of somewhat rounded breccia clasts which are early relative to the tetrahedrite and chalcopyrite. Minor rounded milky quartz breccia clasts are present which are of pre-mineralization(pre-Ag & Cu) time. Wallrock borders the vein on the bottom and top of the photograph (scale 30 divisions to an inch).

The Gem and Dago Peak stocks and the inferred Atlas pluton are major intrusive rocks present in the district. The genetic role of the intrusives in mineralization is currently a subject of debate. The Belt rocks in the district have been deformed and metamorphosed to lower greenschist facies which is evidenced by the recrystalization of quartz grains and the formation of sericite grains parallel to the poorly developed schistosity (Landis, et al., 1984 states that the regional metamorphism is of upper greenschist facies). The relative age of metamorphism is uncertain but the realignment of sericite grains due to pre-ore shears suggests ore deposition after metamorphism.

METHODS OF STUDY

The aim of this thesis is to help clarify the genesis of the Bunker Hill deposits by characterizing the ore-forming fluids, so characterization of the fluid inclusions is the principal study method. Field sampling was accomplished during the summer of 1981 with the goal being to collect as much non-sheared vein material and euhedral crystals for fluid inclusion study as possible. Fluid inclusion study was carried out by microscopic investigation and instrumental analysis of fluid inclusion liquids and gases.

Microscopic investigation involved the observation of doubly polished thin plates at temperatures from below $-100^{o}C$ to nearly $500^{o}C$, as required by the inclusions under study. A Linkam heating-freezing stage was employed which used liquid N_2 gas as a coolant and a heating element for temperature control. The reader is referred to Hollister, et al, 1981, and other sources for a description of the methods of fluid inclusion microscopic investigation.

Gas analyses were carried out by thermally decrepitating inclusions and analyzing the resulting gases with a quadrupole type mass spectrometer (a description of the method used is given in the appendix). Analyses of inclusion fluids were made by crushing samples in a vacuum, leaching with a 1 % solution of ultra-pure HNO_3 and

analyzing the leachate by atomic absorption spectroscopy, specific ion electrode, turbimetric methods and high pressure liquid chromatography; Na, Ca, K, Mg, Mn, Fe, Zn, Cd, Ag, Pb, Cu, As, SO_4 and Cl were the principal anions and cations determined. The reader is referred to the appendix for more information concerning the procedures employed.

FIELD OBSERVATIONS

Crystals suitable for microscopic investigation of fluid inclusions occur within various orebodies and structural settings in the Bunker Hill mine. En echelon tension gashes associated with the zone of reverse-shearing occur in the 24 stope of the Quill orebody (fig. 9). These gashes are typically 1 to 3 meters in length, 1/2 to 20 cm wide and composed of a milky white, massive quartz. Often vugs are present which contain euhedral quartz crystals and sphalerite crystals (fig. 10), and less commonly, galena crystals. Chalcopyrite crystals are rarely present in minor quantities. A sericitic(?) gouge-like filling of uncertain composition occurs in the intercrystalline spaces. Field observations and hand specimens indicate that these gashes are closely related to or contemporaneous with main stage Bluebird mineralization. The tension gashes are fold-form localized and probably concurrent with the end of the deformation. Many samples of Bluebird mineralization were taken from these gashes so a detailed description is given here to clarify possible ambiguities for those who will need to interpret this data or work in the district in the future. These en echelon gashes (fig. 11), should not be confused with the near-horizontal joint sets which also contain crystals, generally less than 1/2 cm in size. Field evidence indicates that these are not fold-form related and are post-main stage mineralization, hence were avoided in

Figure 9. Plan of the Quill orebody (11 level). The stopes are outlined and numbered 21, 23 and 24. Lower levels are offset in the direction of fold-form plunge to the WNW and upper levels to the ESE. The blue shading indicates the zone of reverse shearing which is also the zone of the most intense mineralization. The yellow shading indicates mineralization following favorable quartzite units. Sample sites are indicated by letter without reference to level.
(After mine maps by the Bunker Hill staff)

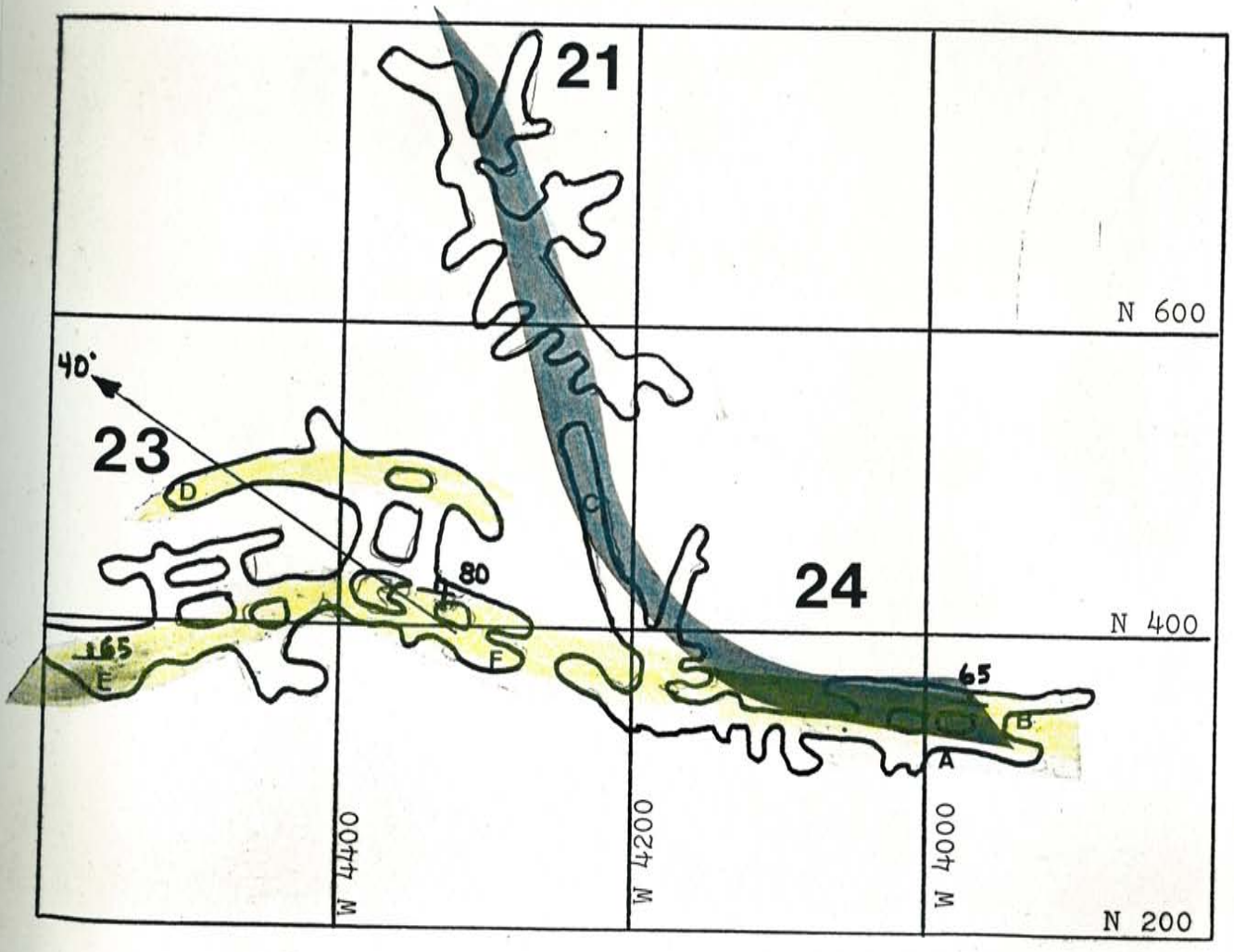

Figure 10. A typical euhedral quartz and sphalerite crystal group found within the vugs of the en echelon shears (100-35-24). A minor amount of the sericitic(?) gouge-like material which commonly filled the "open-space" of the vugs is still present on this specimen after it has been quickly washed.

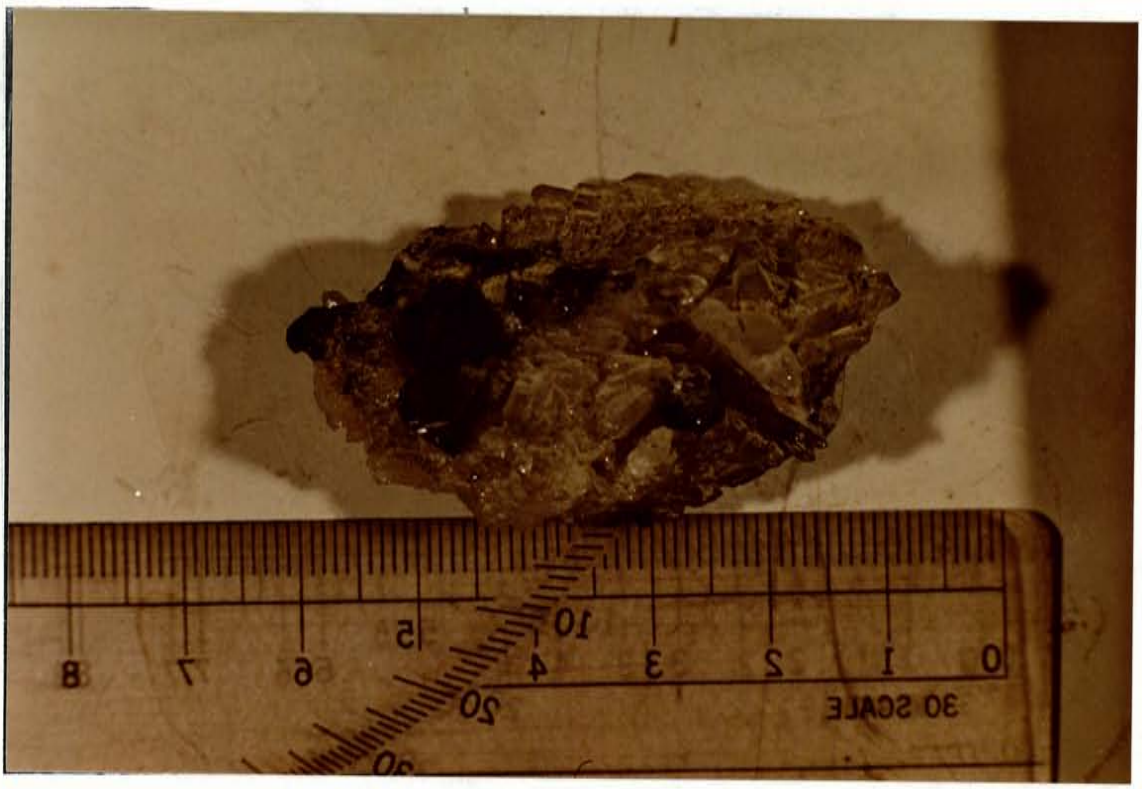

Figure 11. En echelon tension gashes (110-35-24). Perpendicular outcrop (N-S and cutting bedding), to photos 2 and 3 (E-W and subparallel to bedding).

Photo 1. Top of photo.

Figure 11.
En echelon tension gashes (110-35-24).
Photo 2.

Figure 11.
En echelon tension gashes (110-35-24).
Photo 3.

Figure 12. Fracture-controlled mineralization (110-35-23).

Figure 13. Bedding separation near a small parasitic fold and collapse breccia (110-35-23). Unidentified carbonates(?) 'C' may be tremolite(?) rich.

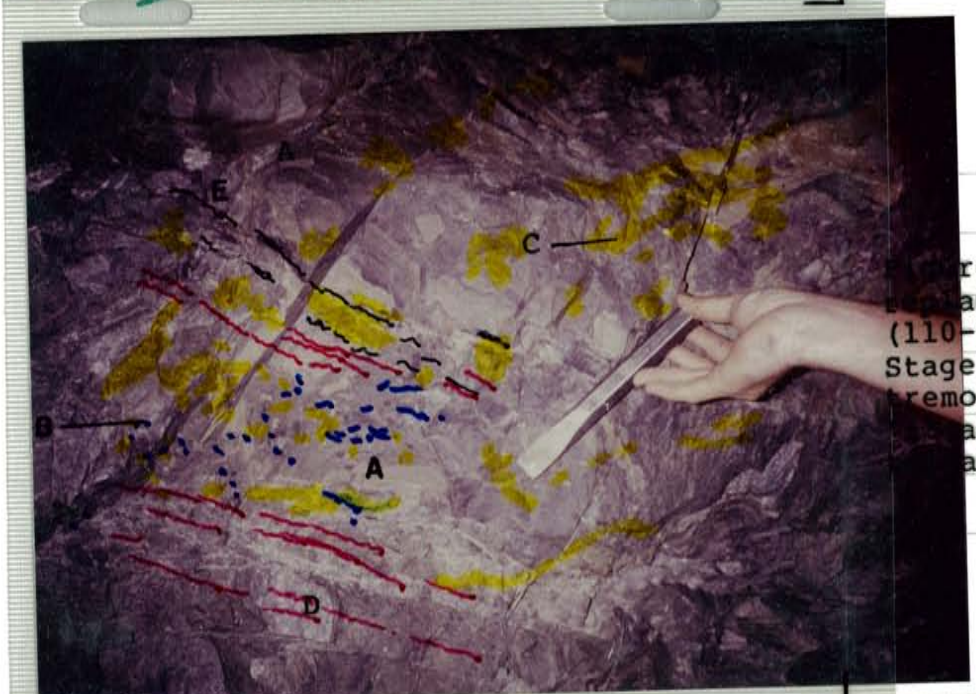

Figure 14. Irregular replacement textures (110-35-23). Stage 'C' may be tremolite(?), stage 'A' and 'B' may have anhedrite(?).

selection of samples for study. Although they do contain small amounts of sulfides in some areas they generally barren in others.

The en echelon tension gashes (fig. 11) are generally shallow dipping and may be a part of a conjugate system resulting from the same a stress field. Several different sets of tension shears are outlined in the three photos of figure 11; set 'A' may be a conjugate shear to shear plane ' C' ' of photo 3, set 'D' may be a product of shear plane ' C' ' or reverse shear plane 'B' of photo 2. In all photos the apparent compressional direction 'E' may produce a direction of relative tensional stress 'F' and all the outlined shear and tensional planes. The apparent direction 'E' is roughly west-southwest trending (note that the stress directions given are not the directions of the maximum compressional axes). Note that main-stage Bluebird replacement veins are oriented parallel to direction 'F'. This indicates that they may be the logical result of the compressional stress field and are oriented in the direction of relative tension. The Bluebird veins seem contemporaneous with the en echelon shear's stress field but contain different mineralization, with an early siderite stage 'X' followed by sphalerite 'Y'. Euhedral sphalerite ' Y' ' occurs in vugs within the shears in photo 2. The early siderite stage 'X' has been brecciated and off-set within the quartz shears but the sphalerite stage has only been

weakly off-set in the quartz shear zone. This indicates that the shears are of Bluebird time. In photo 1 a siderite-sphalerite-galena veinlet cuts the quartz shears and indicates that many of the euhedral crystals in the vugs may be of this late-Bluebird time. Note that the right hand side of photo 1 shows the quartz shears cut by a bedding shear(?) and bounding abruptly against a main stage Bluebird vein consisting of replaced wallrock of the "Blue" and "Brown" ore types. The wallrock within the shear zone is sometimes only weakly mineralized (origin of the term 'bleached' in the literature?). This indicates that a ground preparation stage may have occurred prior to mineralization event 1.

Only clear and euhedral quartz crystals from vugs within the en echelon shears have been studied in this thesis. In the future, the milky quartz of these shears should also be studied.

The character of the mineralization is often very irregular (fig. 12). Mottled textures 'A' are the result of irregular replacement along fracture planes. Note that Bluebird-sphalerite vein 'B' has a very irregular outline which is determined by replacement along shears. The wall rock is complexly sheared and filled with pre-mineralization quartz 'C' (this quartz was not studied). Where bedding planes have been separated during folding

"collapse-breccias" were formed (fig. 13). Here the character of mineralization varies from "soaked" ore 'A' in the footwall of the bedding shears to "crackle-breccia" 'B' in the hanging wall. Psuedo-stratiform mineralization 'D' occurs as replacement of permeable layers within the quartzite. Unidentified carbonates 'C' are interstitial to the collapsed bedding and seem to have formed after the main stage Bluebird mineralization as evidenced by Bluebird-soaking breccia clasts 'E'. Quartz shears 'F' may be post-mineralization(?) and were not studied. The general sequence of mineralization is "Brown" ore 'C' (fig. 14) which is equivalent to the Bunker Hill term- "soaked" ore (The mineralogy of this "soaked" ore is uncertain and may contain either siderite, sericite or light sphalerite, therefor study of a polished section may be desirable.), "Blue" ore 'A' and 'B' where 'B' is simply more concentrated "Blue" ore in localized spots. Quartz fractures 'D' are later than mineralization but have an orientation similar to "Blue" ore mineralized fractures 'E'. The local increase in "Blue" ore 'B' may indicate a period of ground preparation prior to this stage of mineralization.

When a mineralized zone is viewed in section, across bedding, the mineralization is seen to be controlled by bedding (fig. 15). The photo shows a mineralized face of the Revett quartzite ready for blasting. 'D' is the direction of bedding, 'A' and 'B' are mineralized "Brown"

Figure 15. Control of mineralization by bedding (110-35-23).

Figure 15. Control of mineralization by bedding (110-35-23).

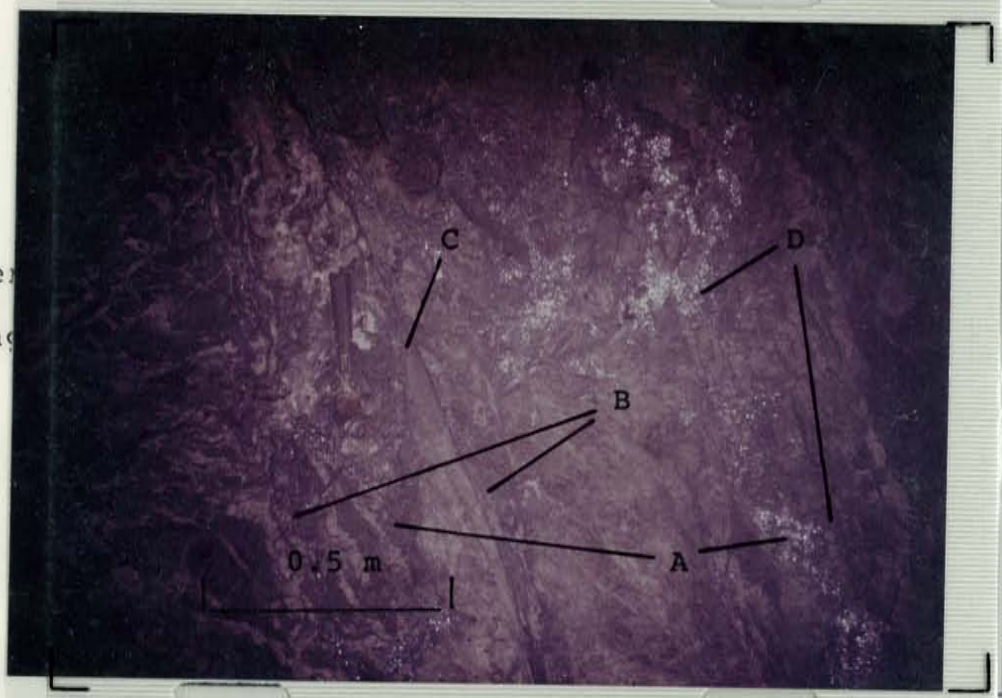

Figure 16. Steel-galena mineralization within the Quill orebody having an irregular character in section, coplanar to bedding (110-35-24).

Figure 17. Textural relati in a block of main stage Bluebird mineralization (110-35-21).

Figure 18.
Pre-mineralization quartz (110-35-21). Questionable photo orientation?

Figure 19.
Orbicular texture (130-35-23).

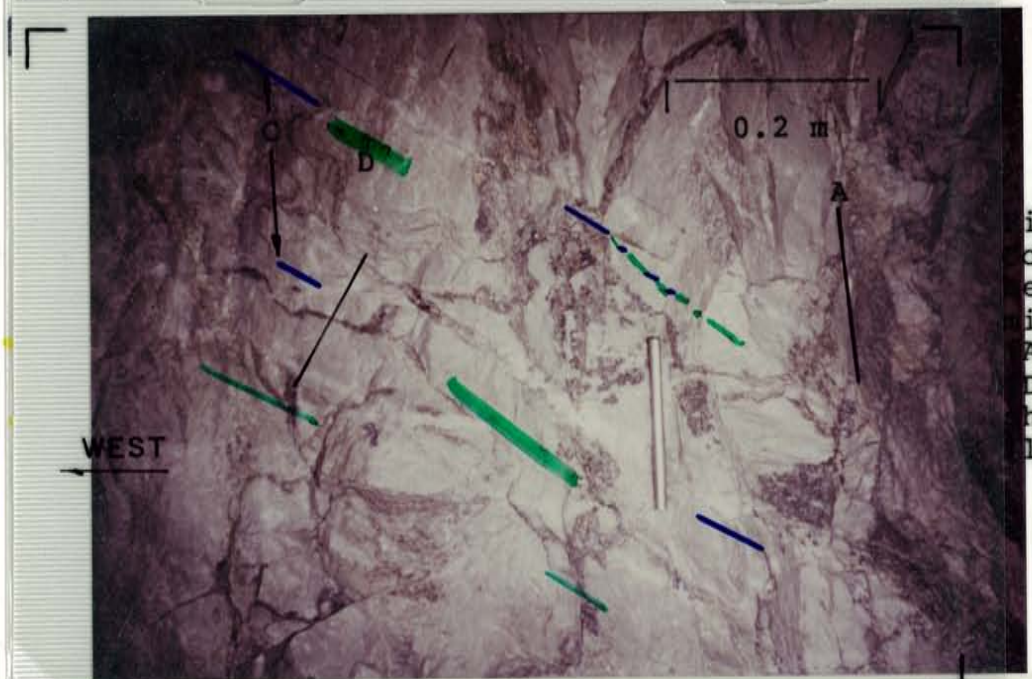

igure 20.
omplex relation
etween Bluebird
ineralized zone
A), quartz shears
D) and mineralized
hears(C)
130-35-23)

and "Blue" ore respectively. Later steel-galena mineralization 'C' is irregular in distribution and does not closely follow bedding.

When the mineralization is viewed in a section co-planar to bedding, the control by bedding, if present, is not apparent (fig. 16). The paragenetic sequence of mineralized soaked ore 'A', quartz shears 'C' and sideritized wall rock 'B' are uncertain in this photo. Steel-galena mineralization 'D' is later than the other stages and very irregular in distribution.

The irregular nature of the ore is visible in a block of main stage Bluebird ore (fig. 17). The "Blue" soaked ore 'A' is bounded by psuedo-stratiform mineralization 'C' in a weakly mineralized quartzite matrix 'B'. The boundary between the two ore types is irregular and seems to be a function of a ground preparation event prior to the emplacement of the "Blue"-soaked ore. The boundary between the previous textures and the main stage, heavily mineralized vein zone is also very irregular with evidence for both replacement and brecciation visible in figure 17. The psuedo-stratiform ore is bounded by irregular replacement-like textures while the soaked "Blue" ore is present as both angular and rounded breccia clasts in the main-stage vein. The main-stage vein consists of both "Brown" ore 'D' and later "Blue" ore 'E' which differ in

texture from "Blue"-soaked ore 'A' in that the main vein mineralization seems to have been formed in an intensely brecciated matrix, which has also probably undergone a period of deconsolidation during ground preparation.

The pre-mineralization (pre-reverse shear) milky quartz from which gas analyses were made is shown in figure 18. The pre-mineralization quartz 'P' is offset by shears mineralized with "Blue" ore 'E'. The wall rock 'A' is probably slightly oxidized in this photo and should be distinguished from the sideritic "Brown" ore 'X' which formed prior to the "Blue" ore 'Y'. Pre-mineralization quartz 'C' is dragged into the shear planes 'E'. The direction of the pre-mineralization shears is parallel to a well defined cleavage 'D'.

Among the unusual features observed in Bluebird mineralization is the occasional occurrence of "orbicular" textures (fig. 19). This texture consist of concentric oblate spheres of non-mineralized wall rock 'A', "Brown" soaked ore 'B', and a rim of "Blue" soaked ore 'C'. The long axis of the "orbicule" in figure 19 coincides with the approximate direction of relative tension while its short axis roughly coincides with the direction of relative compression. Thus a stress field producing conjugate shears 'D' and 'E' may be responsible for the formation of these textures. The non-mineralized wall rock is probably merely

a product of incomplete ground preparation- which probably consisted of deconsolidation of the quartzite. A quick microscopic inspection of a chip of "Brown" soaked ore 'B' indicates that disseminated sphalerite is responsible for the color, with only traces of galena (later stage?), and no obvious siderite present. Some of the quartz shears bear complex relations to mineralization (i.e. fig. 20). The bulk of the wall rock in this example is poorly mineralized and borders abruptly against a well mineralized zone 'A'. Mineralized zone 'A' cuts the quartz shears 'D' and appears to be later. Parts of the quartz shears appear to have been mineralized with siderite and sphalerite of the same type as main stage 'A'. It seems that the milky quartz is earlier than the main-stage Bluebird mineralization. Clear quartz and sphalerite crystals were sometimes present in vugs in these shears and are thought to be close to or contemporaneous in paragenetic time to main stage mineralization.

Sometimes the quartz shears were present in the stope roof (fig. 21). This figure shows that the milky quartz 'A' is earlier than mineralization. The milky quartz shear is fractured along conjugate planes 'X' and 'Y'. The opened fracture spaces were then filled with "Brown" and "Blue" ores 'F' and 'D'. The subangular quartz clasts 'A' indicate that both open space and replacement may have occurred. After(?) the "Brown" and "Blue" ores were emplaced, later

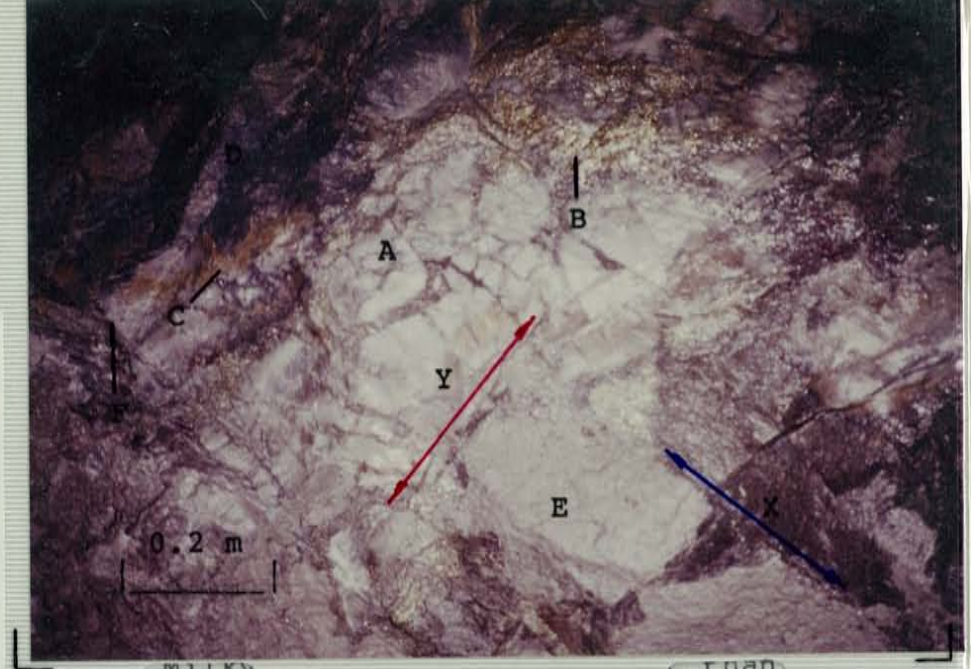

Figure 21. Quartz shear in the stope roof (130-35-23), see text p. 35.

Figure 22. Quartz shear in the stope roof (100-35-24). See page 38.

Figure 23. A typical Bluebird vein (110-35-21). See text page 38 for an explanation.

Top of photo (fig. 23).

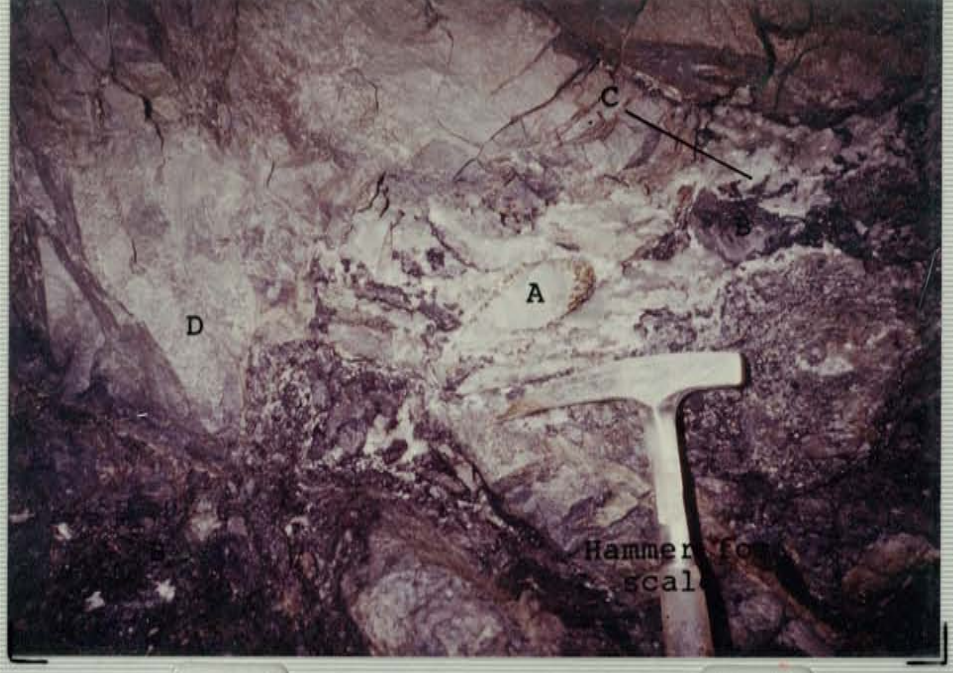

Figure 24. Calcite in collapse breccia (110-35-23); see text page 39.

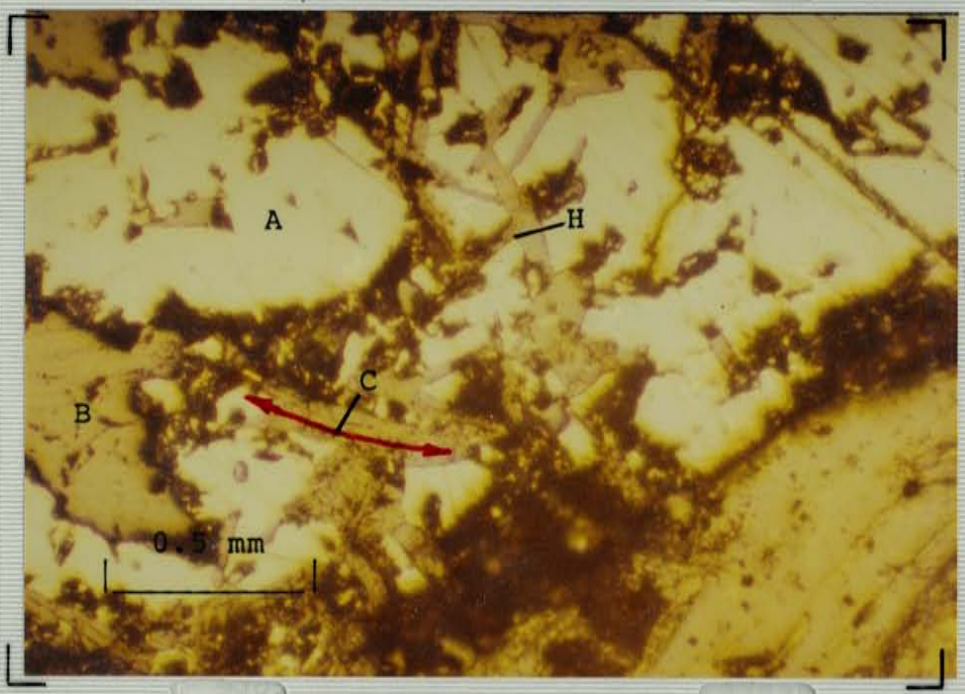

Figure 25. Sericite within the collapse breccia ore (110-35-23).

Figure 26. Load cast with pyrite (p. 40).

pyrite and chalcopyrite 'B' mineralization occurred (about 30 % chalcopyrite::pyrite in handspecimen). Unidentified carbonate 'C' is of an uncertain age, but probably post-"Blue" ore. 'E' is mine dust.

In another example of a quartz shear exposed in a stope roof, abundant euhedral quartz and sphalerite crystals are present (fig. 22). Lesser quantities of euhedral galena cystals were also present. Milky quartz 'A' is earlier than "Brown" ore 'D' and "Blue" ore 'C'. The direction of elongation of a large vug containing euhedral crystals 'B' is parallel to shear direction 'E'.

A final example of a Bluebird vein (The attitude of the vein is N60W75S and the attitude of the bedding is S30W58W; the photo plane is subparallel to the strike of the bedding (110-35-21)), illustrates the irregular character of mineralization (fig. 23). Both the wall rock 'C' and the heavily mineralized vein zone 'A' show evidence of intense shearing. Wall rock 'C' however, is weakly mineralized. The strong mineralization of the vein zone may be due to ground preparation through chemical dissolution and/or more open fracturing. The footwall wallrock 'B' shows irregular boundaries with the vein zone, with angular breccia clasts extending into the vein. Note that the footwall-breccia clasts of 'B' are very weakly mineralized. In the footwall wallrock in area 'G' an intense "Brown" soaked ore indicates

that this stage of mineralization closely followed a period of ground preparation or occurred by replacement. The later "Blue" ore largely defines the vein and appears to replace the "Brown" ore. Late stage pyrite 'D' and galena 'E' are post "Blue" ore. Milky quartz 'F' is pre-mineralization. Only minor rounded, remnant breccia clasts of siderite are present, too small to be visible in the photograph. Angular wallrock clasts are present as stringers parallel to the wallrock borders.

When calcite is present it is post-"Blue" ore (fig. 24). This figure shows clear, euhedral calcite 'C' filling open space created by dissolution of "Blue" vein ore 'B'. "Brown" ore occurs in "Crackle-breccia" 'D'. "Blue" ore occurs as a collapse breccia filling in the hinge of a minor parasitic fold (Note the rotated blocks of mineralized quartzite at the base of the hammer). Non-mineralized, rounded quartzite clast 'A' is enveloped with a late, but pre-calcite, pyrite stage.

Sericite and chlorite are present as late stage vug fillings. Sericite has also been observed within the "Blue" ore of the collapse breccia of figure 24. The polished section in figure 25 shows non-directed sericite 'H' enveloped in sphalerite 'A'. Quartz grains 'B' appear to be remnants of the quartzite host. Whether this sericite is hydrothermal or re-orientated metamorphic sericite is

uncertain. Bent sericite 'C' could have been deformed during mineralization.

A final example of the wallrock in a non-mineralized exploratory drift shows that alteration extends over a broad area (fig. 26). The euhedral pyrite 'P' in load cast 'A' (over load bar 'B') is probably metamorphic in origin. Grain size differences eliminate a detrital origin. The host rock is a sericitic quartzite or argillite.

Although most of the obvious alteration associated with mineralization consists of sericitization, sideritic carbonitization and pyritization, some areas within the Quill orebody show extensive deconsolidation of the wallrock (particularly in the 120-35-24 stope). This deconsolidation consists of a very irregular, non-fault associated dissolution of the intergranular carbonate cement (and possibly much of the quartz). The zone of deconsolidation is so extensive that the entire access drift was flooded with sand when this zone was first breached! The typical unwashed deconsolidated wallrock is very fine grained and was thought to be unmineralized except for abundant sericite (fig. 27). Within the stope irregularly distributed green and reddish patches were present within the deconsolidated zone indicating a complexly varying geochemical environment of formation. The reddish patches were thought to be late hematite stains. Smokey massive and vein quartz sometimes

Figure 27. Typical deconsolidated wallrock (120-35-24). A pellet of dry pale-green sample on cardboard, size is slightly larger than 1 cm. The sample crumbles to a fine powder when touched.

envelops portions of the deconsolidated zone. The almost complete remobilization of sulfides indicates that the deconsolidation event is post main-stage Bluebird mineralization.

A quick microscopic inspection was made of a sample of the pale green deconsolidated wallrock just prior to completing the final copy of this thesis (date: 12-23-84), with the intention of quantifying the quartz-sand grain size. The rounded quartz-sand was uniformly less than 0.2 mm to about 0.1 mm (well sorted). About 1 % rounded sphalerite grains were present, typically about 0.05 mm in size. About 1 % ruby-silvers(?) were present but were only visible under high power. They typically occurred as bright crimson-red micro-crystals, uniformly about 0.005 mm in size, on quartz and formed after the deconsolidation. Approximately 10 to 30 % of the sample was composed of an unidentified, late stage mineral with a grain size of 0.05 to less than 0.002 mm. The unidentified mineral was clear, prismatic and showed an inclined extinction (eliminating sericite; tremolite, hemimorphite and Pb minerals are possibilities). The reddish patches in the deconsolidated wallrock should be investigated to determine if high concentrations of ruby-silvers(?) are present.

MICROSCOPIC TEXTURAL OBSERVATIONS:

Several interesting textural observations were made during the microscopic investigation of fluid inclusions. The first is the indication of the presence of open space during mineralization at the microscopic level. In the euhedral quartz crystals which seem to be associated with Bluebird sphalerite, miniature vugs commonly occur (fig. 28). This example contains euhedral quartz crystals which must have formed in the availiable open space. Sphalerite 'S' occurs as open space miniature crystals and as trapped interfacial fillings (between quartz crystals) which resemble replacement textures but are probably not (The interfacial fillings probably formed in open space.). Note the abundant primary inclusions, many of which are oriented along quartz crystal faces. The alternate deposition of quartz and sphalerite is probably a function of the availiability of nucleation sites and changing fluid chemistry on a very small scale. The completely included sphalerite shown in figure 29 probably formed in open space, as indicated by the thin interfacial mineralization 'A'. The abundant fluid inclusions may be the result of a multitude of miniature quartz crystals growing and meeting. An example of fluid inclusions trapped on a growth plane is shown in figure 31. Note that here the inclusions are planar and contain uniform amounts of the vapor phase relative to the liquid (about 10% vapor). In figure 28 the

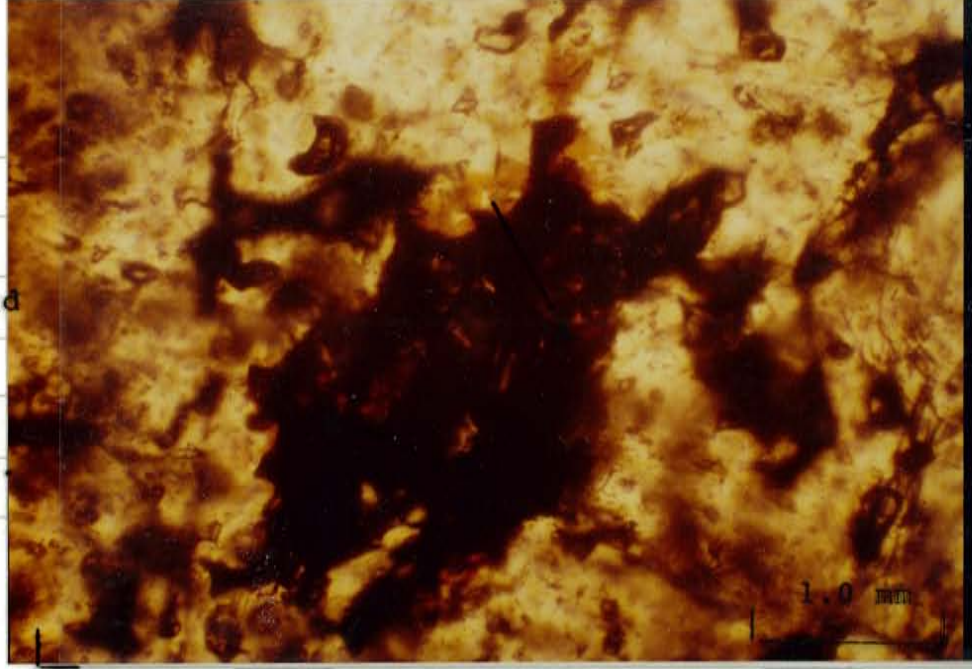

Figure 28. Sphalerite included within quartz (110-35-24). Note the presence of both aqueous and gaseous inclusions.

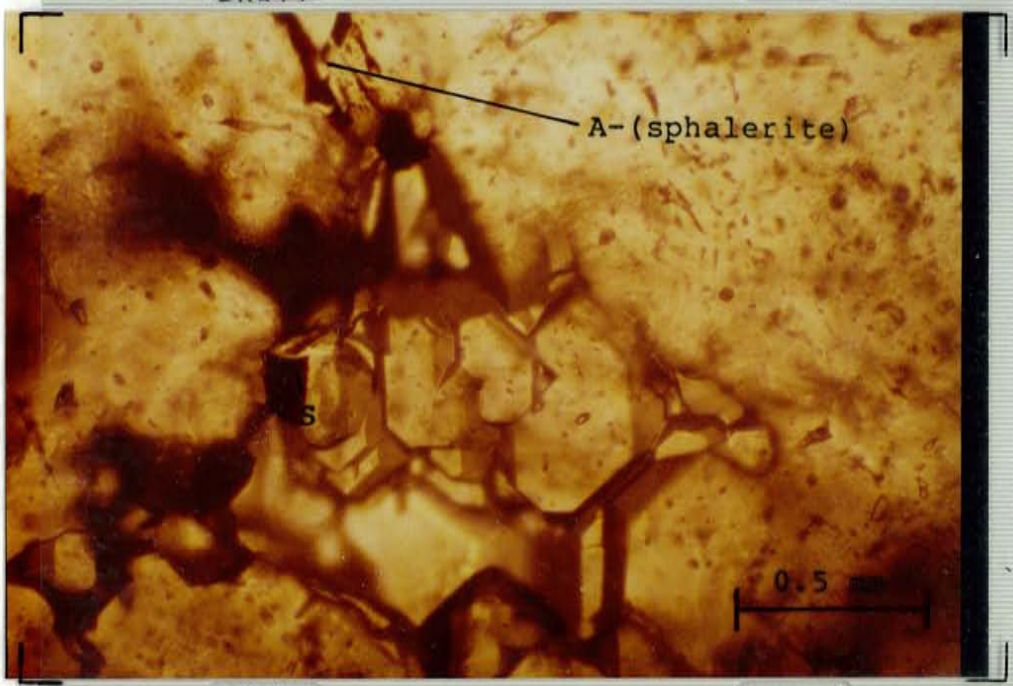

Figure 29. Miniature vug in a quartz crystal (110-35-24). Most inclusions are of an aqueous type in this photo.

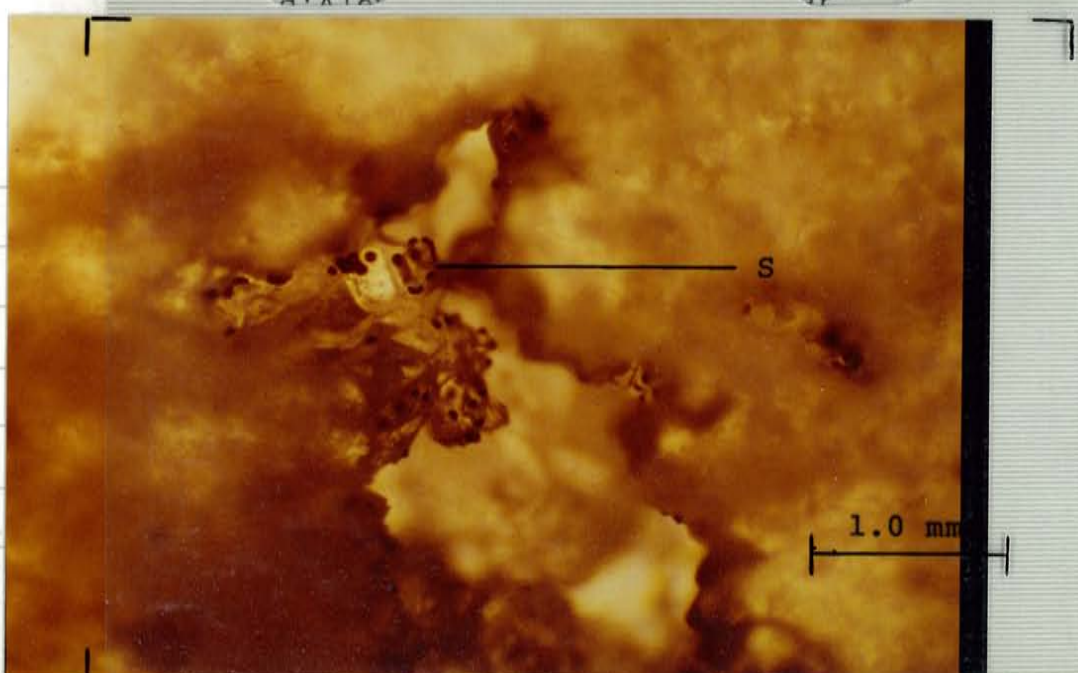

Figure 30. Sphalerite(?) on quartz within a vug in a crystal (110-35-24).

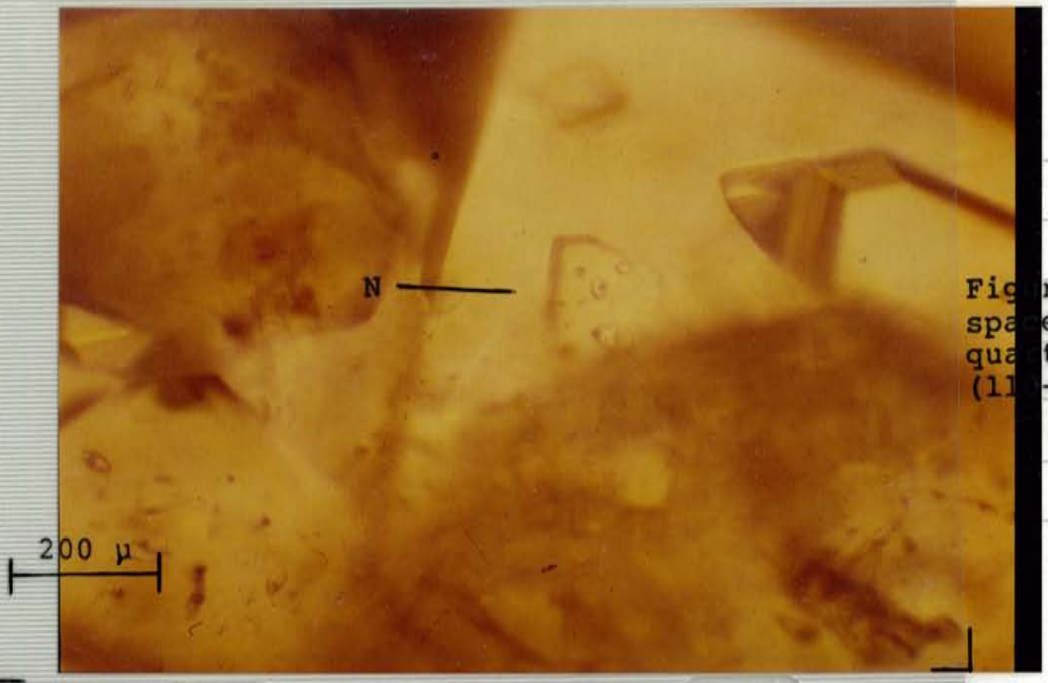

Figure 31. Open space within the quartz crystals (11[illegible]-35-24).

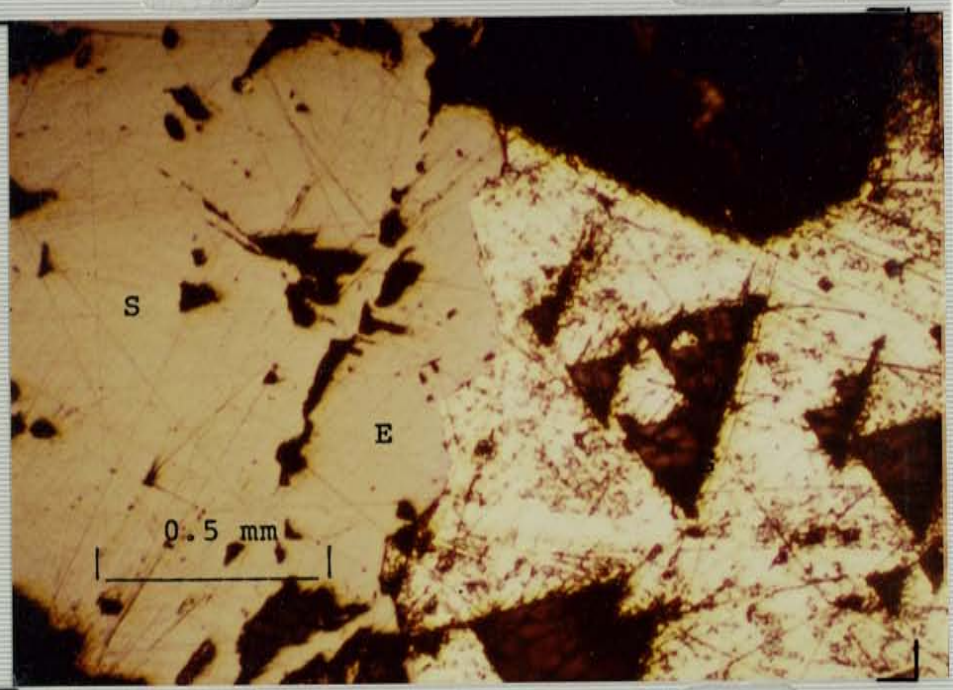

Figure 32. Mutually embaying grain boundary between galena and sphalerite (100-35-24), from euhedral crystal group within a vug in a milky quartz shear (fig. 22).

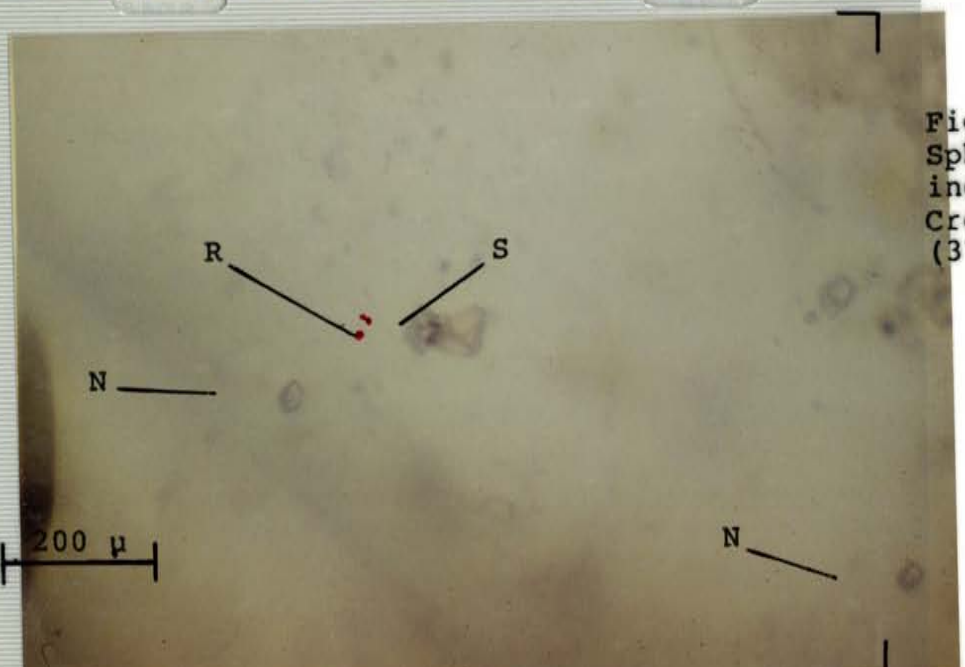

Figure 33. Sphalerite inclusion in Crescent quartz (37-11-9 Hook).

V::L ratios are also fairly uniform. Figure 30 is a photo of a miniature vug in a quartz sample. It shows euhhedral sphalerite deposited in open space upon quartz crystals. In summary, some open space was present at the microscopic level during mineralization.

Some textures may be misleading (fig. 32). Here the grain boundary 'E' between a euhedral sphalerite 'S' and galena 'G' crystal group mutually embays both minerals. Upon close examination, the grain boundary is seen to be composed of short linear segments which may be euhedral crystal faces. The lack of other evidence for replacement indicates that this crystal group may have formed in equilibrium and that the grain boundary may be a competitive growth front. Whether the boundary was formed by replacement or was codepositional in origin will indicate an important distinction in the interpretation of the mechanism of mineral deposition. It is very likely that many open space textures could be mis-interpretted as replacement textures both in the Coeur d'Alene district and in other deposits in general. Further textural studies are necessary to determine which interpretation is correct. Sulfur isotope studies of the sphalerite-galena pairs, should they be undertaken, could provide important temperature information for Bluebird mineralization.

In the case of the euhedral quartz from the Crescent-Hook vein (fig. 33), a solitary inclusion of sphalerite 'S' was observed. Dark "specks" 'R' may be ruby silver minerals. Note the presence of varying amounts of vapor in the fluid inclusions 'N'.

The euhedral crystals collected for study often show evidence that replacement occurred during mineralization. The replacement is not strictly volumetric and may not be produced by linked reactions. It might be better considered as a process of dissolution and deposition, occurring over both microscopic and megascopic intervals. Microscopic replacement intervals were observed in euhedral, clear quartz from vugs in the en echelon shears (fig. 34). It is important to note that replacement textures such as in this example were not present in most of the volume of the euhedral, clear quartz crystals. The width of the replacement intervals (intercapillary open space) in this sample is about equal to the width of the sphalerite inclusions 'X'. Fluid inclusion trails parallel to direction 'C' and spaced along the same intervals support this statement. The fluid inclusions in the trails parallel to the long axis of the replacement intervals are usually normal aqueous types 'B' with a vapor bubble but dense gaseous types are also present. In inclusions where fluids are trapped along with a replaced sphalerite remnent, the fluids observed were always of a dense-gaseous nature (fig.

Figure 34. Replacement "intervals" in euhedral quartz crystals (110-35-24 QSG).

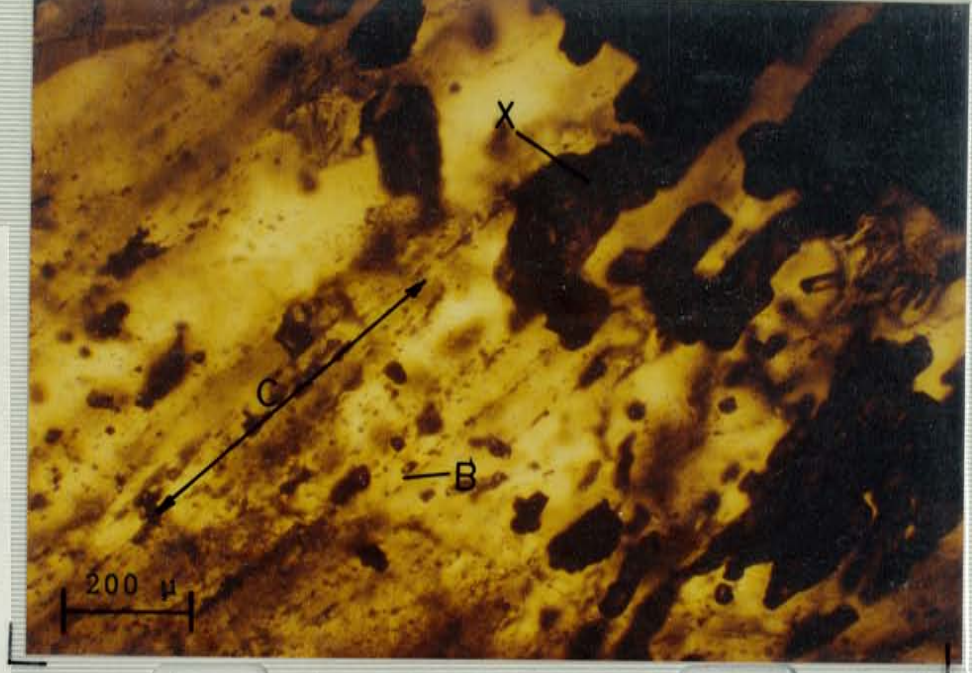

Replacement "intervals" in euhedral quartz crystals, perpendicular to direction 'C' (110-35-24 QSG).

Figure 35. Open space within the replacement "intervals" (110-35-24 QSG). Cross-polarized light.
See text page 50.

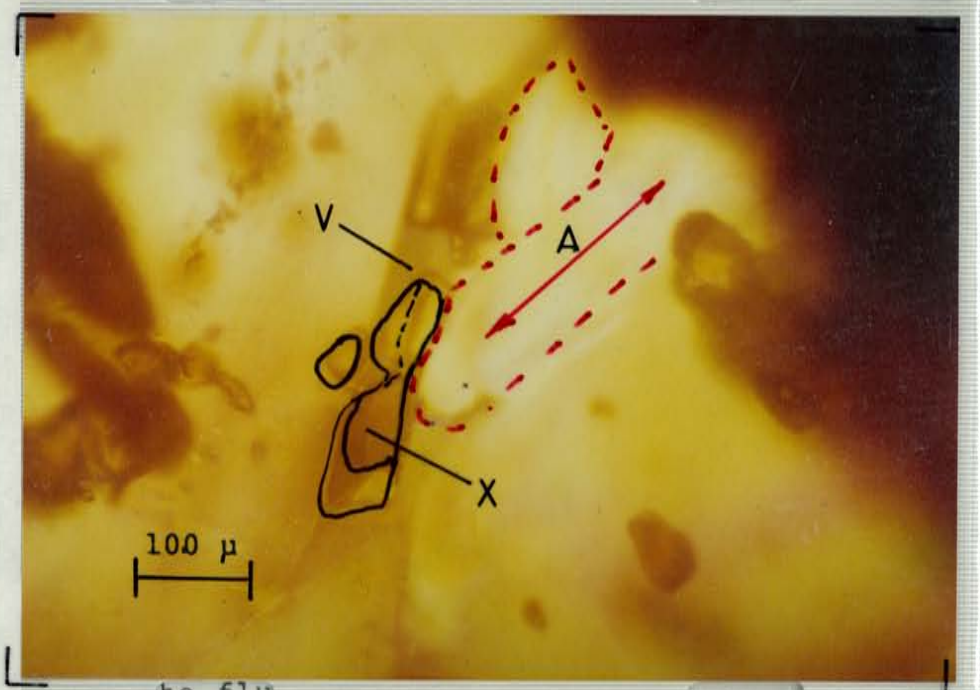

he flu

Figure 35 (photo 2). Same as previous photo but in unpolarized light.

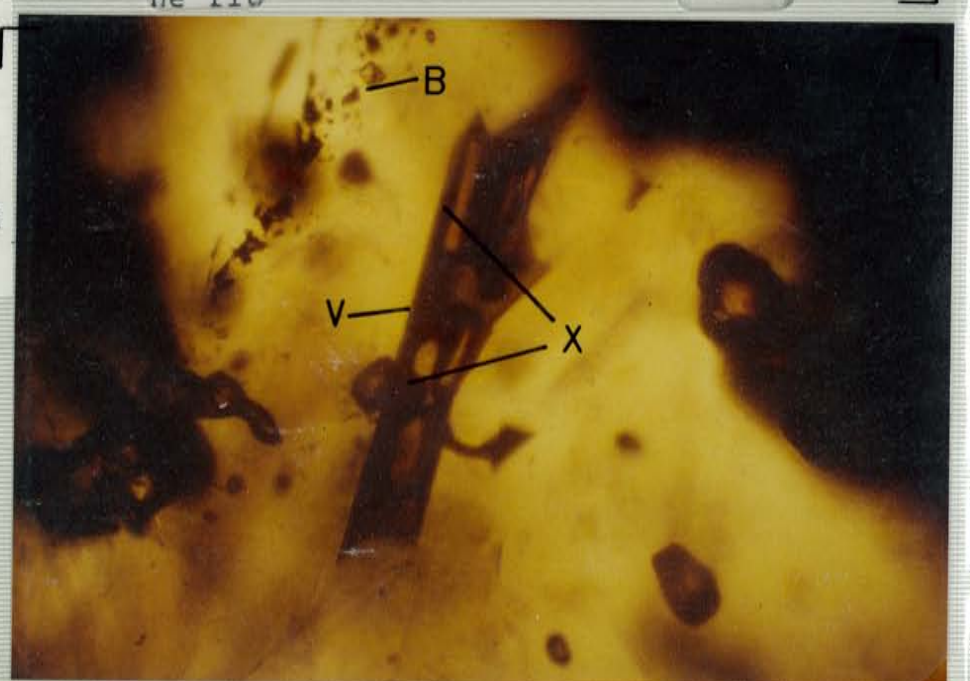

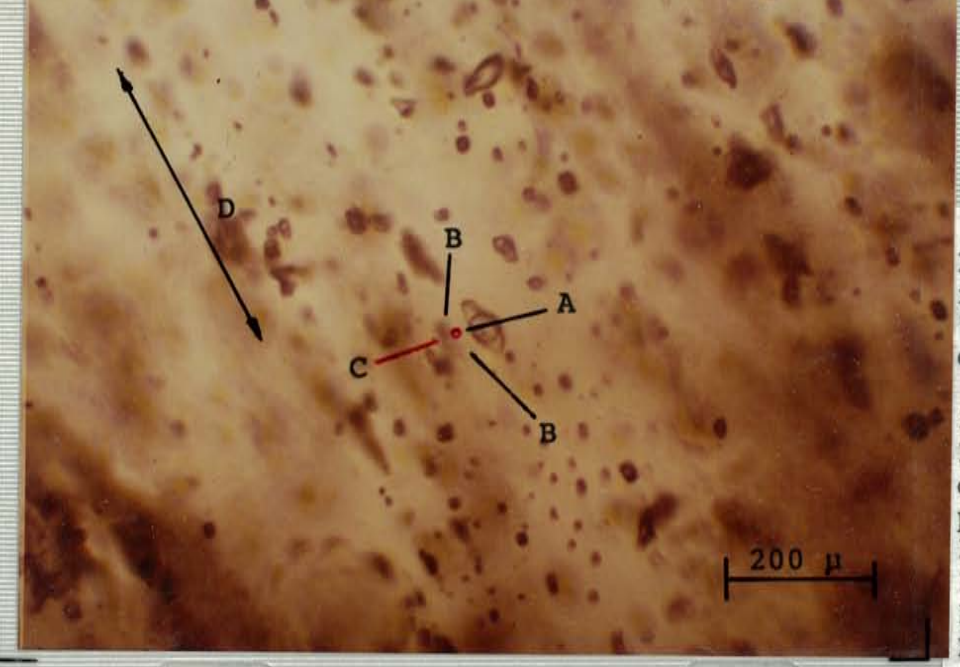

Figure 36. Inferred replacement "intervals" within euhedral quartz (Crescent Hook vein 37-11-9 East). Photo 1. T = +16.3 degrees C (See text pages 50, 57). Phase 'A'; liquid Phase 'B'; liquid(?) Phase 'C'; liquid(?) Direction 'D'.

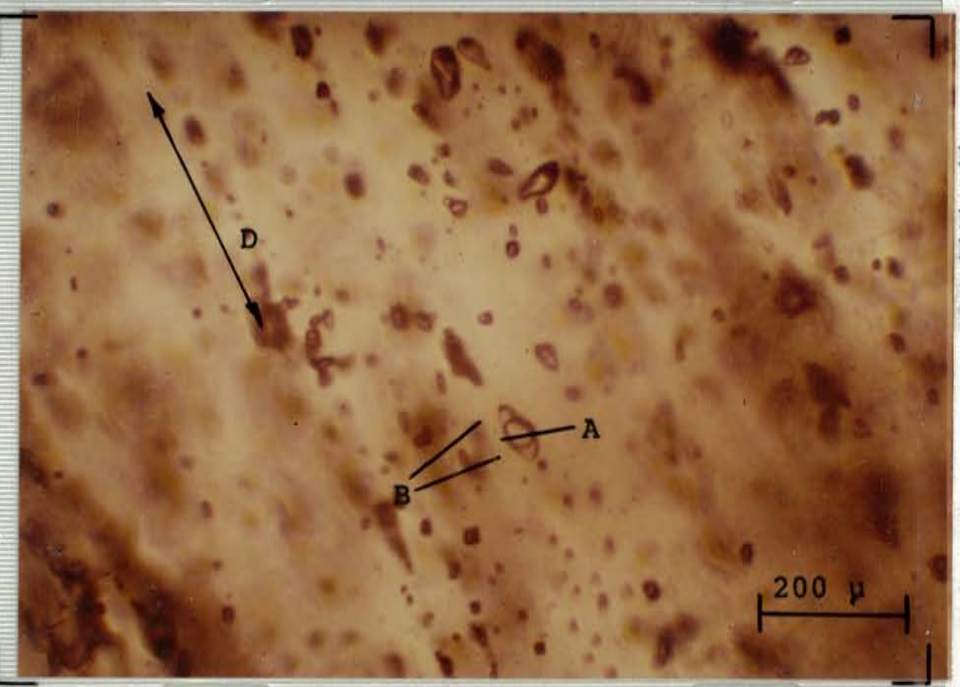

Figure 36 (photo 2). T = + 25 C. Note that phase 'C' has homogenized into phase 'A' T_h (C to A) = +20°C

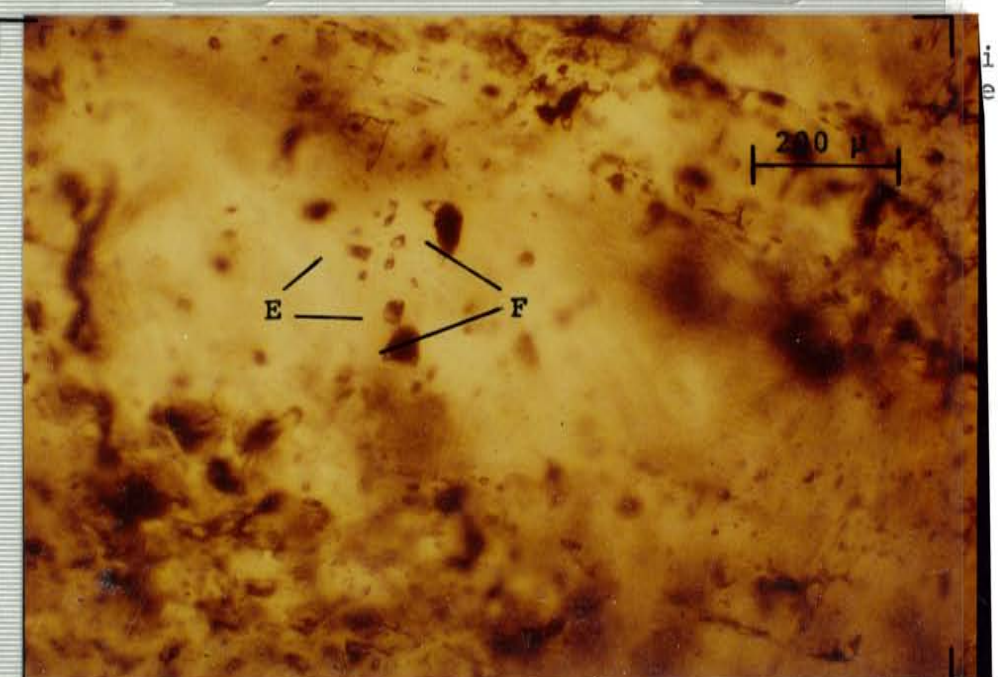

igure 37.
ee text page 50.

Figure 37.
See text page 50.

35). The sphalerite inclusions 'X' have rounded, anhedral dissolution boundaries which indicate that sphalerite recrystallization has not occurred within the dense gas phase 'V'. In cross-polarized light (photo 1 of fig. 35), it is apparent that some small quartz crystals 'A' and a small amount of open space were present during replacement. Aqueous inclusions 'B' indicate that quartz mineralization and sphalerite dissolution probably occurred during aqueous fluid passage through the intercapillary spaces.

The cloudy portions of the euhedral quartz crystals, generally from 10 to about 50 % of the crystal volume, often contain parallel rows of fluid inclusions (fig. 36). The texture of these inclusions in quartz closely resembles that of the quartz of figure 35 except that very few solid inclusions are present, therefore a replacement origin is likely for large parts of many of the euhedral quartz crystals even though they were found filling open space in vugs. The cloudy zones generally occur at the basal zones of the quartz crystals. The fluid inclusion rows 'D' contain both gaseous and aqueous inclusions.

Finally, much of the quartz contained fluid inclusions which showed no obvious textural pattern (fig. 37). The identification of primary vs secondary nature of these inclusions was uncertain and they were avoided during study to avoid ambiguous results. Note the presence of aqueous

inclusions 'E' near gaseous inclusions 'F', both still unfrozen at a temperature of -50°C (110-35-24 quartz). Group 'E' is planar and may have resulted from necking with group 'F'.

FLUID INCLUSION MICROTHERMOMETRY

Over 40 doubly polished thin plates were prepared from quartz, sphalerite, siderite and calcite from both the Bunker Hill and Crescent mines. Fluid inclusions were classified into four basic types at room temperature: type-1A, inclusions with less than 50 % vapor (L + V); type-1B, inclusions with more than 50 % vapor (L + V); type-1C, dry gaseous inclusions (V); type-2A, inclusions with at least two liquid phases and less than 50 % vapor (L'1 + L'2 + V). Type-1A was most commonly observed and is referred to as the normal-type inclusion for this study. Type-2A inclusions persist beyond 31^{o}C and should not be confused with liquid CO_2-bearing inclusions. No attempt has been made to distinguish, by creating a separate category, between inclusions which formed a liquid CO_2 phase during the freezing investigation from those that did not.

Daughter minerals were generally absent in the inclusions from Bluebird veins except as an occasional unidentified "speck". Samples from the 19'J' vein and Crescent-Hook vein, both quartz, frequently contained small orange-red "specks" in their inclusions which were barely visible. These "specks" did not homogenize and may be sulfides trapped during inclusion formation or metastable daughter sulfides. No salt daughter minerals were observed.

All data and discussions of data refer to primary inclusions unless otherwise indicated.

DATA

Melting temperatures of ice and the accompanying salinities in wt.% NaCl were obtained for 53 inclusions (fig. 38). All data fall within the range of 9.5 to 13 wt.% NaCl. The sample group for which the melting point of ice was observable is solely from Bluebird veins and includes 49 type-1A inclusions in quartz and 4 type-1A inclusions in sphalerite. The above salinities were obtained from measurements of the final disappearance of ice. In some cases it was possible to observe that the temperature of first-melting of the ice phase was below the NaCl-KCl-H_2O eutectic of -23°C indicating that significant $CaCl_2$ is present in the inclusion fluids. The exact temperature of first-melting couldn't be measured; however minimum first-melting temperatures of -35 to -25.5°C were obtained from inclusions in samples from both Link and Bluebird veins (data are in the appendix).

During the freezing investigations a number of unusual phenomena were observed. Gas-hydrates were detected in most samples although many individual inclusions did not necessarily form them. Decomposition temperatures for the gas-hydrates, when measureable, fell within the range of below zero to $^{+}11$ to $^{+}13$°C (fig. 39). When inclusions were

Figure 38. Histograms of salinity and homogenization temperature.

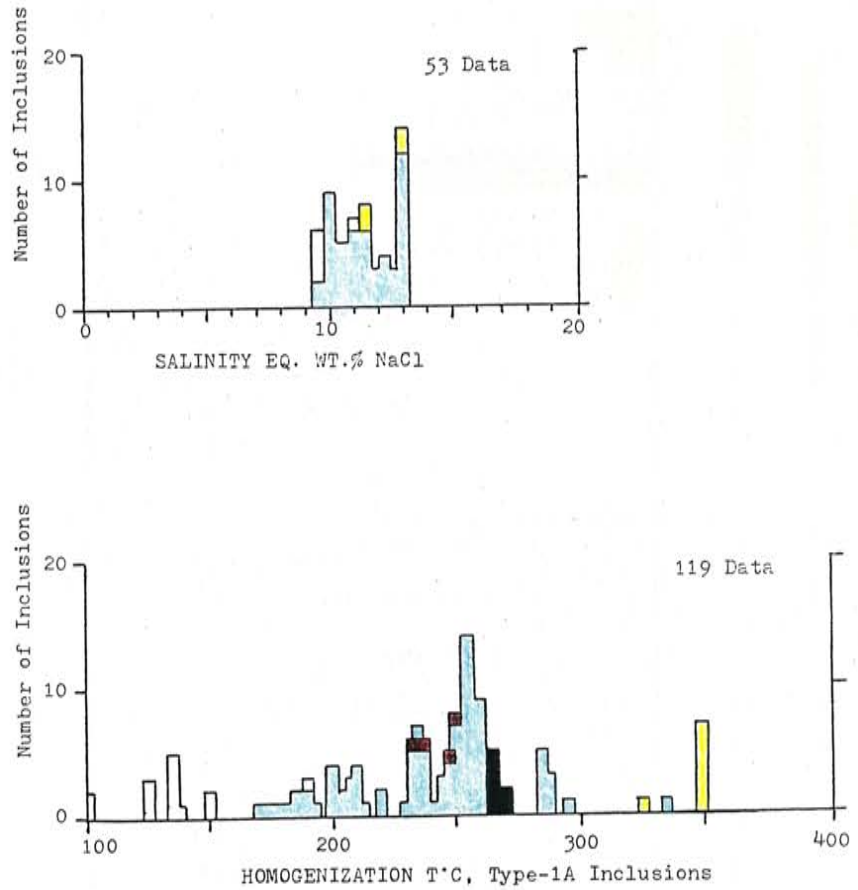

Bluebird quartz

Bluebird sphalerite

Link quartz

Crescent quartz

Secondary Inclusions in Bluebird quartz

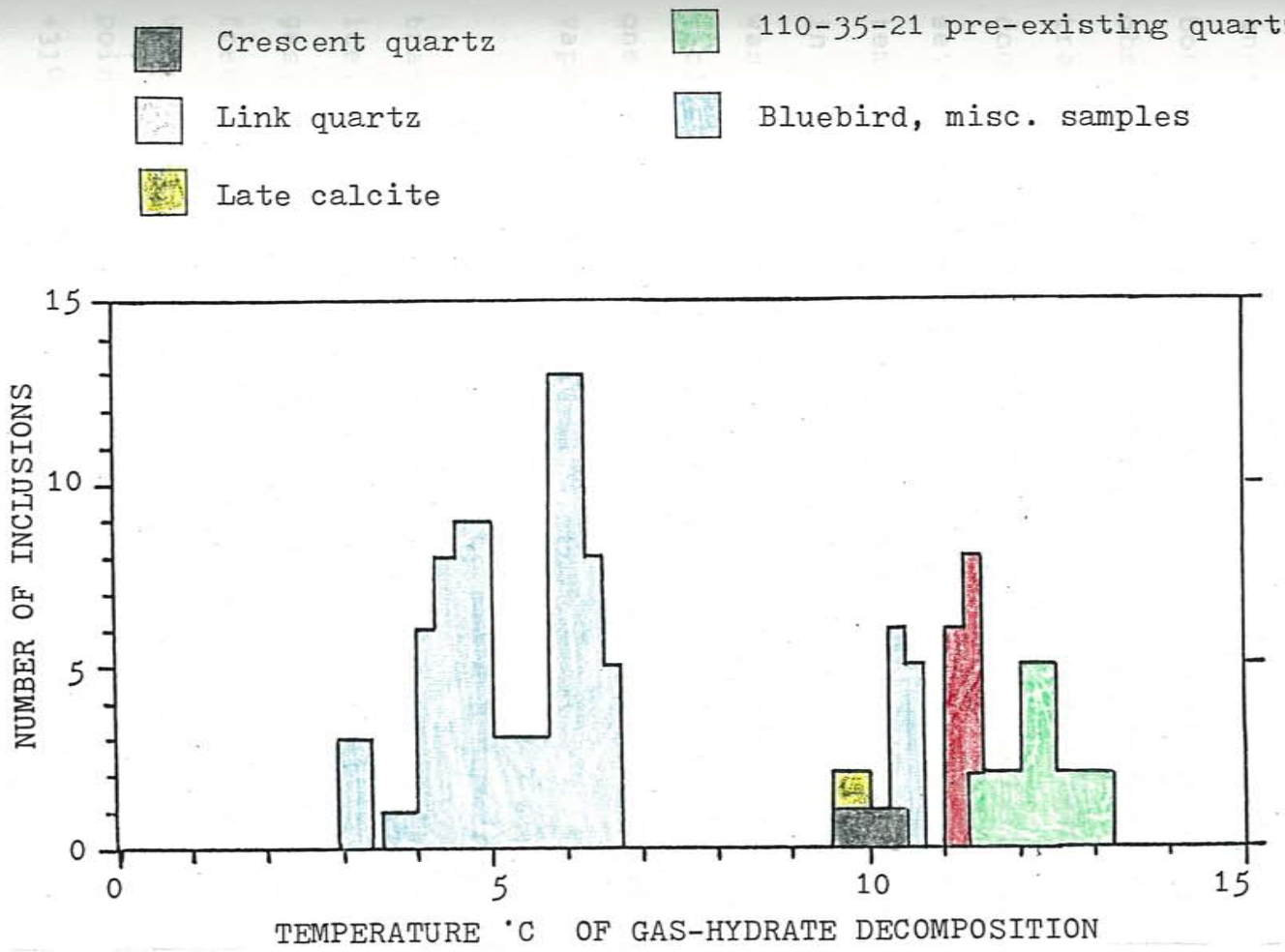

Figure 39. Gas-hydrate decomposition temperatures.
Sample data are in the appendix.

cooled to about -100°C and subsequently heated, no phase transitions were observable in the temperature range of -65 to -55°C during which nearly pure CO_2-solid would become unstable if it were present. At approximately -70°C the borders of an ice rim in a largely gaseous inclusion were observed to melt. This was the only low temperature phase transition observable even though several samples were cooled to about -120°C and allowed to equilibrate for several minutes before slowly heating. At these very low temperatures, two and sometimes three phases were observed in some inclusions. When multiple phases were observed one was a liquid and the others were a vapor and ice. Many inclusions did not completely freeze. Sometimes a rim of one phase 'B' was seen surrounding another phase 'A' with a vapor bubble 'V' (fig. 51, page 84).

At temperatures of -55 to +25°C a number of phase transitions were observable in addition to the melting of ice. Already mentioned was the decomposition of gas-hydrates. In addition to this, a liquid CO_2 phase was frequently observed. This phase was observed rimming the vapor-bubbles and would reach a maximum volume near the points of gas-hydrate decomposition. During slow heating to +31°C the liquid CO_2 phase would decrease in volume until its disappearance, generally below the CO_2 critical point of +31°C. The liquid CO_2 phase was seen to reach the critical point only in several inclusions in quartz from the

Crescent-Hook vein.

Upon close examination many of the "vapor" bubbles were seen to be composites of fluids and a vapor. Since these composite bubbles persisted beyond +31°C, liquid CO_2 is not responsible for this behaviour. Some "bubbles-within-bubbles" did homogenize below -31°C (i.e.; fig. 36). These may be CO_2 related phenomena but are different than the behaviour referred to above.

During heating from room temperature to homogenization, multiple phases were also observable. At room temperature it could be seen that variable amounts of the vapor phase were present in the various inclusions within any sample. Gaseous inclusions and inclusions with from 50 to 5% vapor were observed. Most inclusions however, contained 25-10% vapor or were of a type difficult to see into and probably of a dense, gaseous nature. Most observed homogenizations were of the normal liquid type (i.e.; all data in fig. 38), but some gaseous homogenizations were also noted. The homogenization temperatures of the normal type-1A inclusions did not correspond with that of the gaseous homogenizations within the 110-35-24 quartz sample containing both type-1A and type-1B inclusions. The type-1A inclusion fluids had T_h's of 265 to 230°C while the type-1B inclusions had fluids homogenizing to the gaseous phase between 340 and 326°C (at least 4 which were remeasured to be sure that the inclusions

did not decrepitate; a slight rim of liquid remained in each of these indicating that they are not true gaseous homogenizations). From figure 38 it can be seen that the sphalerite sample from the 14 Brown gave the highest T_h's (six inclusions of type-1A, having T_h's of 352 to 345°C to the liquid phase), while the bulk of the other samples had inclusions homogenizing between 270 to 230°C (all to the liquid phase; type-1A inclusions in quartz). All T_h's were remeasured. Decrepitations below the temperature of homogenization were frequently encountered and indicate high internal pressures within the inclusions. Most decrepitation within 110-35-24 quartz occured at about 250°C while decrepitation in various sphalerite samples occured over a broad temperature range.

A type of multiple phase behaviour was observed in samples from all of the orebodies. This behaviour consisted of the formation of a second fluid phase about the perimeter of many of the type-1A inclusions as they were heated (fig. 40). The second phase was too visible to ignore at temperatures of about 175°C (fig. 55, page 95) and increased in volume to the temperature of homogenization of the vapor phase, at which point it becomes difficult to observe. The observation of the two fluid phases was generally limited to temperatures below the vapor-bubble T_h.

Figure 40. Two types of liquid immiscibility observed during microthermometry.

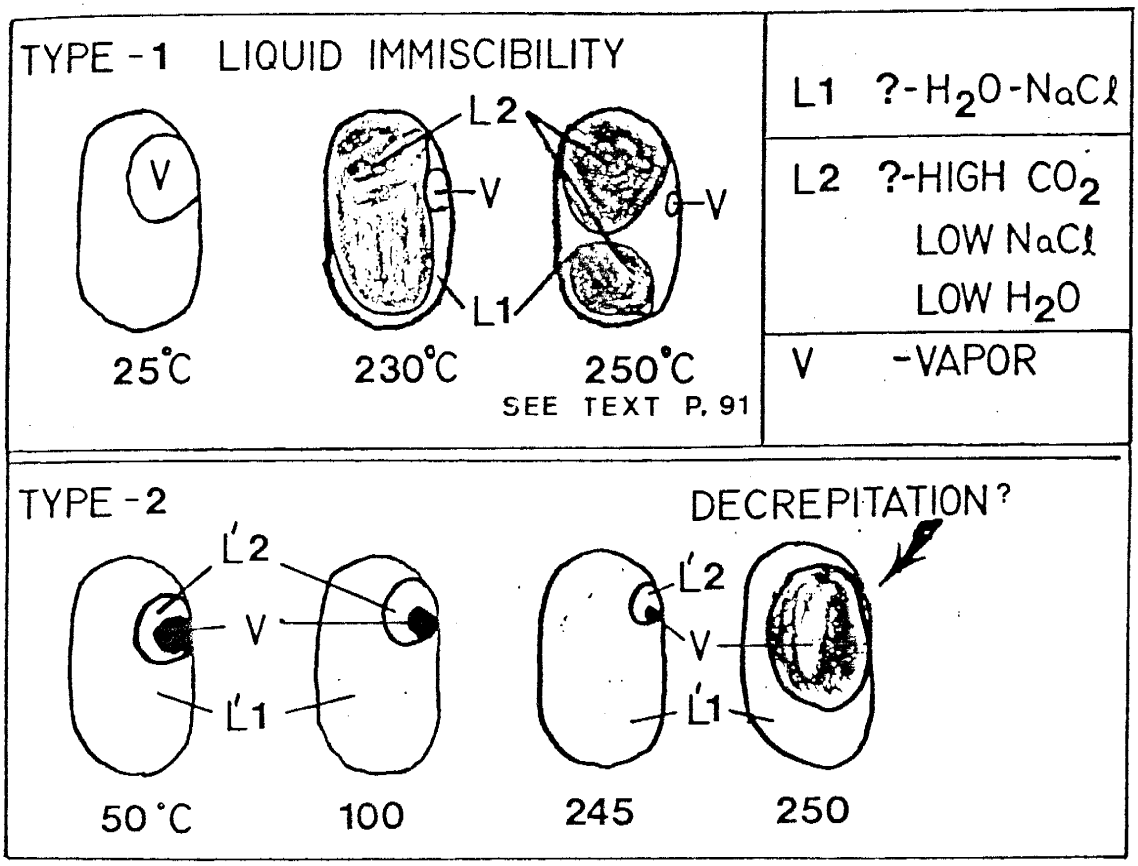

Type-1C inclusions sometimes developed a fluid phase upon heating (i.e.; fig. 56, page 95). Development of the fluid phase occured between 30 and 60°C and reached a maximum volume-percent in the 14 Brown quartz at 140°C. These inclusions had a T_h of 161°C into the gaseous phase. This behaviour was repeatable after cooling.

GAS ANALYSES

Fluid inclusions in quartz, sphalerite, galena and siderite were thermally decrepitated and the resulting gases analyzed on a quadrupole type mass spectrometer. Tables 1 thru 4 of the appendix contain the results of the analyses. A description of the analytical procedures is also included.

Samples were generally heated to 550°C and the resulting gases considered characteristic for the analysis. Upon step-heating the samples it was found that the analyses differed with temperature of fluid inclusion decrepitation (T_d). The data will be presented with the results of the characteristic analyses first and then that of step-heating.

DATA

A high fraction of gases is present in all analyses (fig. 41; Table 1 data range from 90 to 2.4 wt.% gases). Measurements indicate a minimum of 1.27 mole % to over 10 mole % gases were present in the inclusion fluids (appendix Table 4, T_d = 550°C). The principle gases measured in order of relative concentration were CO_2 and N_2, and organics (C_nH_n). Present in lesser quantities were H_2, H_2S, SO_2 and Ar.

Figure 41. Reproduction of Table 1 in the appendix: Gas Analyses

Sample Number	H_2O	N_2	CO_2	CH_4	C_2H_n	C_3H_n	H_2S	SO_2	Ar	Notes
Runs 328-329	79.6	06.9	89.3	0.23	1.75	1.49	0.07	0.21	0.04	550°C Hook Vien,
41-11-7E Qtz		10.3	84.9	0.61	2.44	1.42	0.09	0.14	0.04	Crescent Mine
330-331	?	23.6	71.8	0.51	2.32	1.47	0.05	0.18	0.07	750°C same sample
		32.2	62.2	1.22	2.95	1.28	0.05	0.11	0.07	stepwise temp.
Runs 345-346	12.1	0.90	98.0	.004	1.01	----	.015	0.02	.003	400°C Hook Vien,
41-11-7E Sid		1.40	97.1	0.01	1.47		0.02	.015	.004	Crescent Mine
Runs 306-307	86.8	12.9	85.9	?	?	?	0.06	0.21	0.37	550°C
19'J' Qtz		18.8	79.6				0.08	0.13	0.37	pre-existing xl
Runs 320-321	88.3	12.5	82.5	0.41	2.03	1.97	0.05	0.50	0.05	490°C part of
19'J' Qtz		18.0	76.0	1.03	2.73	1.81	0.06	0.32	0.05	same xl
326-327	?	17.3	32.6	2.71	8.88	3.95	0.95	33.6	0.11	750°C same sample
		25.0	30.0	6.85	12.0	3.64	1.14	21.3	0.11	stepwise temp.
Runs 351-352	96.7	14.7	68.1	0.19	3.36	4.31	0.72	8.27	0.16	400°C
25 Francis Sph		21.4	63.0	0.50	4.83	4.00	0.87	5.26	0.17	
Runs 359-360	81.2*	17.5	52.5	0.68	8.85	19.9	0.03	0.39	0.22	550°C pre-min.
9 Jersy Milky Qtz		23.9	45.5	1.63	11.3	17.2	0.03	0.24	0.21	
Runs 361-362	15.3*	11.6	30.8	0.42	19.7	26.6	0.89	9.84	0.21	750°C same sample
		16.0	27.1	1.01	25.4	23.4	1.01	5.95	0.20	stepwise temp.

Sample Number	H_2O	N_2	CO_2	CH_4	C_2H_n	C_3H_n	H_2S	SO_2	Ar	Notes
Runs 335-336	83.8	21.4	55.3	3.36	8.91	6.89	0.88	3.12	0.12	550°C
110-35-21 Qtz		27.6	45.5	7.60	10.6	5.67	0.94	1.77	0.11	pre-existing xl
Runs 304-305	lost	19.9	51.0	1.29	3.90	7.55	0.21	15.1	.029	NO = 1.04 wt %
12-35-21 Qtz		28.0	45.8	3.20	5.14	6.80	0.25	9.36	.028	T = 550°C, smokey vien Qtz ass/w deconsolidation
Runs 233-234	97.6	37.3	54.7	5.04	0.99	1.58	0.12	0.14	0.12	550°C Main Stage
10-35-24 Qtz		44.9	41.9	10.6	1.11	1.21	0.12	.074	.098	Bluebird Vien
Runs 363-364	27.9*	21.2	50.2	1.88	8.78	15.2	.169	2.42	0.14	750°C 7-15-81B
10-35-24 Qtz		28.1	42.2	4.34	10.8	12.8	.184	1.40	.129	
Runs 347-348	lost	26.2	56.8	0.35	6.12	6.63	0.25	3.72	----	400°C
10-35-24 Sph C		35.0	48.4	0.82	7.65	5.65	0.28	2.18		
Runs 349-350	5.66*	0.39	75.6	.013	4.55	4.49	0.42	14.5	.002	400°C
10-35-24 Gal										Pcm nc= 0.000*
Runs 222-223	97.0	36.2	57.8	1.01	0.67	2.59	.145	1.21	0.42	500°C
11-35-24 Qtz		46.5	47.2	2.26	0.80	2.11	0.15	0.69	0.38	
Runs 230-231	? *	25.4	71.9	.072	0.33	1.30	0.37	0.27	0.32	550°C
11-35-24 Qtz										
Runs 256-257	lost									

Figure 41. Reproduction of Table 1 in the appendix: Gas Analyses

Sample Number	H_2O	N_2	CO_2	CH_4	C_2H_n	C_3H_n	H_2S	SO_2	Ar	Notes
Runs 260-261	95.0	33.6	42.5	0.84	5.22	15.8	0.44	1.30	0.31	550°C
11-35-24 Qtz		43.0	34.6	1.89	6.23	12.9	0.47	0.73	0.28	
Runs 353-354	97.5	34.6	52.0	0.99	3.53	8.30	.031	0.18	0.36	300°C
11-35-24 GA Qtz		44.1	42.3	2.21	4.20	6.74	.033	0.10	0.32	
Runs 355-356	67.4*	15.0	72.4	6.18	2.88	3.38	.020	0.10	----	500°C same sample
		19.5	60.0	14.1	3.49	2.80	.021	.059		NC peaks off-cen.
Runs 357-358	8.17*	15.7	78.6	0.40	2.46	2.70	.027	0.11	0.05	750°C same sample
		22.2	70.9	0.98	3.26	2.44	.031	.070	0.05	stepwise temp.
Runs 336-337										
Runs 312-313	43.4	75.0	22.4	0.32	0.43	1.30	.018	.035	0.19	540°C, NO = 0.33
11-35-21		82.0	15.6	0.61	0.44	0.90	.016	.017	0.15	Milky Qtz
Runs 343-344	36.3*	49.7	24.5	6.36	7.36	9.42	.033	2.19	0.47	750°C Milky Qtz,
110-35-21A		54.8	17.2	12.3	7.58	6.62	.030	1.06	0.37	pre-reverse shear
Runs 341-342	74.9	59.3	28.9	9.88	0.56	1.05	.013	0.16	0.18	550°C same sample
		61.5	19.1	18.0	0.54	0.70	.011	.072	0.13	stepwise temp.
Runs 316-317	lost	43.2	40.3	1.45	8.97	5.26	.075	0.56	0.21	380°C
14 Brown Sph		51.7	30.7	3.04	10.0	4.00	.074	0.30	0.17	

Sample Number	H_2O	N_2	CO_2	CH_4	C_2H_n	C_3H_n	H_2S	SO_2	Ar	Notes
Runs 238-239	lost	35.6	60.9	2.30	----	----	.038	.064	1.09	550°C single xl
14 Brown Qtz		45.0	48.9	5.09			.040	.035	0.96	
Runs 337-338	95.0	18.5	77.2	0.72	1.40	2.03	.008	.060	.060	550°C
14 Brown Qtz B		25.8	68.7	1.77	1.82	1.80	.009	.037	.059	
Runs 339-340	39.3*	24.9	63.2	1.05	4.76	5.63	.032	0.17	0.21	750°C same sample
		33.1	53.5	2.43	5.90	4.76	.035	0.10	0.20	stepwise temp.
Runs 365-366	57.1*	17.7	71.0	0.28	3.91	6.08	.038	0.72	0.22	400°C
14 Brown Qtz		24.8	63.3	0.69	5.11	5.42	.044	0.44	0.21	
Runs 367-368	1.42*	6.41	89.3	0.31	1.45	2.44	----	0.11	----	550°C same sample
		9.61	85.2	0.81	2.02	2.33		0.07		stepwise temp.
Runs 369-370	30.8*	20.7	23.5	1.03	19.3	34.4	0.17	0.77	.094	750°C same sample
		26.6	19.2	2.32	23.1	28.1	0.18	0.43	.084	stepwise temp.

The data indicate that N_2::CO_2 decreased with time. Pre-mineralization quartz had a N_2::CO_2 greater than 3::1, Bluebird-vein quartz and sphalerite 1::1 to 1::3, Link-vein quartz 5::6 to 1::4, and Crescent-vein quartz 1::2 to 1::8, the lowest ratios observed (mole %).

The total organic gas content of the inclusions is variable and shows no difference with respect to paragenesis or individual sample (T_d = 550°C, characteristic analyses). The relative abundance of individual organic species however, varies with sample location and type (fig. 42). Samples associated with mineralization plot in a similar area of CH_4-C_2H_n-C_3H_n triangular space. Samples from pre-mineralization quartz and most Bluebird quartz samples plot outside this space (T_d = 550°C). At least some of the Bluebird quartz samples are thought to represent a time of sphalerite remobilization (by replacement textures).

The H_2S content of the inclusion fluids is variable and shows no systematic trends with respect to vein paragenesis (T_d = 550°C characteristic analyses). Pre-mineralization quartz does however, have the lowest H_2S content of the veins with 0.01 to 0.016 mole % if only the gas fraction (no water) is looked at. Bluebird quartz showed about 0.1 mole % H_2S in its gas fraction, Link quartz about 0.07 mole % and Crescent quartz about 0.09 mole % (T_d = 550°C).

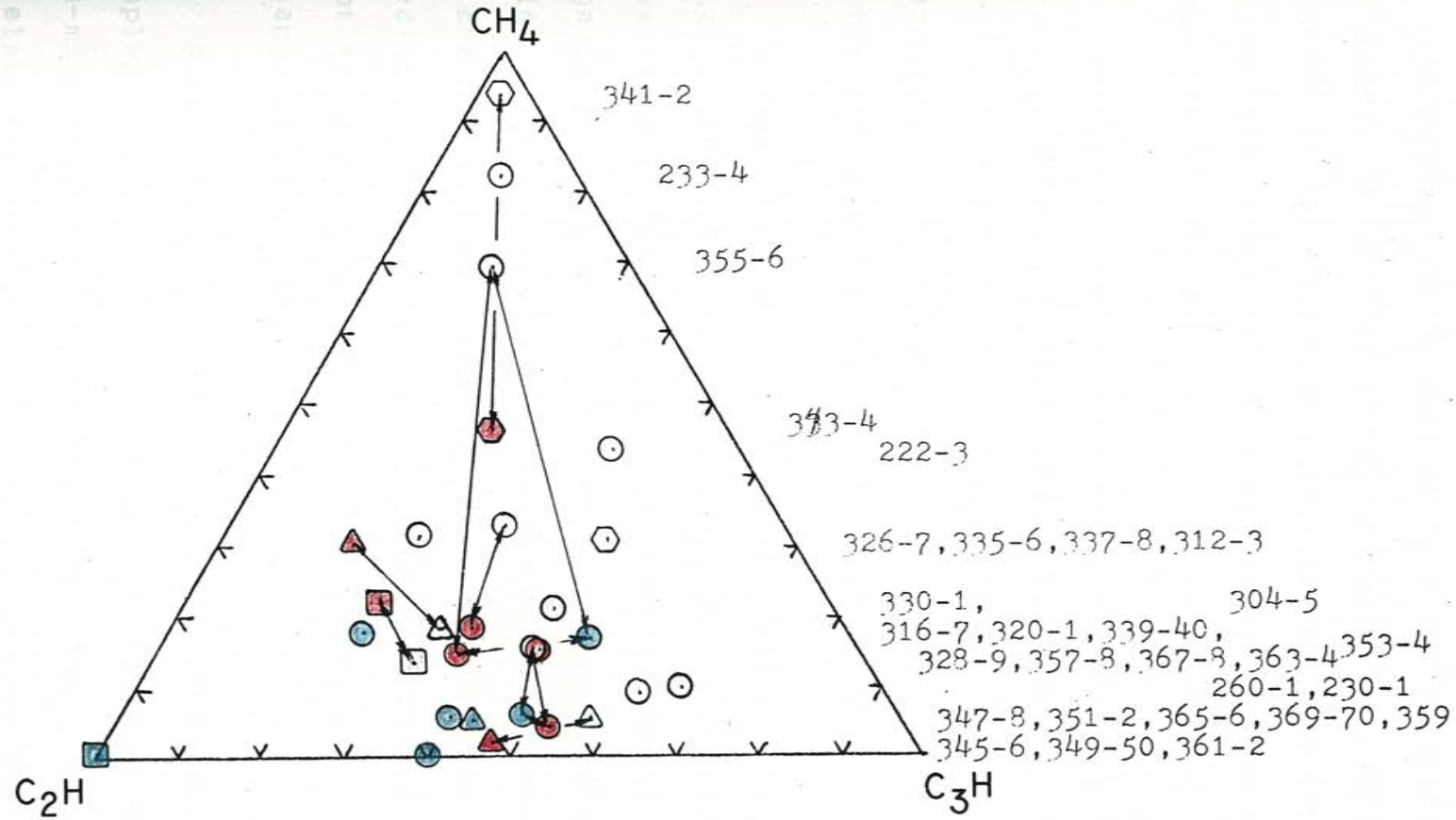

Figure 42. The variation in organic species as a function of sample and temperature of decrepitation. This diagram shows a C2Hn polarity for 'mineralization-associated samples'.

In summary of the data at T_d = 550°C (characteristic analyses), an increase in CO_2::N_2 with vein paragenetic sequence is the only significant trend. Samples decrepitated stepwise with temperature yielded different compositions, the observations of which follow:

Samples decrepitated at the first step in temperature- generally less than 550°C, showed 1.27 to over 10 mole % gases. Inclusion fluids decrepitated at the high temperature step- in the interval of +550 to 750°C, showed higher gas contents, to over 90 wt.% gases.

Compositionally, the 750°C step was most often N_2 rich, total organic rich (C_nH_n), and H_2S rich compared to the lower temperature step (s). The combination of N_2 and total organic increase with T_d can best be seen in diagram form (fig. 43), the red samples being the 750°C runs. The 750°C Td steps also show a similar relative abundance of organic species with the samples associated with mineralization and plot in or trend towards that area of CH_4-C_2H_n-C_3H_n triangular space (fig. 42).

A correlation exists in H_2S::C_nH_n in stepwise T_d samples in pre-mineralization quartz, Bluebird quartz and non-mineralization Link quartz (fig. 44). In these samples a relatively constant H_2S::C_nH_n exists even though the mole % H_2S and C_nH_n vary by large amounts between the different T_d steps. No such correlation exists in the Link and

Figure 43. The variation in total organics-CO_2-N_2 as a function of sample and decrepitation temperature.

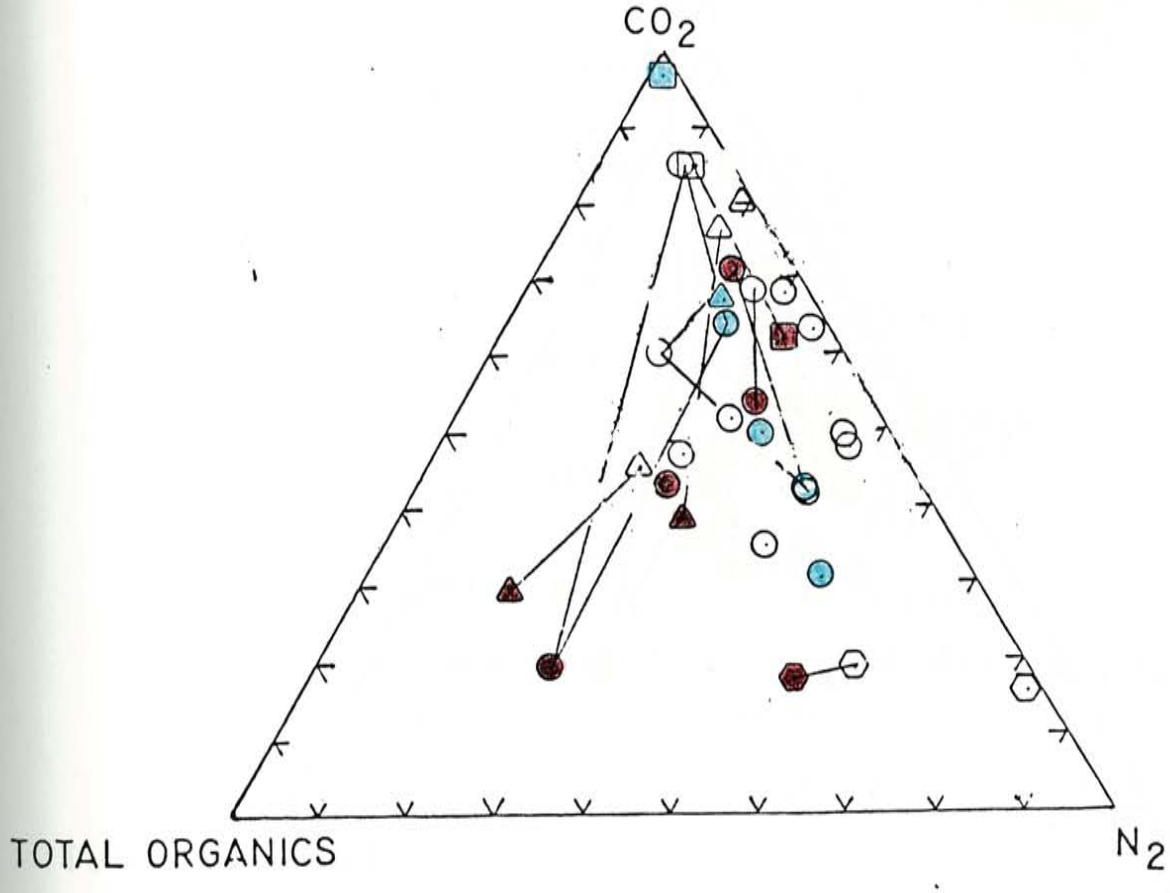

Figure 43. The variation in total organics-CO_2-N_2 as a function of sample and decrepitation temperature.

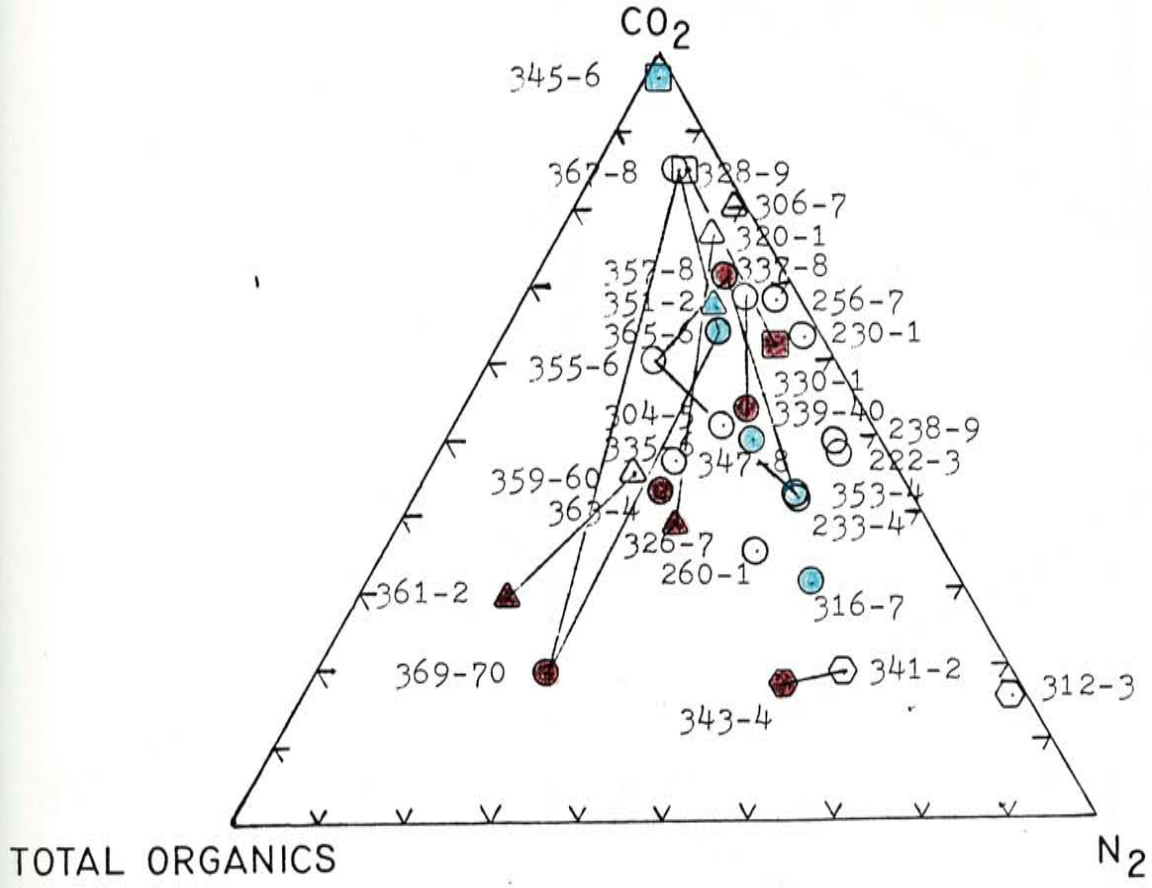

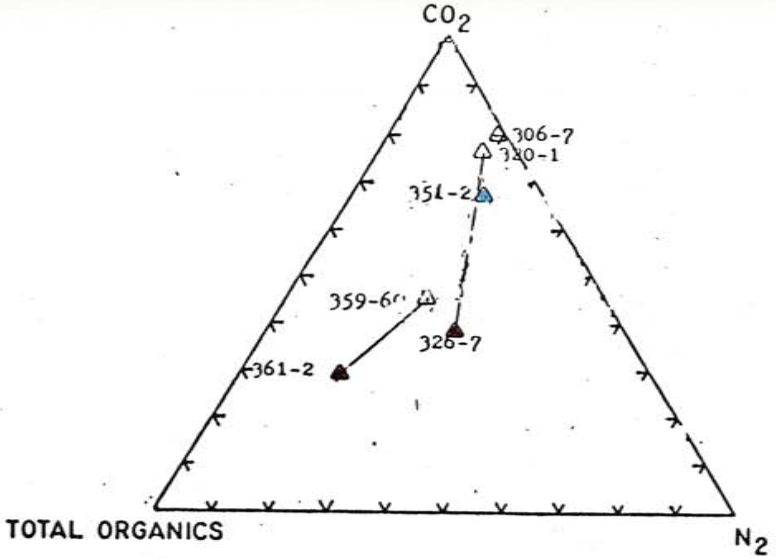
CO2
306-7
330-1
351-2
359-60
326-7
361-2
TOTAL ORGANICS
N2

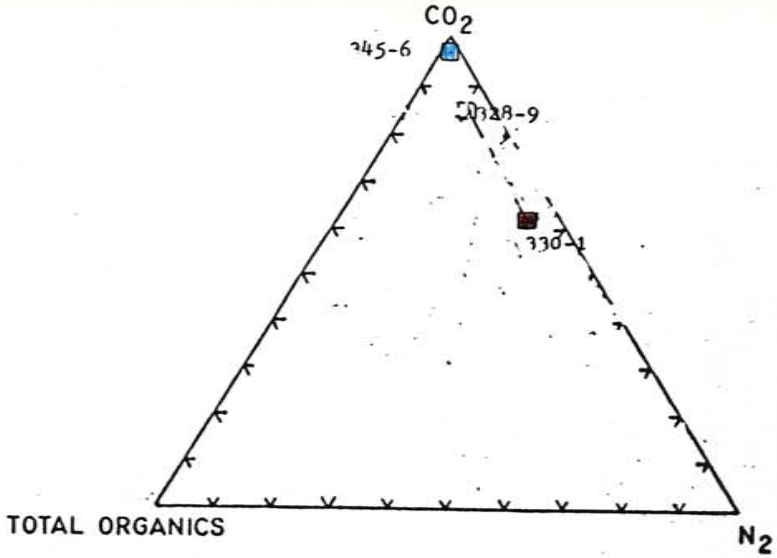
CO2
345-6
328-9
330-1
TOTAL ORGANICS
N2

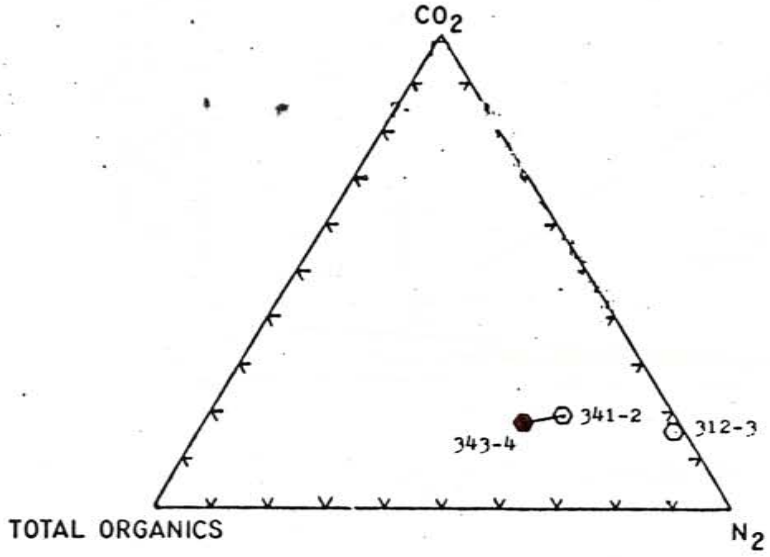
CO2
341-2
312-3
343-4
TOTAL ORGANICS
N2

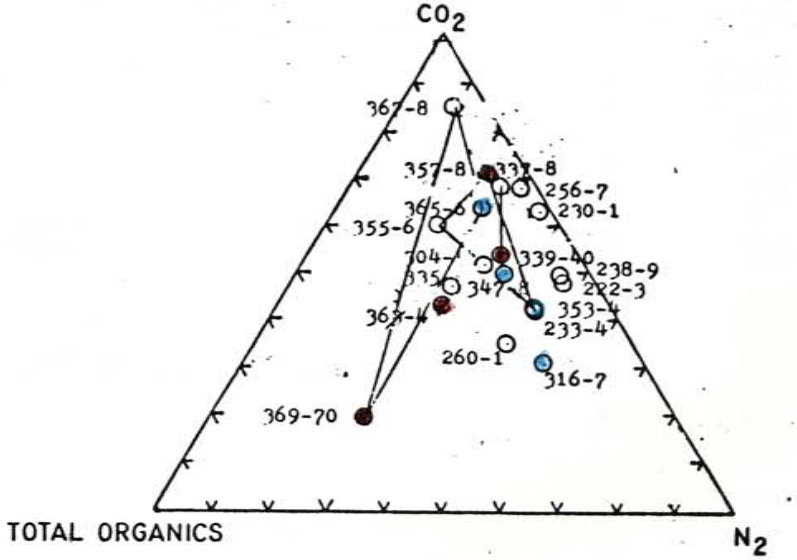
CO2
367-8
357-8
337-8
256-7
230-1
355-6
339-40
238-9
222-3
353-4
233-4
260-1
316-7
369-70
TOTAL ORGANICS
N2

Figure 44. The variation in H_2S with organics. Low slopes indicate relatively constant ratios of H_2S::organic components, even though both values vary in mole percent by large amounts within different inclusions.

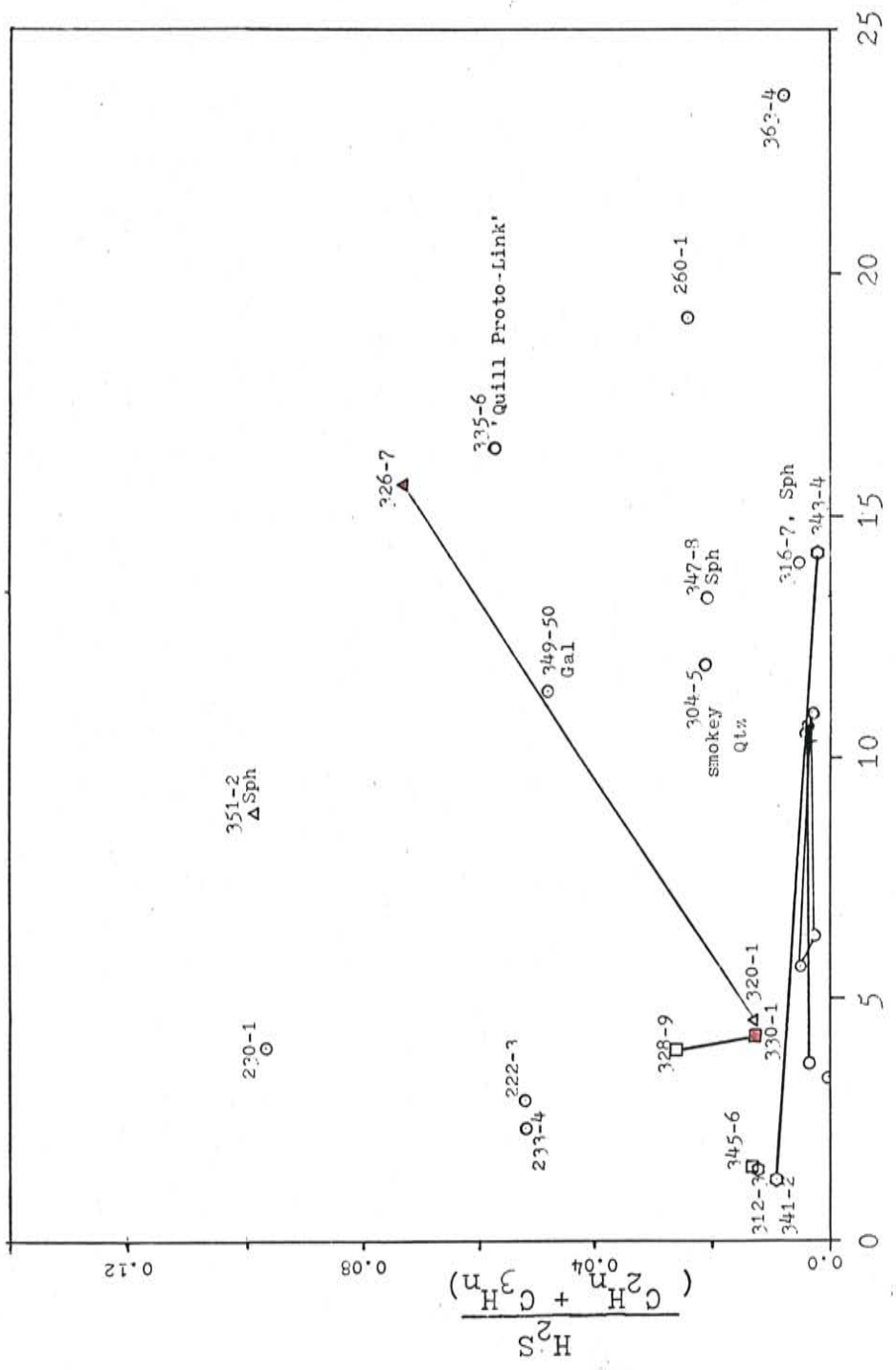

Crescent quartz inclusion fluids. A large scatter in the data of samples measured at a T_d of 550°C indicate that this correlation is inconsistent.

FLUID INCLUSION LEACHATES- DATA

Eight samples and sixteen blanks and standard solutions were analyzed for Na^{+}, Ca^{2+}, K^{+}, Mg^{2+}, Mn^{2+}, Fe^{2+}, Zn^{2+}, Cd^{2+}, Ag^{2+}, Pb^{2+}, Cu^{2+}, As^{2-}, $SO4^{2-}$ and Cl^{-} (appendix Table 5). Because of sample size requirements only Bluebird vein quartz and sphalerite and pre-reverse shear milky quartz were analyzed for their inclusion-water trace elements. Blanks number 1 thru 14 were run before any samples in case of possible contamination problems. After eliminating the identified contamination sources, quartz-rod blanks 16 and 20 were run. These two blanks represent the background levels of contamination present in the Bluebird-vein and pre-reverse shear analyses.

The major cations observed in the analyses are Ca, Na and K, in the order listed. Calcium occurs in concentrations roughly equal, to triple that of sodium, while potassium occurs in concentrations of about two-thirds to less than half that of sodium. Only in the pre-reverse shear milky quartz are the cation ratios different, where K is about equal to Ca, with half as much Na.

Of the other cations analyzed, Mg and Pb are definitely present. Magnesium is present in trace quantities to a significant fraction of the total cations. The determination of the exact levels of concentration is not possible because of the nearness to the background

(generally half to a third of the analyzed Mg values). In the case of Pb, however, the background levels are often well below the analyzed values of the samples. In some cases Pb is present in concentrations as high as 10 % of the Ca ion concentration (runs 17 and 19). More generally, Pb was present in trace quantities as evidenced in the rest of the sample analyses.

High levels of Mn and Fe were detected in some samples, but whether or not these levels are due to contamination by impurities in the samples must be considered. In the case of Mn both sphalerite runs showed very high concentrations while the quartz runs showed concentrations an order of magnitude lower. Sphalerite run 24, which was leached with dilute acid, showed Mn levels six times as high as run 15- which was leached with water only. This indicates that the Mn was present in the sphalerite crystal lattice and not in the fluid inclusion waters (in high concentrations). Since the Mn is apparently easily dissolved by acidic solutions, the other trace levels of concentration observed in quartz may be due to minute sphalerite impurities. The high Fe concentrations present in runs 19, 23 and 24 may be due to siderite inclusions, which were sometimes observed as impurities during microscopic investigations.

The backgrounds of Zn and Cu were too high to obtain any data from the samples (backgrounds from runs 16 and 20). This may also be the case for Cd (run 16). In the analyses for Ag, no detectable concentrations were observed.

Of the anions, Cl^- is the dominant species with only trace levels of SO4 and As. Only one sample, run 19, showed sulfate levels significantly above background (about 5 times the background). Four runs; 17, 18, 21 and 23, showed trace levels of As. Chlorine levels were highest in the pre-reverse shear milky quartz. The Bluebird-vein analyses showed levels of about 1/4 to 1/5 of the Cl levels in the pre-reverse shear quartz.

DISCUSSION: FREEZING DATA AND SALINITY

The freezing point depressions of water-ice and inferred salinities of 53 Bluebird vein inclusions all fall within a tight range of 9.5 to 13 wt.% NaCl (fig. 38, page 54). The presence of significant $CaCl_2$ is noted but should not cause more than +1 wt.% salinity error as the freezing point depression curves for NaCl and $CaCl_2$ are nearly coincident in the region of interest (Hollister, Crawford 1981, p. 88-90 and fig. 4-7).

All of the inclusions yielding salinities were from Bluebird veins. Crescent and Link vein quartz samples were studied under the same freezing conditions as the Bluebird vein samples but ice melting points could not be observed, hence no salinities. It is believed that the principle reason why no salinity data was obtainable in the Crescent and Link veins is due to the high gas content of their fluid inclusion waters. By this I mean that the water-rich inclusion types have a higher gas content in the Link and Crescent quartz than in the Bluebird quartz. The formation of gas-hydrates was observed and is believed to be responsible for the lack of a distinct and measureable water-ice phase. Both Link and Crescent inclusions also contain hydrate forming gases other than CO_2. This is indicated by decomposition temperatures greater than $+10^{o}C$ (fig. 39, page 55). Carbon dioxide hydrates must decompose

at temperatures lower than +10°C (Collins, 1979). The composition and characteristics of the Link and Crescent gas-hydrates are uncertain but organic compounds are a likely component.

In reference to the Link and Crescent freezing runs two questions arise: Were the samples throughouly frozen? ... Did a normal water-ice phase form? In answer to the first question, the samples were cooled and held below -80°C for several minutes. It is difficult for me to believe that none of the liquid-rich inclusions froze. In fact a freezing was observed in many of the Link and Crescent inclusions, resulting in a 'crinkly' ice appearance. This may have been water-ice, gas-hydrate ice, or both. Upon heating of this 'crinkly' ice phase of indeterminate composition a first-melting was observed at about -29°C. This indicates that some water-ice was present, the final melting point of which was unobservable. In any case, gas-hydrates were the only detectable phases of an ice nature from about -10°C to their decomposition temperatures.

DISCUSSION: Gas-Hydrates

The decomposition temperatures of the gas-hydrates show a bimodal distribution with 43 data centered on +5°C and 22 data centered on +10 to +12°C (fig. 39, page 55). The gas-hydrates decomposing near +5°C may be composed chiefly of CO_2 hydrate (CO_2-5.75H_2O). The gas-hydrates decomposing

above +10°C must contain other gases in addition to CO_2 as this is the critical decomposition temperature for CO_2 hydrates in the presence of a gas phase (Collins, 1979). It is very likely that these inclusions contain significant concentrations of hydrate-forming organic compounds.

Within single samples, or within groups of samples from the same location, the gas-hydrate decomposition temperatures are reproducible and fall within well-defined areas. This is evidenced by the limited ranges in melting temperatures for individual samples (Data for fig. 39 are in the appendix). The reproducibility of different samples from the same location is evidenced by tight clusters such as samples 2 thru 6. The group whose inclusions yielded gas-hydrates decomposing in the +5°C area is composed entirely of Bluebird vein samples, both quartz and sphalerite. The +10 to +12°C group is composed of Link, Crescent and special classes of Bluebird vein samples. Sample 15 is from a pre-existing quartz crystal in a steel-galena mineralization zone of very late Bluebird time. I shall refer to this sample as representative of 'proto-Link' mineralization because of a mineralization style similar to Link vein steel galena although it occurs in a Bluebird system. Group 14 is composed of one inclusion in very late clear calcite and is not representative of the Bluebird orebody within which it was found. No salinity was determinable. The 14 Brown quartz inclusion group 10 is an

"odd-ball" within the +10 to +12°C group. It is the only Bluebird sample to show such high temperatures of gas-hydrate decomposition that is also not distinguished as being late within Bluebird time by field evidence.

With the above reservation, it may be concluded that the Bluebird vein inclusions form gas-hydrates which decompose at lower temperatures than inclusions from later systems, reflecting either/or both different amounts of dissolved gases and/or different gas compositions with time.

It has been noted by Collins (1979) that gas-hydrate formation may cause errors in salinity estimation by freezing point depression. The crystalization of gas-hydrates results in the removal of water from the residual aqueous phase, increasing its salinity. The salinity increase in the residual aqueous phase is proportional to the amount of gas availiable to form hydrates. In the case of the Bluebird fluids represented by the aqueous Type-1 inclusions, the amount of gases in aqueous solution is limited to about two mole % maximum (by gas analyses). This means that the maximum salinity error due to gas-hydrate formation can be estimated to be about +1 to +2 wt.% NaCl for corresponding 1 to 2 mole % CO_2 (fig. 5, Collins 1979). If salinities were availiable in the Link and Crescent systems much greater errors could occur due to higher gas contents (gas analyses section). Greater errors

could also occur in Bluebird inclusions having higher gas contents.

The presence of hydrate forming gases other than CO_2 causes further complications. If the proportion of species other than CO_2 is large then the error in salinity estimation would increase over that of pure CO_2-hydrate (Collins, 1979 p 1442). The Bluebird gas-hydrates are however, probably composed of mostly CO_2-hydrate. Since the mole percentage of gases dissolved in the Bluebird aqueous phases is limited to about two mole % (gas analyses section), with organic compounds composing only a fraction of a mole %, the organic hydrates will not be present in high enough concentration to cause a much larger salinity error than that already estimated. It is my conclusion that the error in salinity determination was not very large in the case of the Bluebird samples. The salinity error could be significant in other more gaseous samples however, should data be obtained from them in the future.

Several clathrate decomposition salinities were obtained using the methods and conditions prescribed by Collins (1979). The presence of CO_2 liquid, CO_2 gas, CO_2 hydrate and aqueous solution was noted indicating position on the eutectic-upper critical decomposition join of the H_2O-CO_2 phase diagram (fig. 1, Collins, 1979). These gas-hydrates decomposed at $^{+}6.1$ to $^{+}6.2^{o}C$ (group 5 of the

data), which corresponds to an 8 mass % salinity (Collins's data for the appropriate diagram are in terms of mass % salinity). A measurement of 10 wt.% NaCl would be expected for normal water-ice freezing point depression, assumming that mass % is roughly equivalent to weight % (no normal water-ice melting was observed for these two inclusions).

DISCUSSION- Miscellaneous Freezing Observations:

Figure 45 illustrates the detection of gas-hydrates- which are generally invisible to human vision, in terms of a photo sequence. Photo 1 shows a large primary(?) inclusion in sphalerite which formed on a growth plane (130-35-23, T= $-23^{o}C$. It is also possible to interpret this as a secondary inclusion. Photo 1 shows the inclusion after freezing and after first-melting has been observed. Normal water ice 'A' may also contain both aqueous fluids and gas-hydrates in equillibrium at this temperature. The vapor bubble 'B' contains gases at a low pressure and might be considered to be partially evacuated due to gas freezing. Phase 'C' may or may not be the same as any or all of the components of 'A'.

Photo 2 of figure 45 shows the appearance of the same fluid inclusion after it has been heated above the final melting point of ice, allowed to equilibrate and quickly chilled about $-10^{o}C$ (The photo is at a temperature of $-6^{o}C$). The vapor-bubble's borders have changed shape and maintain

Figure 45. Photo sequence showing the detection of gas-hydrates (130-35-23 sphalerite).
Photo 1. T = -23 C
See text page 78.

which

Photo 2. T = -6 C
See text page 78.

Photo 3. T = +1 C

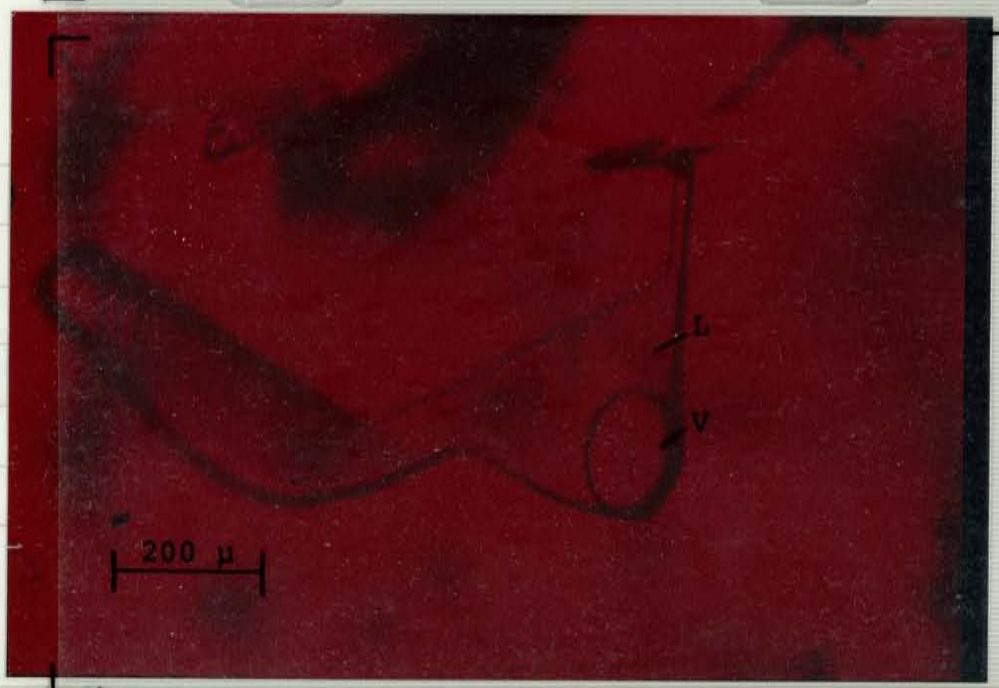

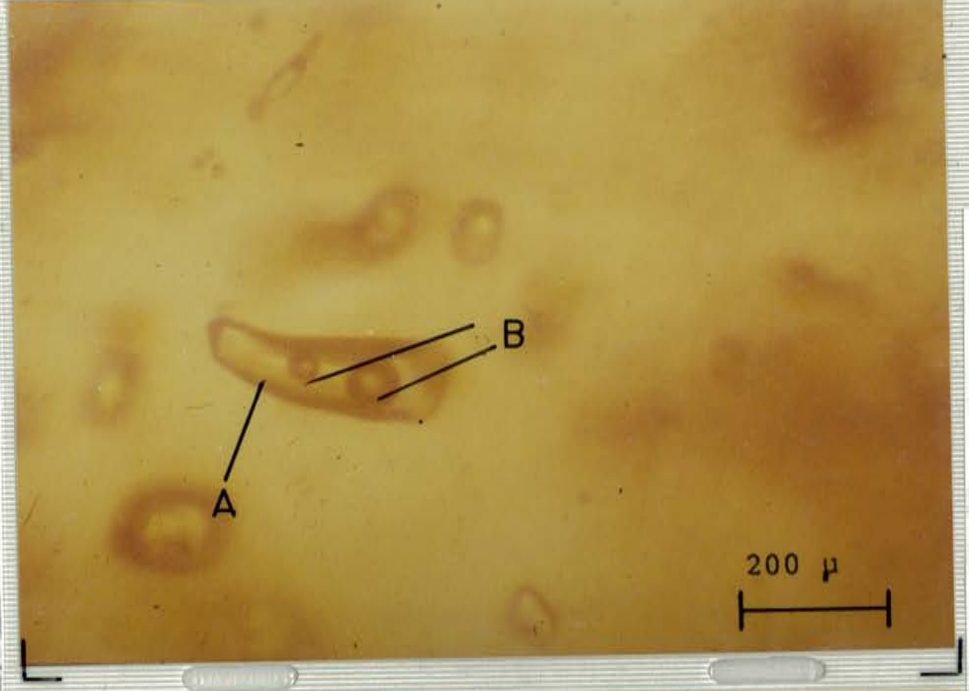

Figure 46.
"Double-bubbles"
T = + 2.6 C (The smaller bubble homogenized at +8.8 C while the larger increased in size).
110-35-24 quartz from a vug in the en echelon shears.

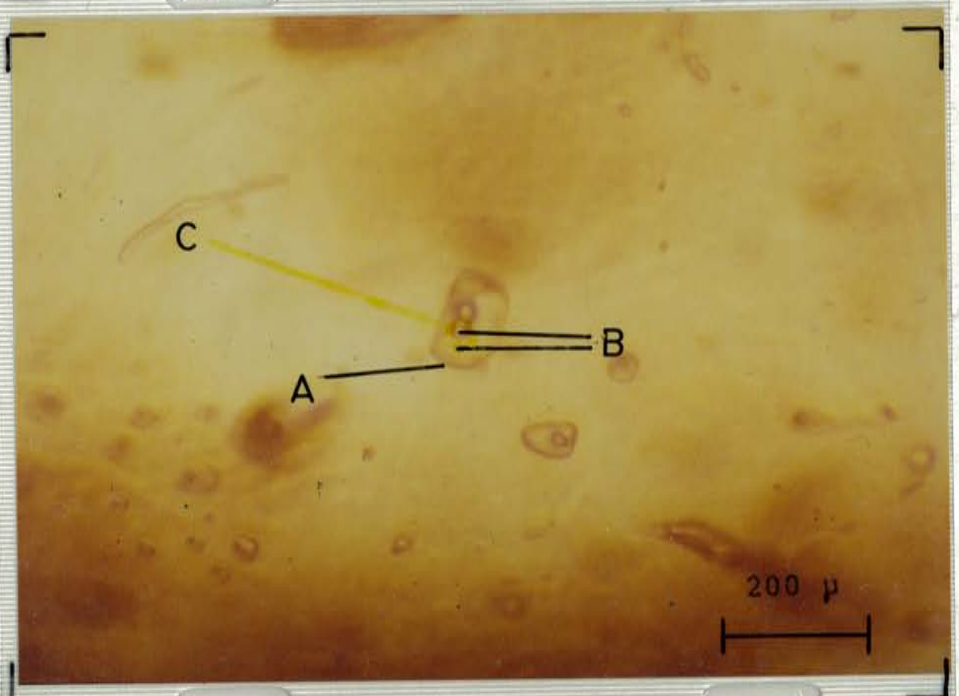

Figure 47.
"Double-bubbles",
T = -9.6 C,
110-35-24 quartz.
Note phase 'C' which is probably mixed gas-hydrates and aqueous solution.

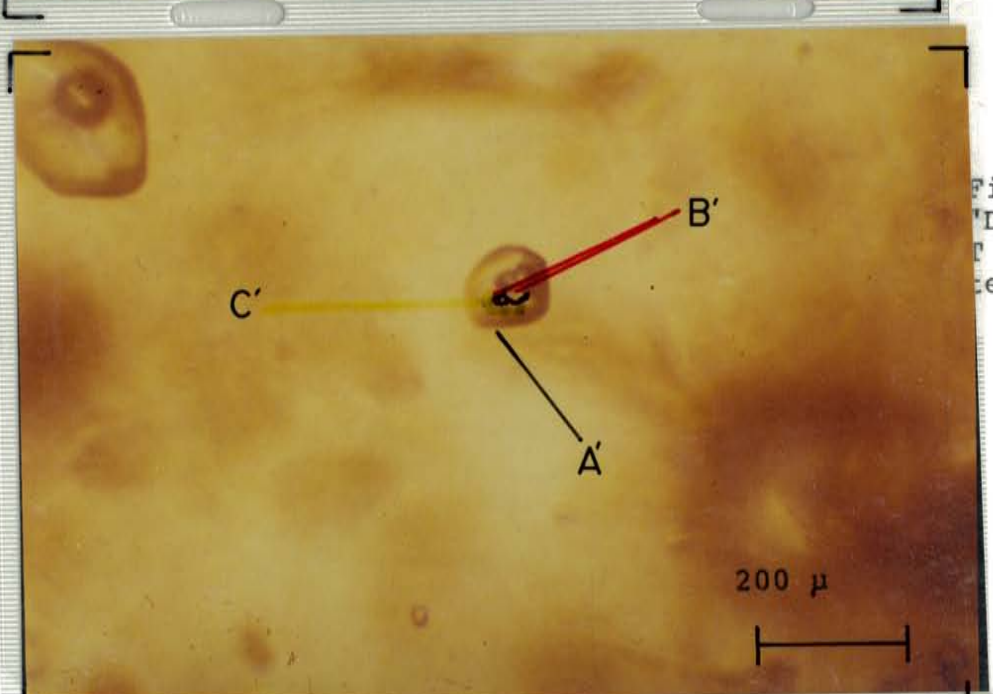

Figure 48.
"Double-bubbles",
T = -4.7 C, see text.

Figure 48.
"Double-bubbles",
T = -4.7 C, see text.

FIG

an irregular outline due to the presence of gas-hydrates in phase (s) 'D'. Photo 3 of the sequence shows the appearance of the inclusion at $+1^{o}C$. Phase 'V' is a gaseous vapor and phase 'L' is an aqueous liquid with some invisible gas-hydrates still present. After gas-hydrates are unable to form when the inclusion is quickly chilled, a lack of nucleation sites for the gas-hydrates will be indicated. The minimum temperature at which this occurs is the decomposition temperature of the gas-hydrates.

Figures 46, 47 and 48 show the presence of "double-bubbles" and complex bubbles due to the formation of gas-hydrates. In figure 46 two distinct phases are evident; Phase 'B' being a vapor or dense-gas is present in two distinct bubbles, which may or may not be of the same composition. Phase 'A' is predominantly solid in nature- as deduced by a lack of bubble movement, and is probably composed chiefly of gas-hydrates, although some aqueous phase may be present. In figures 47 and 48 several inclusions showed the presence of merging or expanding "double-bubbles" which formed as the inclusions were chilled. Note the visibility of a phase 'C' surrounding the bubbles 'B'. The composition and state of this phase is uncertain but may be either liquid CO_2 or a separate gas-hydrate than that in phase 'A'. The "double-bubble" of figure 48 may be different and more complex than that of figure 47. Phase separation within the bubbles is outlined

in black in figure 48, the cause of which is uncertain (T= -4.7°C).

Other freezing observations are shown in figures 49, 50 and 51. The photo sequence of figure 49 shows the contrasting behaviour during freezing investigations of a pair of fluid inclusions occurring close together. In the first photograph (T= 0.0°C)- which is at a lower temperature than the second (+3.1°C), the lower inclusion contains at least two visible phases while the upper one contains at least three. As these inclusions were warmed, one phase 'B' decreased in volume- at similar temperatures, in each of the two inclusions. A point was finally reached in the lower inclusion where all of the ' B' ' phase was dissolved into the ' A' ' phase, at which point a new phase ' V' ' formed (at +3.1°C). The similarity in behaviour of the 'B' and ' B' ' phases suggests that they are similar in composition and probably composed of liquid CO_2 or other liquified gases.

Figure 50 shows a multiphase inclusion containing liquid(?) 'E', vapor 'V' and unidentified phase 'D' at -3.6°C. Phase 'D' had an anomalously high melting temperature of -1.8°C, indicating that either the salinity of this inclusion is very low or phase 'D' is not water-ice. Anomalous inclusions such as the one referred to here were not common in the samples studied and may be secondary in

Figure 49. Photo 1.
T = 0.0 C

Figure 49. Photo 2.
T = +3.1 C

Figure 50.
Multiple phases,
see text.

Figure 51.
T = -29 C

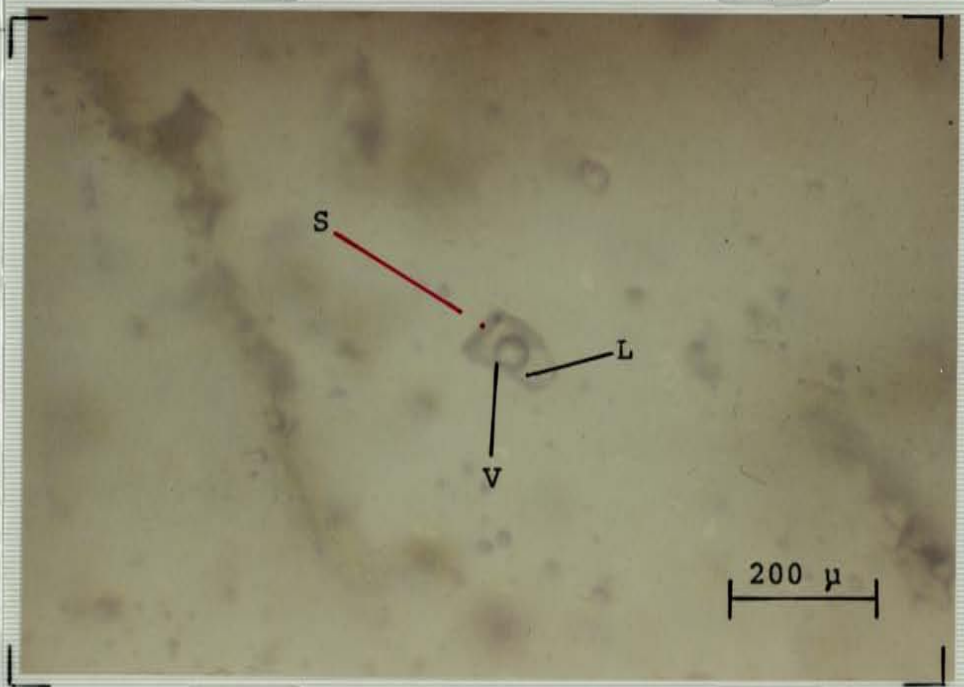

Figure 52.
Fluid inclusion
at T = 25 C.

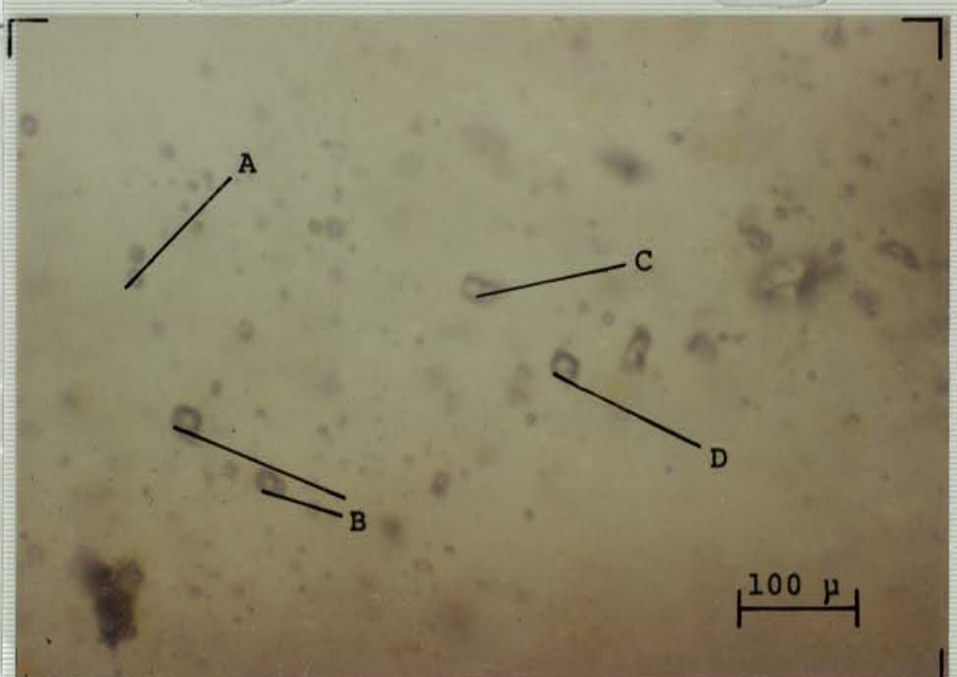

Figure 53.
T = 184 C,
variable ratios of
vapor::liquid.
19'J' quartz

origin.

Figure 51 shows an unfrozen inclusion at a temperature of -29°C. Three phases are visible; Liquid 'A' contains a vapor bubble 'V'. Both phases are enveloped by phase 'B', the composition of which is uncertain. This inclusion remained unfrozen and appeared the same at a temperature of -68°C.

DISCUSSION: Homogenization Data

All of the T_h's should be regarded as minimum temperatures of the ore-forming fluids. They should not be considered true temperatures because there is a strong doubt that the entrapped fluids were boiling in the strict sense of the word. Even though both gaseous and liquid type inclusions are present, they do not homogenize into their respective aqueous and gaseous states at similar temperatures. Homogenization measurements were obtained on only a few type-1B inclusions and they were at temperatures significantly higher than type-1A inclusions in the same sample. If boiling had occurred both inclusion types should homogenize at identical temperatures.

Some miscellaneous heating observations are shown in figures 52 and 53. Figure 52 shows an isolated inclusion containing a clearly visible liquid phase 'L' and a vapor phase 'V' at room temperature (A reddish "speck" is also present which may be a trapped sulfide.). As the fluid inclusions were heated, often the observation of the phases within became very difficult (fig. 53). Figure 53 shows fluid inclusions in the 19'J' pre-existing quartz sample at a temperature of 184^{o}C. Note the variable volumes of the gas bubbles in the different inclusions. Inclusions 'A' and 'C' contain about 15 % vapor, inclusions 'B' contain about 60 % vapor and inclusion 'D' contains over 60 % vapor. As

these inclusions were heated about another 30°C the distinction between the vapor and liquid phases in all of these inclusions became impossible, hence no homogenization temperatures were obtainable. Whether or not this behaviour is caused by critical-point phase transistions is uncertain. This type of behaviour was commonly observed in samples from both the Link and Crescent veins, but not in the Bluebird veins.

While the bulk of T_h's are centered about 250°C, two groups occur at higher temperatures. The group at about 285°C is composed of inclusions from a 120-35-24 quartz sample, all type-1A normal homogenizations to the aqueous phase. The group from 345 to 352°C is composed of six 14 Brown sphalerite inclusions, all type-1A, from a single crystal. The sample was broken into chips and slowly heated so that it is unlikely that stretching due to overheating during study was responsible for these anomalously high T_h's. The tight range in T_h obtained for the six inclusions indicates that this may be a good temperature even though it is significantly higher than the other T_h's observed for type-1A inclusions.

The whole previous discussion presupposes that the fluids in the observed inclusions of the 14 Brown sample are of an aqueous nature, except- of course the vapor-bubble. Upon heating, a 3 phase nature was observed in these

inclusions, particularly as the homogenization point was neared. This indicates the presence of two liquid fluids with large amounts of dissolved gases. It follows that there is the possibility of pre-homogenization stretching, due to high internal pressures which may be required for fluid immiscibility. At temperatures of less than 200°C the solubility of any given amount of N_2 or CO_2 is significantly lower than at the temperatures of homogenization (in aqueous solution).

Another problem concerns the genesis of the secondary inclusions in the 14 Brown sphalerite. Regardless of origin, the secondaries are orientated along cleavage planes and are planar in shape. It is very possible that these secondary fracture systems intercepted the large primary inclusions. This indicates that the secondaries may be products of some type of primary inclusion decrepitation. For this reason the T_h's obtained for the 14 Brown sphalerite sample should not be taken to be representative of mineralization temperatures unless future studies indicate that decrepitation has not occurred.

The bulk of T_h's, centered at 250-265°C, occurred in various quartz samples. These T_h's are much more reliable as minimum temperatures of mineralization than the sphalerite T_h's for several reasons. The first is that quartz has a much higher tensile strength than sphalerite

(at least 850 Bars vs. 400 Bars, Bodnar, et al, 1984). This means that quartz is much more resistant to stretching or decrepitation. Secondly, the inclusions chosen did not bear any obvious relations to secondary inclusions. The chosen inclusions showed primary characteristics such as belonging to growth trails or isolation from planar groupings of inclusions. Thirdly, the T_h's from individual samples were generally very close and the sampling as a whole displays a symmetrical and uniform T_h distribution. This last point is perhaps the most important.

Besides the inclusions of normal type which yielded good T_h's several other types of inclusions were observed (normal inclusions are Type-1A and homogenize to the liquid phase). One type of behaviour commonly observed, especially in planar secondary groups, was a lack of homogenization of the vapor phase after reaching a minimum volume. The minimum volumes of the vapor-bubbles generally were about 5% although considerable variance was observed. The temperatures at which the minimum volumes were observed were most often about 245-250^{o}C, although ranges were seen- especially in planar secondary groups. Within planar secondary groupings of inclusions it was often possible to follow this behaviour along the secondary-plane for temperature ranges of over 20 degrees. This indicates a systematic variation in bulk fluid composition within these planar groupings. Several explanations are possible for

this observed behaviour. One is partial decrepitation, however no evidence of fracture-reopening or fluid leakage could be seen. Another possible explanation is fluid inclusion stretching. This would require pressures of greater than 850 Bars in the inclusions, if the tensile strength of quartz has been correctly estimated. If this behaviour could be demonstrated in primary inclusions then a minimum pressure estimate would be possible. Since it is very difficult to state that any inclusion is undoubtedly primary, all inclusions exhibiting this behaviour were assumed to be secondary. It should also be noted that this behaviour was not reversible by cooling. If these inclusions contained significant amounts of N_2 it may be necessary to freeze the sample below the freezing point of the gas to be sure a phase metastability problem does not exist. The samples were not cooled sufficiently during study to be sure metastability does not exist.

Another type of behaviour observed was the presence of immiscible liquid phases. The term 'liquid' is used here to distinguish between a true vapor or gas phase from any phase in a high density-condensed state (liquid). It is recognized that the observed immiscible liquids may be quasi-gaseous in nature, but are visible as distinctly different phases than the vapor-bubble. At least two types of immiscible liquid behaviour were observed (figs. 55, 56, page 101 and fig. 40, page 59). Type-1 liquid

immiscibility was observed in all Bluebird quartz samples and in the 14 Brown sphalerite sample (i.e.; fig. 55). The observed character of this type of immiscibility was limited to that shown in the intermediate drawing of figure 40, at 230°C. A much less frequently observed variation of this type of immiscibility occurred with the vapor-bubble present in the less-dense L_2 phase. This type of observation may be transitional to Type-2 immiscibility, where the L'_2 phase is generally less than 30 % of the inclusion volume. The separation of the L_2 phase, in Type-1 immiscibility, was observed only in secondary inclusions from the 14 Brown sphalerite sample from which T_h's were obtained. It is believed that the separation of the L_2 phase occurred only because of the flattened nature of the secondaries produced along cleavage planes. In more rounded inclusions the vapor-bubble was often observed to spin violently around the circumference of the L_2 phase until homogenization. After the vapor-bubble is homogenized it becomes very difficult to observe the L_1 phase and the behaviour of the immiscible liquids is uncertain. Only in the 14 Brown sphalerite secondaries were the immiscible liquids clearly visible after homogenization of the vapor-bubble. In this case the T_h of the vapor-bubble was variable between separate secondary inclusions and generally not recorded. The highest T_h observed for a secondary vapor-bubble was 271°C in the 14 Brown sample, the two

immiscible liquid phases visible to above 300°C- at which point the L_2 phase began to lose clarity and become indistinguishable from the L_1 phase, much as in critical point observations rather than homogenizations. Upon cooling to low temperatures the vapor-bubble suddenly re-emerged and produced the same T_h as previously recorded. Because this observation was limited to secondary inclusions no general deductions can be made except that it is possible to have co-existing immiscible fluids beyond the homogenization of the vapor-bubble. Whether or not they exist in primary inclusions is uncertain.

Another type of immiscibility frequently observed is that labeled 'Type-2' in figure 40 (also fig. 56). It is assumed that the compositions of the immiscible liquids may differ from those of the corresponding Type-1 fluids, so they have been labeled L'_1 and L'_2. It is very difficult, in some cases, to observe the final homogenization of the vapor-bubble. Often, when the vapor-bubble reaches a few percent of the inclusion volume, the L'_2 phase grows to over 30 % of the inclusion volume. This behaviour has been observed to occur at temperatures similar to those observed for vapor-bubbles exhibiting a lack of homogenization, previously discussed. These two phenomena may be related and many of the vapor-bubbles in the previously discussed case may really be immiscible fluids. Inclusions showing Type-2 immiscibility often contain more than one

"vapor-bubble" within the L'_2 phase, sometimes up to three. When this has been observed the inclusions could not be homogenized. After the L'_2 has expanded, the change in phase ratios is not reversible upon cooling (L'_2 will only increase in size).

Another immiscibility related observation is the emergence or increase in volume of a liquid phase in gaseous inclusions as they are heated (fig. 54). It may be that the supposed gaseous phase is actually a complex fluid. In the case of the 14 Brown quartz sample photographed, the liquid phase was first noticeable at about $+37^{o}C$, reached a maximum volume-percent at about $140^{o}C$ and had nearly disappeared by $160^{o}C$. A $T_h = 161^{o}C$ into the gaseous phase was then observed. After cooling the inclusion to $+14^{o}C$ and re-heating, the same observations were made at the same temperatures indicating reproducibility. The sample had to be cooled to about $110^{o}C$ before the liquid phase would reappear each time indicating that gaseous phase homogenization had occurred. A second inclusion located nearby displayed almost identical results, differing only a few degrees in phase emergence and homogenization temperature. A sample from the Quill orebody also had a group of inclusions displaying similar results.

Figure 54. Photo 1. Photo sequence showing the emergence of a liquid phase from gaseous inclusions, as they are heated (14 Brown quartz). T = +28 C.

Photo 2. T = +36 C. The liquid phase has emerged.

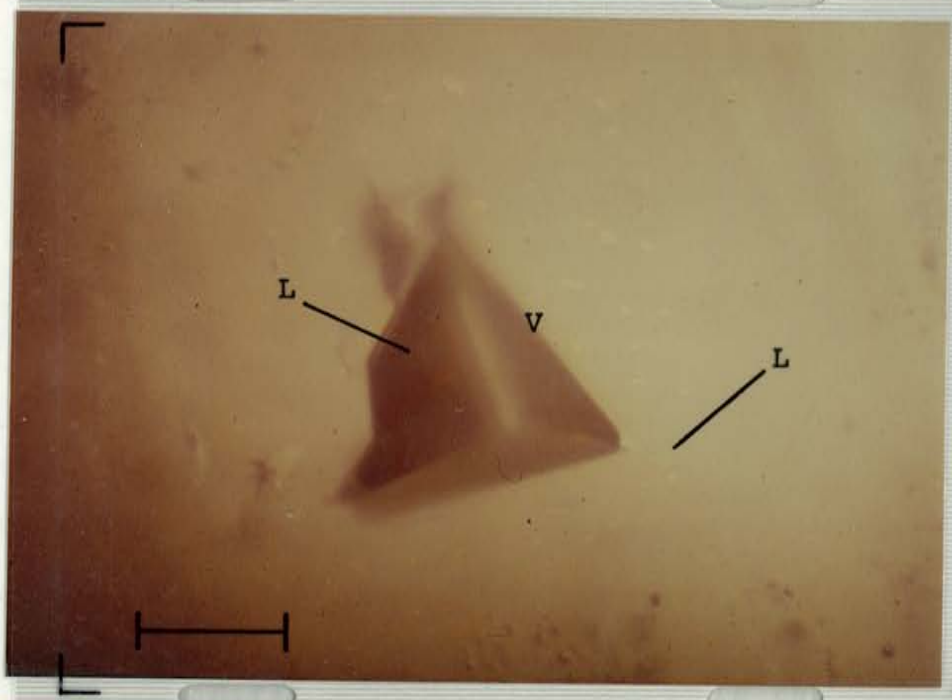

Photo 3. The liquid phase has increased in volume. T = +80 C. See text page 93.

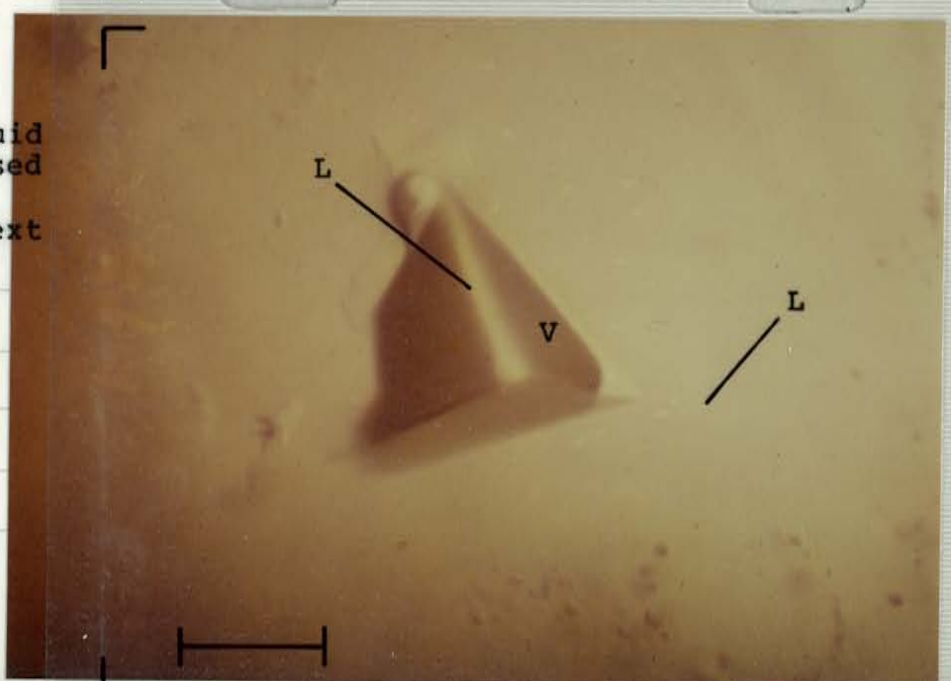

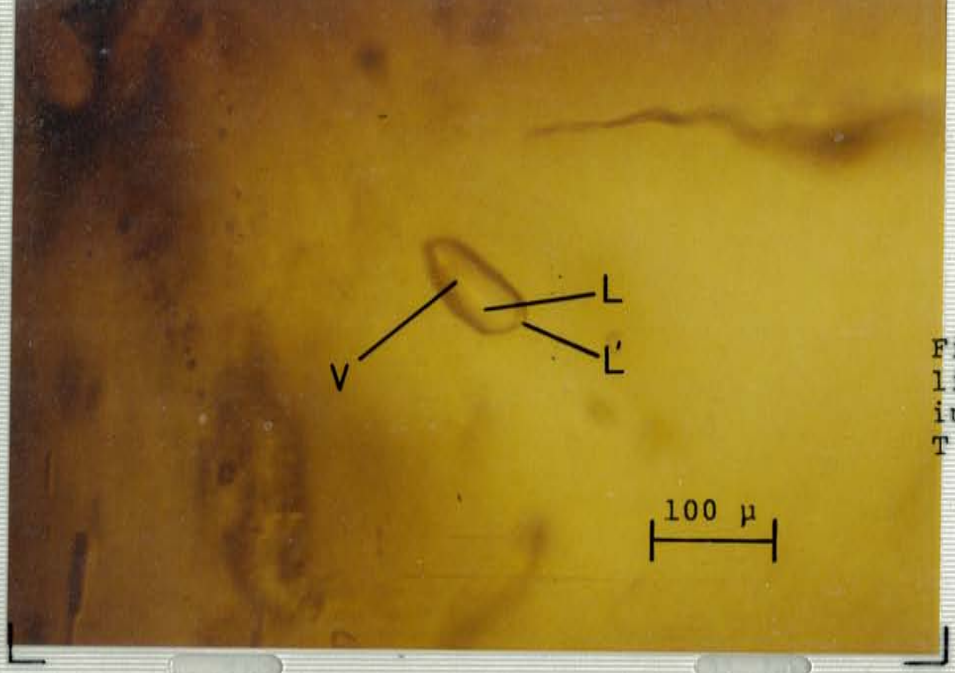

Figure 55. Type-1 liquid immiscibility in Bluebird quartz. T about 175 C

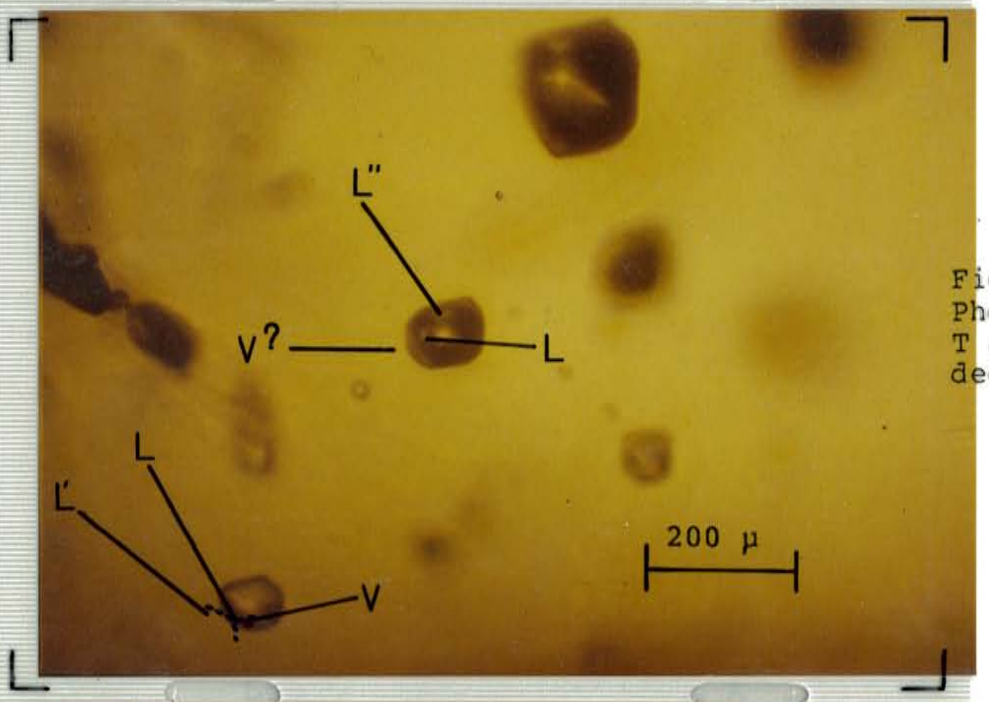

Figure 56. Photo 2 at T about 245 C, decrepitated?

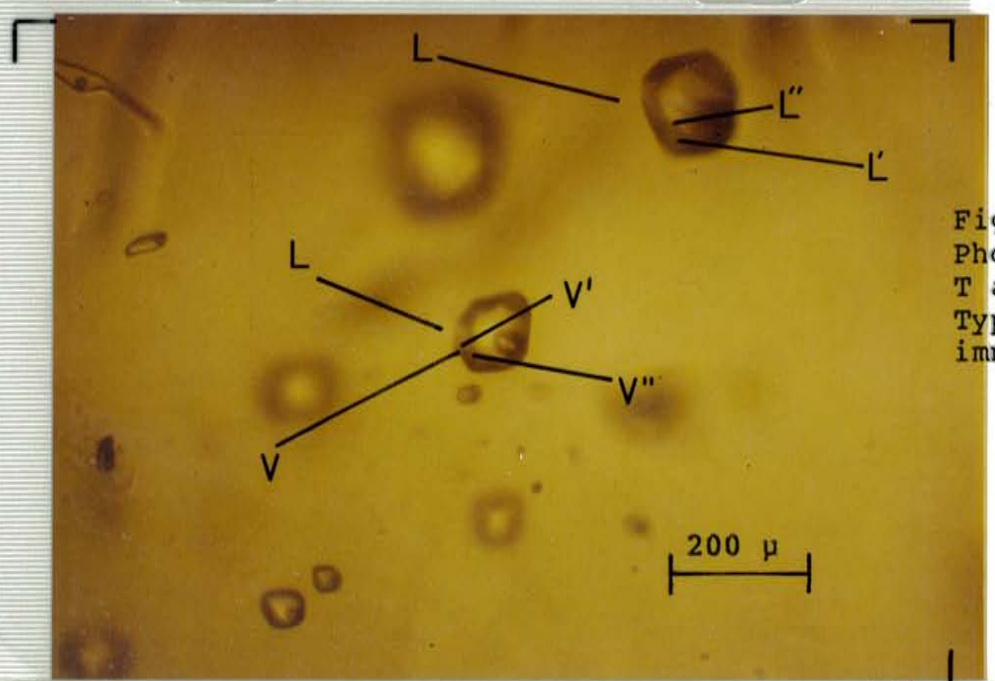

Figure 56. Photo 1 at T about 200 C. Type 2 liquid immiscibility.

DISCUSSION OF GAS ANALYSIS DATA

The analyses of the Bunker Hill and Crescent mine fluid inclusion gases are unusual in several respects; 1. Most reported analyses show only a few wt.% gases (Roedder, 1972) while analyses of this study contain a wide range- to over 90 wt.% gases. 2. High N_2 fluid inclusion content (Discovery by Dave Norman). 3. Compositional heterogeneity of the analyses.

The wide range in wt.% gases and composition within individual samples during stepwise thermal decrepitation indicates the presence of different inclusion types. Inclusions of the same type with similar fluid compositions should follow similar paths of pressure vs. temperature and decrepitate at similar temperatures. Compositionally different fluids however, follow different P-T paths and may decrepitate at different temperatures. At least three types of inclusions are necessary to account for the diversity in gas analyses; a water-rich type to account for the analyses with only several wt.% gases and a N_2 rich-H_2O poor type to account for analyses of these respective compositions. All three types of analyses were observed in a single sample of 14 Brown quartz decrepitated stepwise with temperature.

Analyses of inclusions with 2.4 to 5 wt.% gases, such as the Bluebird vein lower temperature decrepitations, are due to aqueous inclusions which may be gas-saturated. Once

fluids homogenize to the aqueous phase, a further increase in temperature will result in a rapid increase in pressure explaining the tendency of these type inclusions to decrepitate at low temperatures relative to gaseous inclusions. It is probable that analyses of this type correspond to type-1A fluid inclusion decrepitations. Whether or not these inclusions are gas-saturated depends upon whether boiling did or did not occur during fluid entrapment.

Analyses showing high wt.% gases indicate the decrepitation of gaseous fluid inclusions or inclusions containing large amounts of gases relative to water. If these inclusion types are heated beyond their temperatures of formation the corresponding pressure increase will not be as large as in the case of homogenized aqueous fluid inclusions. This may account for the higher temperatures observed for these type analyses (750°C vs. less than 550°C for the aqueous types). The reason for the different internal pressures for the different inclusion types is that the slopes of the isochores differ for fluids of different compositions. Even for liquid and vapor trapped at boiling, different isochores are followed at temperatures beyond entrapment. Thus vapor inclusions must be heated much more than liquid inclusions to reach the same pressures required for decrepitation, if these pressures are higher than that at homogenization.

Most often the analyses were carried out at 550°C without stepwise temperature intervals. Stepwise analyses however, indicate that both gaseous and aqueous types of inclusions may decrepitate by 550°C and that some analyses may represent a combination of the two types. This is especially suspected in the case of the analyses showing about 20 wt.% gases at 550°C and should be kept in mind when interpreting the results.

A remarkable result of the analyses is the very high N_2 content of the inclusions (Dave Norman). High N_2 fluids have been reported only in inclusions from evaporite deposits and as a major constituent of many natural gases. High N_2 contents have also been reported in a group of analyses in pegmatitic quartz but Roedder (1972) feels that these analyses represent contamination during the crushing by steel balls and are therefore unreliable. High N_2 fluids have not been reported from other igneous rocks except in the case of some whole rock analyses where the N_2 is very probably due to atmospheric contamination (Roedder, 1972). A sedimentary environment is therefore implicated in the origin of high N_2 fluids. The Bunker Hill and Crescent fluid's high N_2 content implies that they were derived from the Belt Supergroup or underlying sedimentary rocks, probably during basin metamorphism.

Nitrogen has a low solubility in water at near surface pressures, hence high pressures are required to dissolve the amounts measured in the aqueous inclusions. Figure 63 (page 122) shows the Henry's law constant relations for the gases measured, giving an indication of the relative gas solubilities. Of the major gases present- nitrogen and carbon dioxide, nitrogen has a Henry's law constant about five times higher than carbon dioxide. This means N_2 will be the predicted phase to boil-off or effervese. Whether or not N_2 effervescence occurred requires a complicated discussion of the Henry's law calculated minimum pressures, observed gas trends and a discussion of the possibilities of liquid immiscibility. The question of N_2 effervescence will therefore be discussed after these other subjects in more detail.

DISCUSSION- CO_2::N_2 Ratios:

Because the CO_2::N_2 ratio varies with inclusion type within an individual sample care must be taken in any interpretation of its trends. The specific types of inclusion fluids responsible for the trends must be recognized. Pre-mineralization quartz has the lowest CO_2::N_2 ratios, followed by Bluebird quartz and sphalerite, "proto-Link" quartz, Link quartz and Crescent quartz in order of increasing CO_2::N_2. This order is followed in both the characteristic runs (T_d = 550°C, fig. 57) and in the water-rich inclusion types (fig. 58). The aqueous

Figure 57. $CO_2::N_2$ as a function of T_d.
Lines connect stepwise T_d runs.

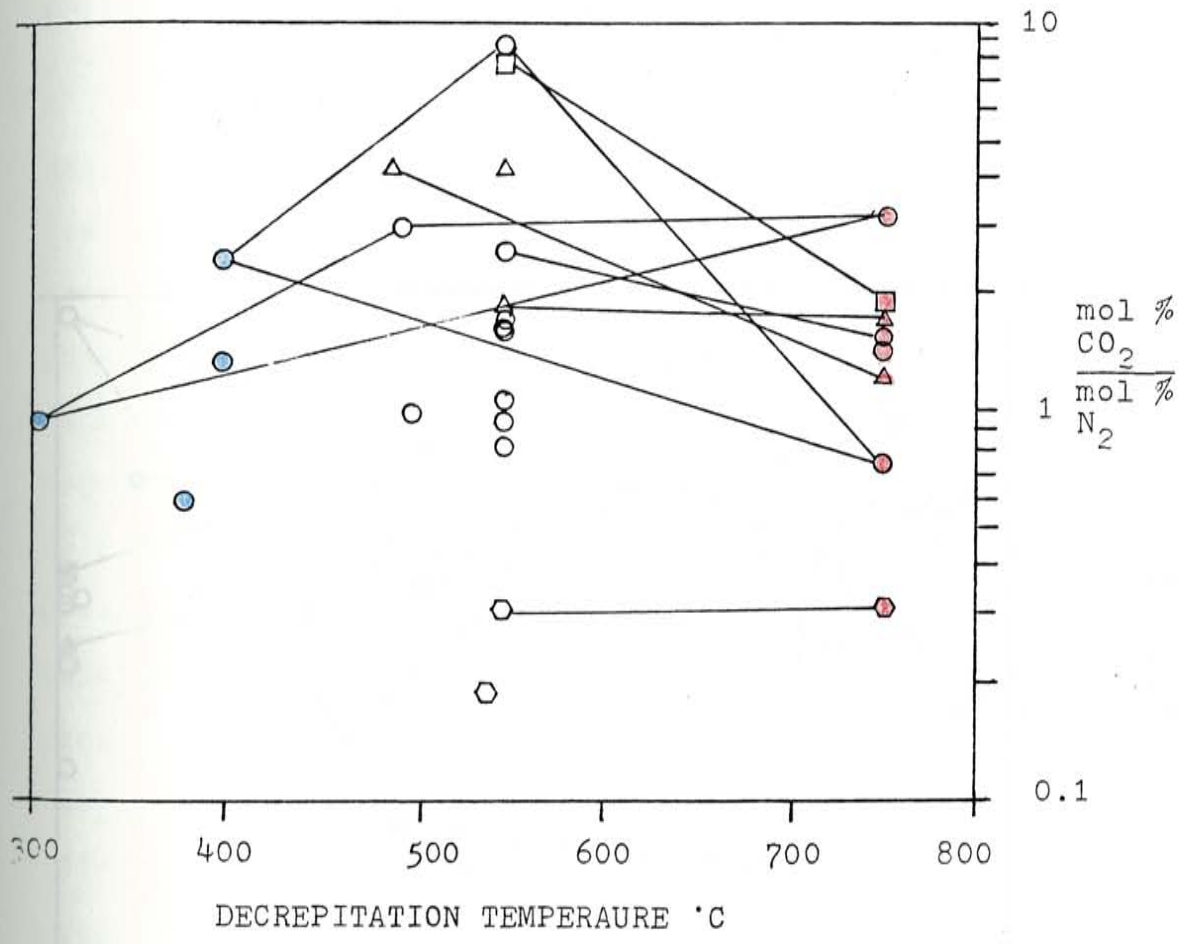

Figure 58. $CO_2::N_2$ as a function of wt.% H_2O.

The right-hand side of the diagram indicates a trend in the aqueous inclusions from pre-mineralization, Bluebird, Link and Crescent fluids (hexagon, circle, triangle and square respectively). Red- T_d = 750°C

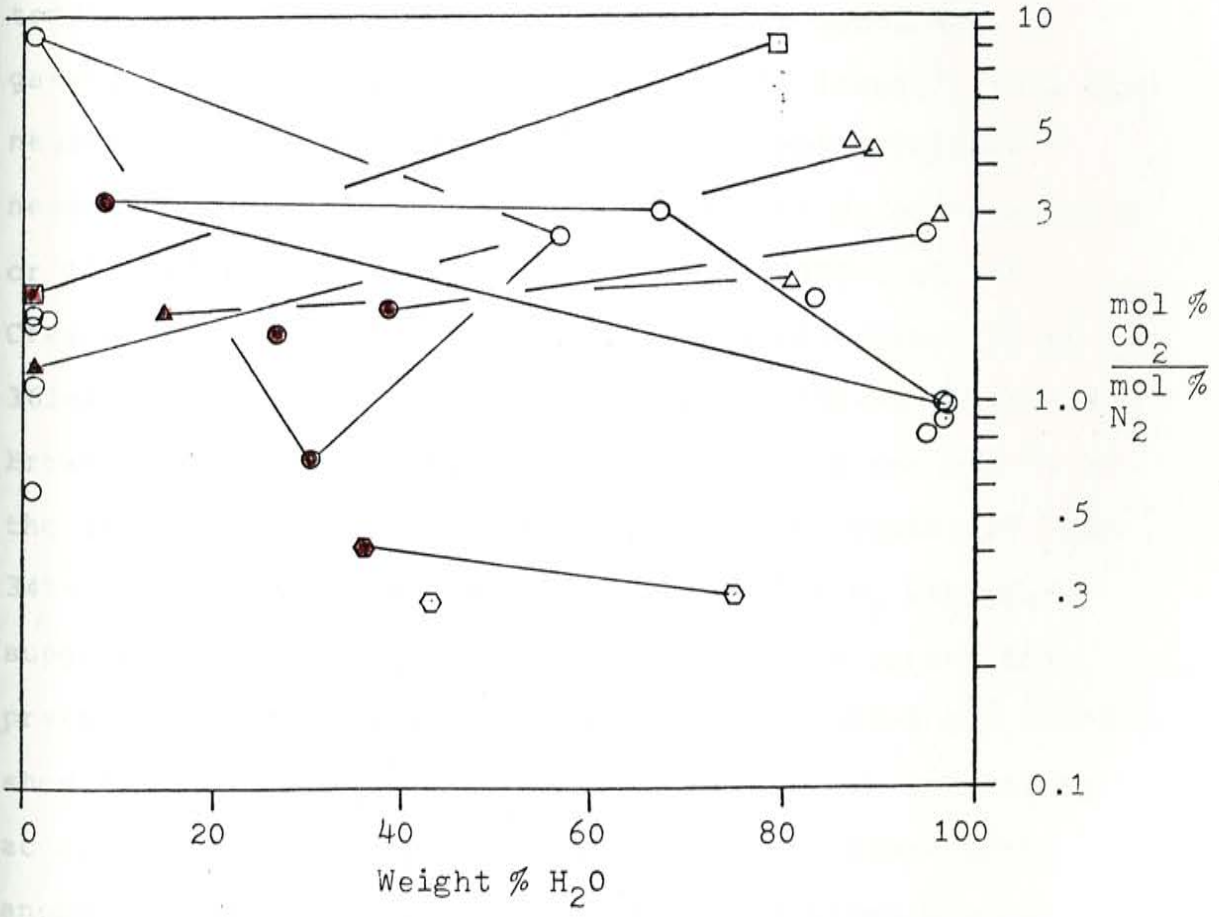

inclusion types rather than the gaseous inclusion types are responsible for this trend (fig. 58). Gas analyses may therefore be a useful 'tool' in distinguishing vein paragenetic sequence, especially if used in addition to structural modeling as both structural regime and the CO_2::N_2 in the aqueous phase seem to have specific trends over a large time span.

The CO_2::N_2 ratios vary with the temperature of stepwise thermal decrepitation (fig. 57). Stepwise T_d runs are connected by lines- positive slope with increasing temperature indicating the higher T_d runs (generally gaseous) contain more CO_2 relative to the lower T_d runs and negative slopes indicate the opposite. Most slopes are negative, the cause of which may be either N_2 effervescence or liquid immiscibility; runs 328-9 and 330-1 of the Crescent Mine, 320-1 and 326-7 of the 19'J' vein, 359-60 and 361-2 of the 9 Jersy (milky quartz), 337-339-40 of the 14 Brown and finally, runs 365-6 plus 367-8 and run 369-70 of the 14 Brown. The pre-reverse shear, milky quartz of runs 341-2 and 343-4 shows nearly identical CO_2::N_2 ratios, suggesting that no N_2 effervescence occurred during this pre-mineralization event. Runs 353-4 plus 355-6 and 357-8 show a CO_2 increase in the higher T_d run which can not be accounted for by Henry's law boiling. Inclusions with anomalously high CO_2 also occur in the 14 Brown quartz sample- run 367-8. These type inclusions are suspected to

occur in many of the analyses made at only T_d = 550°C because of gas ratio considerations which will be discussed shortly. The immediate importance of these inclusions is to complicate the possible determination of the sequence of orebody paragenesis thru CO_2::N_2 gas ratios. Of greater importance, is determining whether or not these inclusion types were formed as a result of liquid immiscibility, specifically by the NaCl-H_2O-NaCl system (or a more complex system, possibly involving N_2 immiscibility).

CONSTRAINTS ON LIQUID IMMISCIBILITY:

A discussion of the NaCl-H_2O-CO_2 system- which exhibits immiscible liquid behaviour at high temperatures and pressure, is given by Pichavant, et al. (1982). Several "limits on the interpretation of fluid inclusion data" concerning the existence of immiscibility have been listed by Ramboz, et al. (1982), in a companion paper to the one above.

The first constraint is that the inclusion content has not changed since trapping. Necking-down, leakage or natural decrepitation could not account for the anomalously high CO_2 content previously referred to, due to the much greater insolubility of N_2- if one wants to derive these inclusion types directly from gas-saturated liquid type inclusions. The low wt.% H_2O with high CO_2::N_2 type

inclusions represented by runs 357-8 of the 110-35-24 Quill-Bluebird quartz and runs 367-8 of the 14 Brown-Bluebird quartz could not even be generated by necking off a N_2 enriched gaseous type inclusion (which would be an expected fluid if Henry's law boiling occurred), since the gaseous type inclusions with high N_2 content also have much more H_2O than the analyses with a high CO_2 content.

The second constraint is that "no chemical or physical changes occurred in the inclusions after trapping due to reaction with the host mineral". Since the inclusions in question are in quartz, no reaction is likely with the host mineral. The possibility of solid inclusions (impurities) reacting to produce the anomalous CO_2 is not likely because of the gaseous nature of the CO_2 rich inclusions. Increasing CO_2 content by carbonate dissolution would be limited with the small amount of water available and the observation of entrapped carbonates in gaseous inclusions during microscopic inspection would be expected. No such inclusions were observed. Thermal release of CO_2 during analysis step-heating is unlikely because higher and lower T_d runs and other runs at similar temperatures, do not show anomalous CO_2. Thermal release of CO_2 adhering to quartz would be expected to be a systematic problem rather than an anomaly. Thermal reaction during decrepitation (impurities would be necessary) is also unlikely because runs 369-70 do not show CO_2 enrichment, yet were decrepitated at a higher

temperature than runs 367-8.

A third constraint on interpretation of immiscibility concerns the "space-time relationships between the various sorts of inclusions". In the case of the 14 Brown sample, runs 365-6 and 367-8 can be related thru the use of gas ratios. The N_2::(C_2H_n + C_3H_n) ratios are nearly the same for the 400°C and 550°C runs (2.36 and 2.21 for the respective mole % ratios). Figure 59, which shows the relative proportions of CH_4, C_2H_n and C_3H_n and figure 60(Table 3 of the appendix) both indicate that the organic compounds of these runs were similar. Both CH_4 and the C_4Hn hydrocarbons are relatively 'enriched' in the 550°C step but the close agreement in other ratios suggests a prior equilibrium between the two inclusion's fluid types. The magnitude of CH_4 enrichment and CO_2 enrichment in the 550°C run relative to the 400°C run is very similar. The CO_2 to N_2 ratio of runs 367-8::365-6 is 3.48 and the CH_4::N_2 ratio of the 550°C step divided by the 400°C step is 3.03. A possible depletion in H_2S, SO_2 and Ar exists in the 550°C step relative to the 400°C step.

The 750°C step shows a depletion in CO_2::N_2, relative to the 400°C step, which is exactly the inverse of the CO_2::N_2 enrichment in the 550°C step. That is, the 750°C step is depleted in CO_2 by a factor of 3.53 and the 550°C step is enriched in CO_2 by a factor of 3.48, both relative

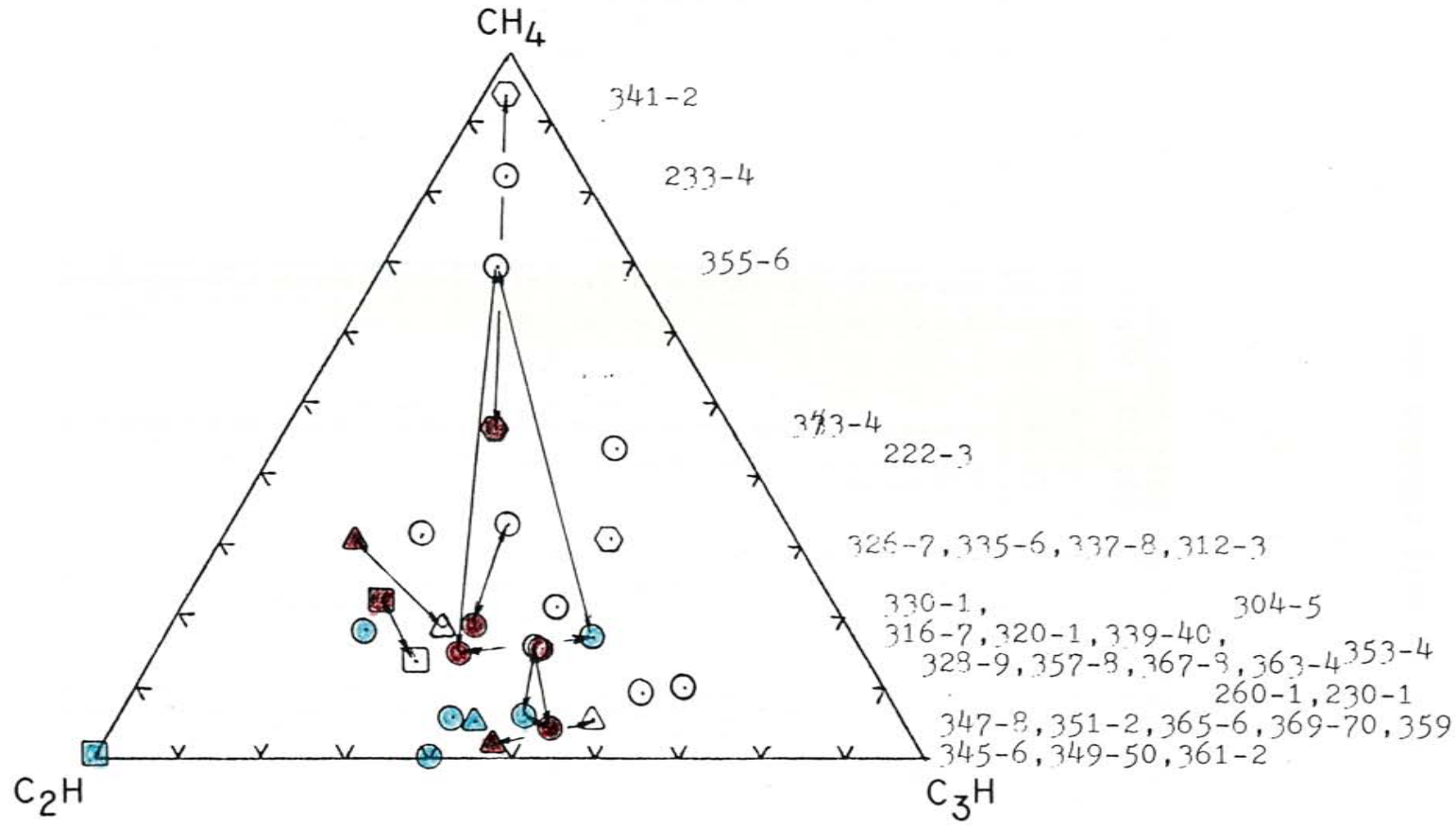

Figure 59. The variation in organic species as a function of sample and temperature of decrepitation. This diagram shows a C2Hn polarity for 'mineralization-associated samples'.

Figure 60. Reproduction of table 3 of the appendix.

Organic mass spectra line ratios.

Table 3. Organic compound line spectra ratios.

SAMPLE	C2::C3	C3::C4	C4::C5	C5::C6	C3::C5	C2::C4
328-9	0.764	29.6	17.6	------	530.	22.6
330-1	0.737	22.9	8.57	------	196.	16.9
345-6	1.10	37.4	------	------	------	41.
306-7	0.523	22.8	7.30	0.333	166.	12.
320-1	0.504	9.25	6.91	1.06	63.9	4.6
326-7	0.413	12.2	2.16	1.20	26.4	5.
351-2	0.474	10.1	5.23	1.88	52.8	4.8
359-60	0.260	27.9	4.78	0.668	133.	7.25
361-2	0.583	12.6	5.91	0.88	75.	7.34
335-6	0.38	9.6	7.1	1.2	68.	3.65
304-5	0.30	13.	3.2	1.7	41.	3.9
233-4	0.49	19.	5.3	0.53	101.	9.31
363-4	0.48	21.	6.1	0.62	127.	10.
347-8	1.86	14.	4.0	1.6	58.	26.
349-50	0.85	11.7	2.4	1.8	28.	9.9
222-3	0.14	11.	13.5	0.99	150.	1.54
230-1	0.13	7.7	6.5	1.0	50.	1.0
256-7	------	------	------	------	------	------
260-1	0.20	11.9	3.8	------	45.	2.4
260'	0.24	10.5	3.5	0.94	37.	2.5
353-4	0.23	16.	6.9	------	109.	3.7
355-6	0.66	16.	6.5	1.1	101.	10.6
357-8	0.75	16.	13.	0.17	212.	12.
236-7	0.75	36.	------	------	------	27.
312-3	0.20	29.	4.3	0.68	126.	5.7
343-4	0.76	10.	4.5	0.29	46.	7.6
341-2	0.50	13.	5.4	0.24	71.	6.5
316-7	1.7	13.	6.3	1.1	82.	22.1
238-9	0.52	23.	4.2	0.26	96.	12.
337-8	0.43	31.	4.5	0.54	137.	13.
339-40	0.71	20.	8.7	------	170.	14.
365-6	0.46	20.5	3.0	0.53	62.	9.4
367-8	0.49	9.4	7.1	0.62	67.	4.6
369-70	0.36	30.	4.2	1.07	126.	11.

to the 400°C step (note the symmetry!). The 750°C step is CH_4 enriched, relative to the 400°C step. The 750°C step is CH_4 enriched, relative to the 400°C step, by a factor of 3.18, which is similar to the 550°C step (CH_4::N_2 of each run, relative to the other). From Table 3 it can be seen that the organic line spectra ratios of the 750°C run do not closely resemble either of the two lower temperature runs at first glance. The major difference between this run and the two lower temperature runs is a small amount of C_3H_n enrichment and lower C_6H_n. This is probably not a major difference considering the general variability of the organic line spectra, but should be kept in mind. The H_2S::(C_2H_n + C_3H_n) ratio of the 750°C step is close to that of the 400°C step despite a 500 % change in the mole % values of C_2H_n + C_3H_n. This indicates that the H_2S either behaves like the organics or is dissolved in them, if this type of relation can be widely observed in other samples.

In summary, the 14 Brown data discussed above probably support near contemporanity of the three inclusion types of the particular sample analyzed. Heterogeneous trapping of unmixing or immiscible fluids is indicated. The inverse relation of CO_2 enrichment and depletion relative to N_2 discussed above also indicates that CO_2 formation by reaction did not occur because of the symmetry between the runs.

In the case of the 110-35-24 Quill (Bluebird quartz) sample of runs 353-4, 355-6 and 357-8, the two higher T_d inclusion types seem related. Both have very close $CO_2::N_2$ ratios and similar organic line spectra. The 300°C run on the other hand, has a much lower $CO_2::N_2$ ratio. The difference in the $CO_2::N_2$ ratio of the 300°C run relative to the higher temperature runs can be explained as a result of liquid immiscibility in the H_2O-NaCl-CO_2 system however. The relative CO_2 enrichment in the 500°C run to the 300°C run is 3.21 and that of the 750°C run relative to the 300°C run is 3.33 ($CO_2::N_2$ at the higher temperatue step divided by the lower temperature step). These values are very close to the CO_2 enrichment value of the 14 Brown 367-8 step and suggest a common origin. The $N_2::(C_2H_n + C_3H_n)$ values for all three of the Quill stepwise decrepitation analyses are similar to the 550°C step. The 300°C step differs mainly in C_2H_n depletion relative to the higher temperature steps. All this probably indicates that the fluids forming these inclusion types were close to being in equilibrium with each other. This also probably indicates that the time of trapping of the fluids is close between the inclusion types.

Another set of constraints concern "homogenization phenomena". The first concerns contemporaneous trapping of the inclusions, already discussed above. The second requires that the two inclusion types "must homogenize at the same temperature" or "range of temperatures". This

point is probably valid for the samples studied and is discussed in the section on fluid inclusion microthermometry (partial homogenizations may be excepted from this criteria). The third constraint listed by Ramboz is that the two fluid inclusion types should have similar pressure behaviour upon heating and therefore should decrepitate at similar temperatures. This condition is probably not valid for the samples studied, possibly due to their high N_2 content. At temperatures lower than trapping the gases in the aqueous inclusions behave according to Henry's law, but largely gaseous inclusion types follow a different P-T relation- probably closer to the Ideal gas law. Different slopes occur in the isochores after homogenization. In either case the inclusions may decrepitate at different temperatures. If the aqueous type inclusions were not "gas-saturated" and do not represent a Henry's law N_2 boiling event, then the vapor bubble will homogenize at a lower temperature then that of entrapment, allowing for a very different P-T path upon heating and a lower temperature of decrepitation. Note that this interpretation does not disallow boiling at greater depths or even intermittent N_2 boiling episodes at a similar space and time within the deposit.

A third phase- a nitrogen and organic enriched, somewhat gaseous phase is also present, which may interact with the other two phases when it comes into contact with

them. This third phase must be at least partly immiscible with the aqueous phase but in the case of the high CO_2 content "gaseous fluids", the extent of miscibility is unkown. If it is hypothesized that the anomolously high CO_2 content fluids are generally in equilibrium with the aqueous fluids then the CO_2 rich phase must also be required to have a limited miscibility with the N_2-Organics rich phase- if all three phases are simultaneously present.

ORGANIC COMPOUNDS:

The organic contents of the analyzed fluids vary in concentration and type of organic compounds. These types of variation may occur between different mineralization events or within single events (fig. 59 and fig. 61). Organic compound variation within a single event is reflected by changes in the amount and/or type of organics with the temperature of fluid inclusion decrepitation (as noted by color in the triangular plots). Inclusions decrepitating at the 750°C step generally are enriched in total organics relative to those decrepitating at lower temperatures (runs 369-70, 361-2, 363-4, 326-7 and 343-4). Exceptions to the above generalization are runs 357-8 and 330-1. It has already been noted that run 357-8 is suspected of representing immiscible CO_2 enriched fluids and can be seen to be doubly anomalous on the triangular plot in terms of direction of fluid compositional 'variance' with temperature.

The total organic compound variation between samples is large but not greater than that found within some single samples (i.e.- stepwise T_d runs 365-6, 367-8 and 369-70, 14 Brown quartz). It is interesting to note that the Link samples 359-60 to 361-2 and 320-1 to 326-7 span the same approximate space as the 14 Brown sample referred to above (fig. 59). The Crescent quartz sample also occupies a

Figure 61. The variation in organic compounds in a single stepwise Td sample, as shown by the line spectra in graphical form.

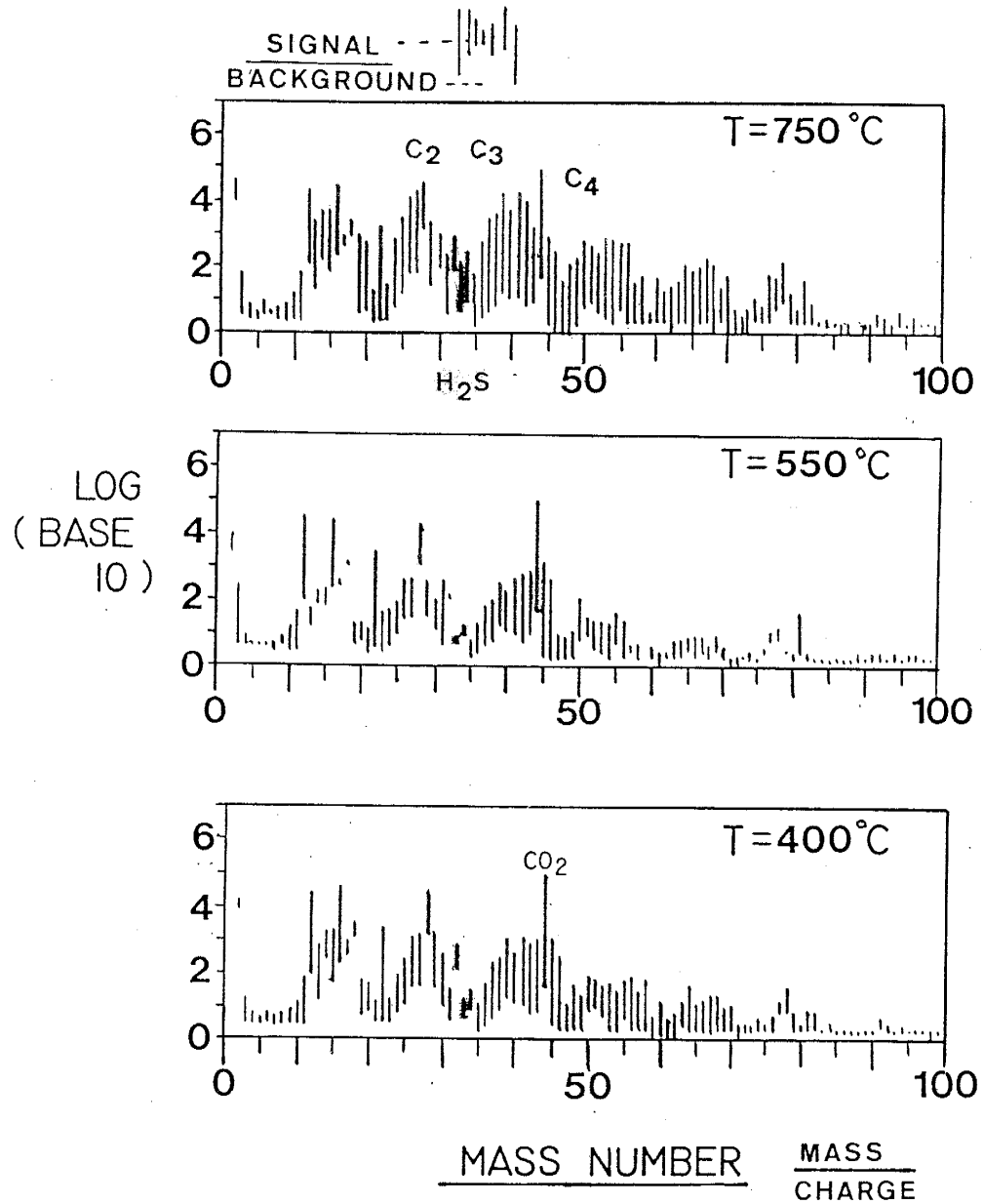

Figure 61. The variation in organic compounds in a single stepwise Td sample, as shown by the line spectra in graphical form.

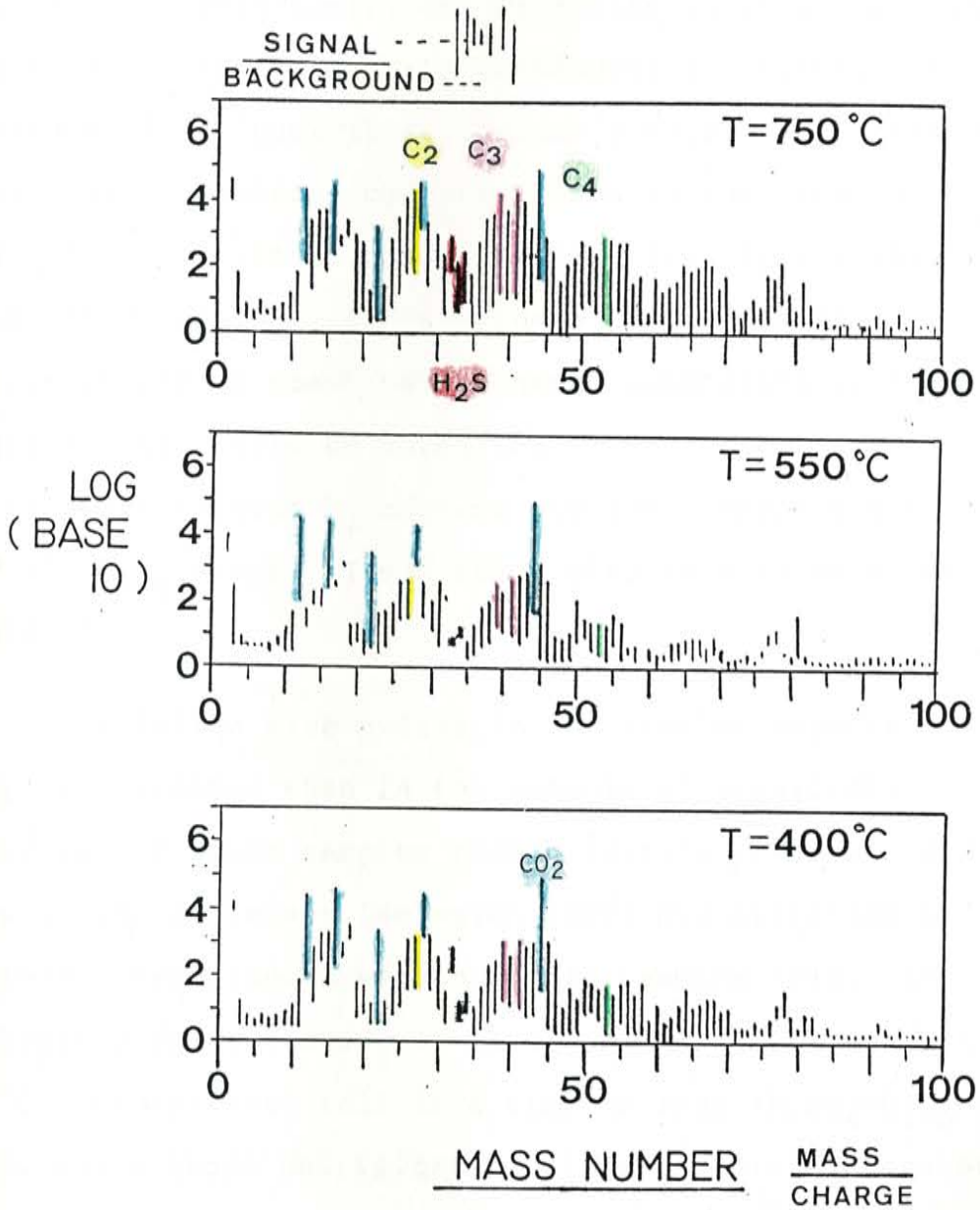

similar portion of the triangular diagram. This overlap in total organic content vs. N_2 and CO_2, suggests that either complexly varying trends of organic content occurred with the fluid evolution between orebodies (due to the basin metamorphic evolution?), or- more likely, that the organic contents of the fluids were continuously varying. The presence of at least three phases- previously discussed, could easily generate complex trends in the total organic content of any single phase due to differing viscosities and rates of migration. It is assumed that these three principle phases sometimes exchange components when they contact. It should be noted that there is a positve correlation between N_2 content and total organic content in the 750°C T_d steps. These steps also tend to have low water contents.

A variation also exists in the type of organic compounds (rather than in the amount- as previously discussed) between samples from different orebodies and also between the different inclusion types decrepitating at different temperaures within single samples (fig. 59). Inclusions decrepitating at low (i.e. 400°C) or high (i.e. 750°C) temperatures fall in a similar area in CH_4-C_2H_n-C_3H_n space while those decrepitating at intermediate temperatures (i.e. 550°C) fall closer to the CH_4 or C_3H_n poles. The only intermediate T_d inclusions to fall near the C_2H_n pole are those from Link and Crescent vein samples and the

late-Bluebird "proto-Link" sample (runs 328-9, 320-1 and 335-6 from a steel-galena vein). The group of samples located near the C_2H_n pole in the triangular diagram represent 'mineralization-associated' space- that is the samples are either sphalerite crystals from the Bluebird veins, pre-existing Link quartz (which was formed during Pb mineralization as indicated by euhedral galena inclusions) or Crescent quartz (tetrahedrite- Ag time). Some 750°C T_d fluids from Bluebird samples also plot in this region (runs 339-40 and 357-8) but the lower T_d (550°C or less) fluids do not. The trend towards the C_2H_n pole may be due to fluid evolution with time or may be the result of organic compound fractionation during deposition. In the case of the Link and Crescent stepwise T_d's the C_2H_n polarity must have been due to bulk-fluid evolution since very little variation exists between the T_d steps 320-1 compared to 326-7 and 328-9 compared to 330-1. Whether the bulk-fluid evolution is due to basin evolution- such as metamorphic history, or to a distantly located phase fractionation process is uncertain.

If a hypothesis can be made that in a situation of in-situ boiling the evolved gaseous phases would be light hydrocarbon enriched relative to the residual aqueous phases then this trend should be observed in the inclusions of such trapped fluids. In the case of the Crescent and Link samples the opposite trend is observed (appendix Table 3).

The N_2 enriched gaseous phases are heavy hydrocarbon enriched (runs 326-7 and 330-1). This may be possible evidence against in-situ boiling, or- since the organic compounds are not the predicted phases to boil-off, they may not behave in this manner. The organic compounds may simply be more soluble in the gaseous N_2 phase than in the aqueous brine?

DISCUSSION- H_2S Trends and Correlation to Organic Compounds:

The general trend of increasing H_2S content in the series pre-reverse shear quartz, Bluebird quartz, Link quartz and Crescent quartz is most evident in the calculations in terms of gas fractions- excluding water (Table 1, appendix). This trend also occurs in terms of mole % H_2S, water included (Table 4, appendix). In terms of mole %, including water, there are several samples which show excessively high H_2S contents that do not fit this trend.

A plot of the ratio- $H_2S::(C_2 + C_3)$ on the ordinate axis, to the $(C_2 + C_3)$ mole % total, as the abscissa, was made to determine if a correlation exists between H_2S and hydrocarbon content (fig. 62). Pre-mineralization quartz and many of the Bluebird samples show a uniformly low $H_2S::(C_2 + C_3)$ although the mole % total $(C_2 + C_3)$ varies within the stepwise T_d of individual samples. Stepwise

Figure 62. H_{2S}::(C_2H_n + C_3H_n) vs. Total organics.

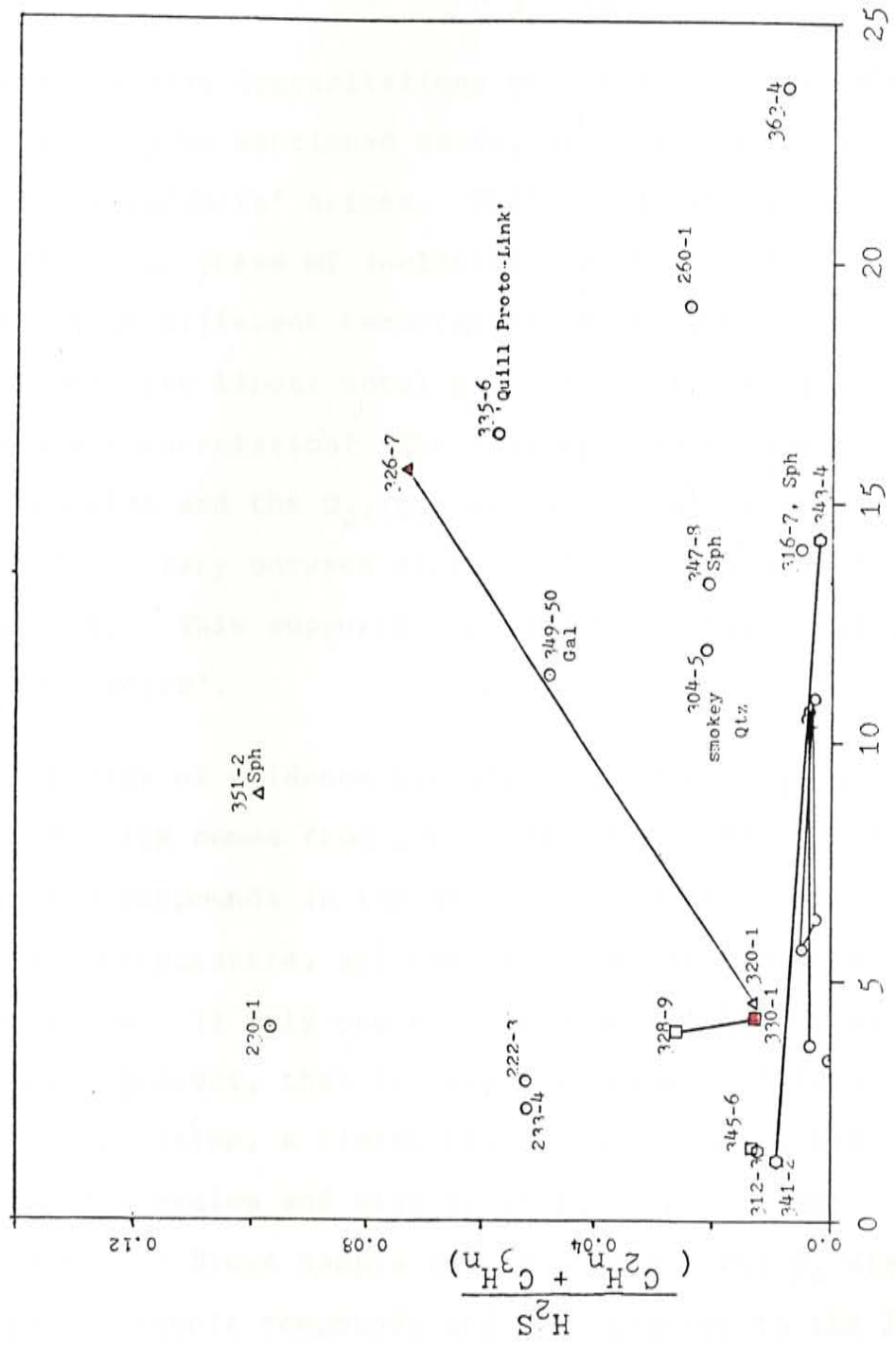

decrepitated inclusions in the Link and Crescent samples show a higher $H_2S::(C_2 + C_3)$ which also varies inconsistently in relation to the $(C_2 + C_3)$ mole % total.

Of the stepwise decrepitations of the pre-reverse shear and Bluebird samples mentioned above, the question of H_2S and organic 'reservoirs' arises. That is- is there more than one source or phase of inclusion type which is decrepitating at different temperatures or only one, responsible for the linear total H_2S content to total organic content correlation? The line spectra of the organic compounds and the $C_2::C_3$ ratios for the various inclusion fluids vary between stepwise decrepitations (Table 3 and fig. 59). This supports the idea of multiple H_2S and organic 'reservoirs'.

Another line of evidence supporting multiple H_2S and organic reservoirs comes from interpretation of the actual mole % organic compounds in the gas fractions vs. decrepitation temperature, and comparison to the observed $C_2Hn::C_3H_n$ ratio. If only one reservoir of H_2S and organic compounds were present, that is only one phase containing them during deposition, a linear trend would be expected between the low, medium and high T_d steps. This is not observed in the 14 Brown sample as the intermediate T_d step is depleted in organic compounds and H_2S relative to the low and high T_d steps (runs 365-6, 367-8 and 369-70). If we

would assume a hypothetical single inclusion type source for the organic compounds and H_2S and assume that they were dissolved principally in one phase, a given mole % water should also be assigned to this phase, if aqueous in nature. In the case of the 14 Brown (Bluebird) runs, no assumed mole % water content for the hypothetical phase works. One would have to assume a largely gaseous nature for the phase containing the organic compounds and H_2S to account for the measured water in the various steps, but then the non-linear T_d vs. total organic and H_2S trend indicates more than one inclusion type source. If any H_2S and organic content correlation can be made to a specific phase, it seems that it would be a N_2 enriched phase (14 Brown and Quill Bluebird samples). Whether or not this trend exists is uncertain.

ESTIMATE OF PRESSURE AND DEPTH OF FORMATION:

Regardless of whether or not Henry's law boiling occurred, a minimum pressure and depth may be calculated by using this relation ($f = K_h X$, where 'f' is the fugacity of the dissolved gas species, 'K_h' is the experimentally derived Henry's law constant and 'X' is the mole fraction of the gas species in solution). The most reliable minimum pressures (P_m) will be those calculated from samples decrepitated so that only inclusions containing aqueous fluids during entrapment are represented. In practice these turn out to be the lower T_d runs which yielded the highest wt.%'s of water (Table 4 in the appendix).

In addition to the Henry's law relation a 'salting-out' correction is necessary. This derives from decreased solubility of gases due to the increase in the activity of a gas in a brine, relative to pure water. The expression used to correct for salinity is also called the "Setchenow equation":

$$\log \text{gama} = \log K/K' = K_s m_s,$$

"Where K is the modified Henry's law constant for the brine and K' is the Henry's law constant for water, m_s is the molality of dissolved salts in the brine, K_s is the salting-out coefficient and gama is the activity coefficient" (Cramer, 1982).

The modified Henry's law constants and salting-out coefficients used are from a variety of sources in the literature (fig. 63). Of these the data used for N_2 are the most incomplete with no study of the effects of salinity at elevated temperatures. The salting-out coefficient used for N_2 is that of CH_4. At 25°C the salting-out coefficient for N_2 is close to that of CH_4 (K_sN_2 = 0.309 and K_sCH_4 = 0.333, expressed as a natural log function for 1.882 molal NaCl). At 265°C the salting-out coefficients of CH_4 and CO_2 are very similar (fig. 10 of Cramer, p. 13, 1982). It is expected that N_2 would not greatly deviate from CH_4 in its salting-out behaviour at 265°C because of the similar non-reactive properties of the gases. The magnitude of the error of this assumption will probably be the error in the total pressure calculation as it is the largest uncertainty in the available data.

	CO2	N2	CH4	C2+C3
Kh (2M NaCl)	8957	50583	3204	(CH4 used)
Ks	1.92	(1.558)	1.558	
Kh (pure water)		32459		

Test equations: pure water, T in degrees Kelvin

$$\log KhCO2 = 5.31328 - 0.00306T$$

$$\log KhCH4 = 7.35698 - 0.00590T$$

$$\log KhH2S = 4.00871 - 0.00142T$$

$$\log KhN2 = 7.56180 - 0.00567T$$

Figure 63. Henry's law constants and salting-out coefficients used in the pressure calculations. The methane salting-out coefficient is used for N2. Calculated values are at 265°C. Sources of data: CO2 and CH4 (Cramer, 1982), Ar and H2S (Naumov, 1974), N2 and test equations (Nehring, 1981)

The minimum pressures calculated are on the order of 370 to over 600 Bars for the Bluebird aqueous inclusions and 970 to 1700 Bars for Link and Crescent inclusions (fig. 64). It is suspected that the Link and Crescent decrepitations may include some gaseous type inclusions and that the resulting calculated pressures may be high. The Bluebird decrepitations are mostly of the aqueous type and the resulting P_m estimate is probably good. These pressures are reasonable as minimum pressures but are they as true pressures of Henry's law boiling? Using an approximation of 3.5 km/kbar it is probable that no more than 2 km of rock could have existed as overburden during Bluebird time if boiling is assumed (slightly more if the load is hydrostatic). Runs 351-2 yield a P_m of less than 300 Bars (25 Francis sphalerite). Again an approximate overburden during mineralization would be on the order of 2 km, but at present there is nearly 2 km of overburden over the 25 Francis level. Considering that the ore deposits lie in an uplifted block which must have undergone considerable erosion since mineralization, it might be argued that the calculated P_m's are too low to represent boiling fluids. This argument is certainly not conclusive in the Bluebird case, as only about 1 km of overburden exists over the sampling sites, but since these deposits are fold-form related- during compressional tectonics, it might be possible to make a structurally based estimate of

Figure 64. Table of the calculated Henry's Law Pressures for 2M NaCl. T = 265°C, P in Bars.

	gas fugacities							
SAMPLE	H2O	CO2	N2	CH4	C2 + C3	Ar	H2S	Total
328-9	42.0	840.	576.	2.15	13.8	0.52	0.17	1475
306-7	42.0	478.	637.	----	----	2.97	9.1	1170
320-1	42.0	398.	534.	1.9	8.6	0.34	5.9	991
359-60	42.0	422.	1249.	5.4	94.5	2.6	5.2	1821
351-2	42.0	85.	163.	0.24	4.3	0.30	0.22	296
335-6	42.0	254.	870.	15.2	32.7	0.82	0.99	1216
233-4	42.0	49.	299.	4.5	1.0	0.15	2.7	399
222-3	42.0	62.	345.	1.06	1.4	0.66	3.7	456
353-4	42.0	48.	283.	0.9	4.5	0.49	7.1	386
260-1	42.0	73.	516.	1.4	13.9	0.78	0.19	648
337-8	42.0	150.	317.	1.4	2.8	0.17	3.7	517
341-2	42.0	354.	6424.	119.5	8.2	3.2	3.9	6955

mineralization time minimum overburden. If this must exceed 2 or 3 km, serious doubt could be placed upon insitu Henry's law boiling mechanisms for Bluebird fluid evolution.

Recent deep drilling has provided evidence that the increase in pressure with depth is not linear (Kozlovsky, 1984). Low pressure anomalies have been observed in zones of disaggregation below well consolidated rock at depths of below 4000 meters, however the magnitude of the low pressure deviation is too low- less than about 25 % of the projected median total pressure of the overlying and underlying zones, to seriously affect the preceding argument.

DISCUSSION-FLUID INCLUSION LEACHATE RESULTS:

1)- Reliability of the Analyses:

As indicated by the background levels of quartz-rod blanks 16 and 20, all of the concentrations referred to can be expected to be reasonably accurate and free of error due to contamination. A small amount of error may be present in some of the Cl analyses- up to approximately +30 %, (appendix, Table 5, analyses 4, 16 and 20). Low levels in some analyses indicate that the source of the Cl contamination is inconsistent (analyses 11, 12 and 15). High backgrounds indicating contamination from the crush-tubes occurred for Zn, Cu and possibly Cd; for this reason the calculation of the levels of these elements in the crush-tube samples was impossible. Analyses 1, 2, 3 and 9 were contaminated by unwashed Nalgene filters as indicated by analysis 13. This contamination was eliminated by prewashing the filters (analysis 14). A small amount of Ca contamination was introduced by the crush-tubes (analyses 16 and 20). Except for analysis 15 (about +40 % error) and possibly- but to a lesser extent, analyses 18, 21 and 24(+15 to +30 % error), this contamination is insignificant.

The accuracy of the analyses is ensured by comparison to the standard solutions (runs 5,6,7 and 9). The analyzed concentrations obtained for the standard solutions compares well with previous values obtained by Borden Putnam (1980,

reference note: The solution A and B used in this thesis is different in concentration than those used by Putnam, therefor a systematic correction factor is needed when comparing results). A comparison of solution A (Dave Norman's list of what solution A is supposed to contain, analysis-1) with the results from this study (analysis-2) (both analyses are 1::1000 dilutions of the stock solution) follow:

	Na	K	Ca	Mg	Cu	Zn	Fe	Cl
1) Solution A:	39.7	4.0	4.0	2.0	2.0	2.0	2.0	43.2
2) Solution A:	39.2	5.08	4.89	2.1	nd	1.9	0.5	70.

The analyses of this study are very close to analysis-1 in the values for Na, Mg and Zn. They are acceptably close in the values for K and Ca, with a possible error of approximately +25 %. This magnitude of error will not result in any different interpretation of the data than that given and will not significantly affect any of the calculations made in this study (i.e.: salt-geothermometry calculations). The values for Fe and Cl show the largest disparity between analyses 1 and 2. The similar values obtained for Bluebird Cl^- content, even with varying dilution factors, indicate that this value is accurate. Solution 'A' was prepared a long time (1 year?) before this study and may have precipitated some of its contents or may have been contaminated (Cl). A comparison with solution 'B' could not be made because no one could find the contents

list!

2)- Calculation of Salt Balance:

Most published analyses of fluid inclusions are listed in ppm which is easily converted to weight percent by dividing by 10000. Most comparisons between geologic fluids are given these units and this convention is followed here. Molal units are used in the discussion when a comparison of the stoichiometric properties of the fluid inclusion analyses is necessary.

The total salt cations are less than the total anions in all of the analyses (Table 5 of the appendix and figs. 65, 66 and 67). In comparing the molal charge balance between the analyses, the negative charge is generally in excess of the positve charge (fig. 67). The divalent cations make the charge balance more equal but most of the analyses still show an excess of the negative charge, which is due almost entirely to Cl^-. Comparison to other published analyses shows that this commonly occurs (Roedder, 1972). The excess of negative charge may indicate the presence of undetected cations.

Figure 65. Calculation of the Salt Balance:

		CHARGE BALANCE (ppm)	
SAMPLE	Total Cations	sum '+'	sum '-'
15 less Mn	13900-15400 ppm	20100-22400	15600
17	18700-21000 ppm	28400-33150	79900
18	14600-16100 ppm	20300-23500	83000
19	57800 ppm	101118	77000
21	52900-60600 ppm	76800-91200	423000
22	16200-17400 ppm	20750-23150	109000
23	29400-33400 ppm	46850-52850	96000
24 less Mn	25500-30500 ppm	51100-61100	85000

3)- Comparison with other fluids:

Figure 66. The following table lists the major cation concentrations in molality:

SAMPLE	Ca	Na	K	Mg	Mn	Fe	Pb
15	.1142-.1715	.2141	.0939	.048	(.256)	nil	nil
17	.1971-.2567	.2364	.0862	nil	.0039	nil	.008
18	.1068-.1465	.2224	.1171	.016	nil	nil	.001
19	.7328	.4502	.1110	.035	.022	.182	.008
21	.5140-.7061	.3597	.5499	.079	nil	nil	nil
22	.0883-.1181	.3579	.0992	.010	nil	nil	.002
23	.2769-.3518	.3954	.0749	.012	.0106	.095	.001
24	.3293-.4541	tr	tr	.055	(1.548)	.197	nil

Figure 67. The following table lists the major anion concentrations in molality and the molal charge balance- which is a comparison between the total positive and negative charges, as calculated by the molal salt concentrations:

				MOLAL CHARGE BALANCE	
SAMPLE	As	SO4	Cl	sum '+' ::	sum '-'
15	.0003	nil	.440	.6324-.747	.4403
17	.0013	nil	2.248	.7406-.8598	2.25
18	nil	nil	2.341	.5871-.6665	2.341
19	nil	.0003	2.172	2.521	2.173
21	.0013	.0002	11.93	2.094-2.480	11.93
22	nil	nil	3.074	.6575-.7171	3.074
23	.0002	nil	2.708	1.262-1.410	2.708
24	nil	nil	2.398	1.163-1.412	2.398

The analyzed Bluebird salinities range from 2.0 to about 10.0 equivalent weight percent NaCl from the sum of the positive charges. The low values are probably due to less than 100 % recovery of the salts during leaching but as previously stated, may indicate undetected cations. When the anion (Cl^-) content is used to estimate salinity, a range of 10.9 to 7.9 eq. wt.% NaCl is obtained. This value is in excellent agreement with the freezing point depression salinities obtained for Bluebird samples, even more so when the possible error from gas-hydrate formation is taken into account (see discussion on fluid inclusion microthermometry, pages 74-78). The analyzed pre-mineralization quartz salinity is higher than the analyzed Bluebird salinity, but until more data is availiable no conclusions should be drawn from this observation.

The high Ca content of the Bunker Hill inclusion fluids is a distinctive characteristic (Table 5 of the appendix, concentrations in ppm). Most geologic fluids are higher in Na than Ca but where Na is not predominant Ca usually is (Roedder, 1972). The significance of high Ca fluids is uncertain but metamorphic fluids commonly contain high concentrations of Ca relative to Na or K (Crawford, 1981, p. 166, in Hollister, 1981). Inclusions from igneous rocks contain fluids with variable Ca content, dependent upon rock type (Roedder, 1972, appendix).

Several elemental ratios are useful in characterizing geologic fluids, among these the Na::K ratio is one of the most important (the ratios used are in terms of weight percent). Of geologic fluids in general, the Na::K ratio typically ranges from 10 to 1. Pre-mineralization quartz is anomalously low in this ratio due to a very high potassium content (Na::K = 0.4). The Bluebird samples range from about 3.0 to 1.5. No data are availiable from Link or Crescent samples but in the future their Na::K ratios should be determined to see if a trend exists which may be a useful indicator of vein paragenetic sequence. Most Mississippi Valley-type ore deposits are characterized by Na::K ratios of about 17, metamorphic fluids fluctuate widely on both sides of 1 and the ratios in igneous rocks are dependent upon their source chemistry (Roedder, 1972). A metamorphic source for the Bunker Hill ore-forming fluids is therefore in agreement with the observed Na::K ratios but an igneous component can not be ruled out.

The Ca::Mg ratio of the Bunker Hill fluids ranges widely from about 40 to about 4. Mississippi Valley-type fluids show a rather uniform Ca::Mg ratio between 8 and 4 and other fluid-types deviate widely on both sides of this range (Roedder, 1972). The implications of the Bunker Hill ratios are uncertain.

The K::Cl ratios of the Bunker Hill fluids are similar to those of Mississippi Valley-type deposits. Main-stage mineralization fluids from Mississippi Valley-type deposits show ratios of about 4000 ppm K::115 ppt Chloride in the region where the Alberta Basin fluids also have this same ratio (Hanor, 1979, p. 161-fig. 4.9, in Barnes, 1979). The Bunker Hill fluids show ratios of about 4000 ppm K::80-90 ppt Chloride, plotting close to and just above the above examples. No conclusions as to the source of the fluids can be made from this ratio because both igneous and sedimentary fluids have been observed with similar ratios (Roedder, 1972, appendix).

The Na::Cl ratios of the Bunker Hill fluids are anomalously low in comparison with most Mississippi Valley-type fluids. Whether this reflects a sodium deficient source rock or if fluid geochemistry is the major control upon sodium content is uncertain.

Calculated temperatures are generally higher than the recorded T_h's (fig. 68). This is in agreement with the interpretation that the observed T_h's are minimum, rather than true, temperatures of formation. Note that the pre-mineralization quartz (fig. 68, sample 21) has a significantly higher calculated temperature than any of the Bluebird samples (all other samples). The next highest calculated temperatures are those from the 14 Brown quartz

SAMPLE	T degrees Kelvin	T degrees C
15	611-605	338-332
17	588-584	315-311
18	633-627	360-354
19	554	281
21	756-748	483-475
22	588-584	315-310
23	542-539	269-266

Figure 68: The temperatures shown were calculated from the analytical results of Table 5 in the appendix. The following salt-geothermometer equation was used:

$$1000(T \cdot K)^{-1} = A(\log_{10}((Na)(K)^{-1}) +$$

$$1/3 \log_{10}((Ca)^{0.5}(Na)^{-1})) + 1.3745$$

The concentrations of the elements are in molality and the term 'A' is a constant equal to (0.6151). This equation was derived by David Norman from the data of Fournier and Truesdell (1973).

(sample 18) and 14 Brown sphalerite analyses (sample 15). These temperatures indicate that the 14 Brown orebody may have formed at slightly higher temperatures than the Quill orebody (samples 17, 19, 22 and 23). Caution is advised in relying heavily on the salt geothermometer because the data used to calibrate it are limited and begin to diverge in temperature range of interest here. The error due to minor Ca contamination by the crush-tubes, previously discussed, will not significantly change the calculated temperatures (about $5^{o}C$ change).

CONSTRAINTS ON GENETIC MODELS:

My discussion of genetic models will be confined to the explanation of the ore deposits as they exist today. No consideration will be given as to whether or not syn- or diagenetic orebodies exist in the district since the deposits studied do not display these characteristics in their present form.

Of the most basic characteristics of the ore deposits and of the most controversy in the Coeur d'Alene district is the category of origin of the ore-forming fluids: igneous, metamorphic, meteoric etc... . The results of this study strongly support a metamorphic source for the mineralizing fluids: In particular high N_2 content fluids have only been observed from sedimentary rocks, which indicates that an igneous source is very unlikely. Unless future studies indicate that N_2 exists in igneous environments the presence of this gas in the Belt Supergroup mineralizing fluids can be considered as characteristic of a metamorphic origin (David Norman). The relation of N_2 content to the grade of the metamorphic fluid is uncertain. It is also recognized that sedimentary basins and oil-natural gas-fields in particular, may contain N_2-rich fluids. The origin of these fluids is not clearly understood by the author but is suspected to be related to some of the same processes of basin maturation.

Of the other major problems concerning the genesis of the Coeur d'Alene ore deposits, most prominent is the mechanism of deposition. The necessity for linked replacement reactions has been discredited by the textural observations indicating the presence of open space deposition in a not strictly volume for volume sequence of mineral deposition. The problem now lies in the nature of the fluid phases present at any time of mineral deposition or dissolution.

From the gas analyses it is evident that the Bunker Hill ore deposits were formed in an environment in which at least three principle phases were present. A conventional explanation for multiple phases would be to suggest that 'boiling' had occurred. It is necessary, however, to assess the possibility of generating heterogeneous fluids by mechanisms other than 'boiling'. Studies of metamorphic fluids indicate that CO_2 enriched, or relatively pure CO_2 inclusions exist along with aqueous fluid inclusions (Crawford, 1981 and others). In the case of the Bunker Hill fluids, N_2 rich phases are also present. Since under no conditions should two gaseous phases be present with a third aqueous phase if normal Henry's law 'boiling' occurs, we must look to more complex models to explain the existence of the observed phases. It is important to distinguish between Henry's law 'boiling' and other possible multiple phase generating mechanisms because they imply the possibility of

unique environments of deposition, especially in terms of depth, quite different then that which would be hypothesized from a conventional interpretation.

Two general categories of genetic models may be constructed: Those that incorporate a form of Henry's law boiling at some time during the fluid evolution and secondly, those that do not. The models that do not rely upon a Henry's law boiling mechanism require fluid immiscibility. The first category of models incorporating Henry's law boiling may also incorporate immiscibility. The cause of immiscibility may be regarded as indeterminate for the present time and encompass all non-Henry's law dependent, phase separating phenomena.

To begin with, it should be noted that it is impossible to generate the Link and Crescent fluids from Bluebird or pre-mineralization fluids by Henry's law boiling alone without immiscibility or 'gas charging'. An explanation of this is given in a logic diagram (fig. 69). It should also be noted that evidence for immiscibility during Bluebird mineralization has already been given.

Figure 69. Logic diagram explaining the necessity for fluid immiscibility during evolution of the Crescent and Link fluids (next page). If case A is correct, then gas charging is required if a boiling model with one homogeneous source fluid is assumed.

Crescent quartz:

if:

Bulk fluid Composition of runs 328-9:
88.95 mol % H2O
9.4 mol % CO2
1.14 mol % N2

is composed of:

Aqueous Inclusions + Gaseous Inclusions- (Must be CO2 rich because runs 330-1 have a CO2::N2 = 2)

CASE A: But if the gaseous inclusions have a CO2::N2 of only 2, then the aqueous inclusions must have 7 mole % CO2 (too high?).

CASE B: If the aqueous inclusions have only about 2 mole % CO2, then the CO2::N2 in the gaseous phase is (7.33::1.14). This requires a 3 phase immiscibility.

Note: In either case A, Crescent or Link, if boiling has occurred it can generate a gaseous phase as predicted by Henry's law. A phase immiscibility or gas charging is required to evolve these fluids from Bluebird fluids. Crescent aqueous fluids can not be evolved from Link fluids by simple Henry's law 'boiling'.

Figure 69 continued. Link quartz:

if:

Bulk fluid Composition
Runs 306-7 or 320-1:
94-93 mole % H2O
6::1 mole % CO2::N2

is composed of:

Aqueous Inclusions + Gaseous Inclusions (must be CO2 rich because runs 326-7 have a CO2::N2 = 5::6)

CASE A: If the CO2::N2 of the gaseous inclusions is only 5::6, then 5 mole % CO2 must be in the aqueous inclusions (too high?).

CASE B: If less than 2 mole % CO2 is in the aqueous inclusions, then the CO2::N2 of the gaseous inclusions must be at least 4::1. Comparing to runs 326-7, this requires immiscible gaseous fluids in addition to the aqueous phase.

The next point to consider is whether Henry's law boiling of N_2 and the calculated proportions of other gases occurred. The evolutionary sequence of pre-reverse shear quartz, Bluebird, Link and Crescent quartz shows a definite CO_2::N_2 increase in the gas fractions of the aqueous phases. Upon close examination it is apparent that much of this trend- if not all, is due to an increase in the CO_2 content of the aqueous phases and not to the removal of CO_2 with the 'boiling' off of N_2. As N_2 is the most insoluble and the predicted phase to boil-off, an explanation of the observed trends requires a more complex model than simple Henry's law boiling- even with the presence of immiscible phases. At the very least these fluids could not have evolved from one homogeneous source by Henry's law boiling without a mechanism of CO_2 'charging'. It is possible that the fluid source has undergone evolution, such as during the basin metamorphic history, and become more CO_2 rich with time. This would add to the simplification and plausibility of a Henry's law model incorporating immiscibility.

If one assumes a Henry's law boiling model, another question to ask is: Did the boiling occur insitu or at depth at a level removed from that of mineralization? The disparity of homogenization temperatures of coexisting gaseous and aqueous inclusions and the presence of immiscible phases reject an insitu boiling hypothesis. Boiling at levels deeper than mineralization is a

possibility which the present data can neither credit nor discredit.

The second category of models, those that do not require a Henry's law boiling mechanism, should be regarded as hypothetical but real possibilities. The first of these is the possible generation of excess gases, notably CO_2, N_2 and organic compounds, beyond that soluble in a confined, single aqueous phase. The generation of these fluids is distinguished from boiling in that they may be spacially distant, in terms of time and distance, from the ore deposits they may later form. To be more specific, these hypothetical fluids could be regarded as metamorphic, multiphase, basin fluids (a metamorphic equivalent of conate formation waters). It is expected that these heterogeneous multiphase fluids could vary considerably during migration, in the proportion of any single phase present, due to the different viscosities and surface tensions of the phases.

A second model in the non-Henry's law category involves the generation of immiscible phases in which the gaseous to aqueous phase ratios are fixed by a controlling equilibrium, largely a function of T, P and availiable components. Such systems as the H_2O-CO_2-NaCl system are partially described in the literature (Pichavant, et al., 1982, Sisson, et al., 1981, Roedder and Franck, et al.,- in Rickard and Wickman, 1979). As of the writing of this paper, little is known of

the behaviour of the H_2O-CO_2-N_2-Organics-$CaCl_2$-NaCl system most pertinent to this study. Liquid immiscibility has been reported in the H_2O-CO_2-$CaCl_2$ system at a pressure of 1 kbar and temperatures of 500 to 600°C (Shmulovich, et al., 1982). Shmulovich, et al., also indicate that the region of fluid homogeneity is narrower for $CaCl_2$ solutions than for NaCl or KCl solutions under similar conditions. This means that an increase in $CaCl_2$ content will increase the field of liquid immiscibility over a greater range in temperature, pressure and composition relative to other salts.

It is assumed that the above models probably involve subcritical behaviour of the aqueous phase at the lower temperature regions within the immiscibility fields. If supercritical behaviour of the aqueous phase, or a mixture of sub- and supercritical behaviours occurred, many new mechanisms for generating multiphase fluids may be possible. No further discussion of a possible role of supercritical fluids will be given here because of time limitations and the probability that new studies may be necessary to discuss this subject intelligently. An investigation of the possiblility of trapping supercritical fluids during mineralization is needed, but may have to wait for the establishment of boundaries for the critical and immiscibility fields in terms of minimum pressures and temperatures for any possible phase compositions. If the fluids were supercritical during entrapment then fluid

immiscibility must exist in this state, which has been indicated to occur (Shmulovich, et al , 1982). Specifically, Shmulovich, et al., indicate that there may be a lack of complete miscibility at 1 kbar at any temperature at salt concentrations greater than 6 wt.% in the H_2O-CO_2-NaCl system. $CaCl_2$ is indicated to have a stronger supercritical salting-out effect than NaCl and increase the probibility of open-ended immiscibility.

Within the framework of any chosen model explaining the occurrence of multi-phase fluids, the parameters of pH, f_{O_2}, f_{S_2} etc. can be considered. These variable parameters are considered to be of secondary importance in modeling only as they do not determine how the multiple phases are generated. These parameters are functions in the mathematical sense, of the phases present and may be different in each of the coexisting phases (gas fugacities probably are, pH variability is uncertain). As the metals are probably carried in the aqueous phase, it is recognized that the modeling of this phase alone may provide useful results. Gas fugacities may be calculated directly from the gas analyses as done in this thesis. The effects of any coexisting phases should, however, be taken into account.

One important consideration in modeling concerns the source of the sulfide sulfur. The gas analyses indicate a high probability that sufficient H_2S is carried in the

combined fluids so that no other source is needed.

The increase in F_{CO_2} within the aqueous phase in the sequence; premineralization quartz-Bluebird-Link-Crescent quartz, rejects an increase of pH as the principle mechanism of deposition of the Pb-Ag ores (at least an increase of pH by the decrease of the concentration of dissolved CO_2). The CO_2 trend indicates that Pb chloride complexes would increase in solubility if aqueous phase control of pH by f_{CO_2} occurred. This trend should, however, have bearing upon some of the redissolution and replacement textures observed.

CONCLUSIONS:

Several important conclusions concerning the characterization of the fluids forming the Bunker Hill and Crescent ore deposits may be made from this study, summarized as follows:

1. The fluids of each of the representative types of mineralization; Bluebird- Zn, Link- Pb and Crescent- Ag and Cu, contain widely varying amounts of gases. Both aqueous and gaseous fluid inclusions were observed from all of the vein systems.

2. The gas content of all the veins may be characterized as being high in N_2 and CO_2. Organic compounds are present in varying amounts, often being a

major gas in the non-aqueous inclusions. Hydrogen is present in significant amounts, the quantification of which is uncertain due to analytical problems. Lesser amounts of H_2S, SO_2 and Ar are also present.

The gas compositions of individual inclusions are variable within any single sample. The various types of inclusions decrepitate at different temperatures. This enables the compositions of the aqueous phases to be distinguished from the compositions of the gaseous phases.

Definite compositional trends exist in the gas-fractions of the aqueous fluid inclusions between the orebodies, summarized as follows: pre-mineralization, pre-reverse shear milky quartz has a mole % N_2::CO_2 of 3, Bluebird quartz has a mole % N_2::CO_2 of 1 to 0.3, Link quartz- 5::6 to 1::4, and Crescent quartz- 1::2 to 1::8. CH_4 content decreases in the series, C_2H_n increases, H_2S increases and SO_2 and Ar remain approximately constant.

3. If Henry's law boiling occurred N_2 would be the gas boiled off. It is uncertain whether or not Henry's law boiling has occurred.

4. Numerous indications of immiscible fluids have been observed. It is likely that any model explaining the genesis of the Bunker Hill ores will require a form of immiscibility. The origin of the immiscibility is

uncertain. Three phases appear to be involved in the liquid immiscibility observed; an aqueous phase with low CO_2 content, a gaseous phase with high CO_2 content, and a gaseous phase with high N_2 and organic compounds. Whether or not all three phases are simultaneously present and in equilibrium is uncertain.

5. The presence of abundant hydrocarbons in combination with other observations- most notably the high N_2 content of the fluids, indicates a deep-basin brine as the mineralizing fluid. It is probably of a sedimentary-metamorphic source.

6. Minimum temperatures of formation by fluid inclusion homogenization are 265-250°C. Some higher temperature T_h's were observed but stretching or partial decrepitation may have been involved in the generation of these inclusions. Gaseous and aqueous inclusions did not homogenize at similar temperatures.

7. A Bluebird salinity of 10-13 eq. wt.% NaCl was observed. No salinity was measureable for Link or Crescent quartz, presumably due to the high gas content of their inclusions.

8. Gas-hydrates were observed in Bluebird, Link and Crescent inclusions. A bimodal distribution in decomposition temperature was observed, with Bluebird quartz

gas-hydrates centered on +5°C and Link and Crescent quartz centered on +10 to +12°C. The difference in decomposition temperatures is interpreted as representing contrasting gas composition and concentration.

9. Analysis of fluid inclusion leachates from Bluebird samples indicates that $CaCl_2$ is the dominant salt in the brines followed by NaCl and KCl. Pre-mineralization, pre-reverse shear quartz showed KCl equal to $CaCl_2$ with lesser NaCl. Cl^- is the dominant anion, with only traces of SO_4 detected. Pb and Mg were also detected.

10. H_2S is the dominant sulfur species indicating a reducing environment of low f_{O_2}. The abundance of pyrite and lack of pyrrhotite (except in rare cases) indicate that the f_{O_2} may be roughly characterized.

11. Minimum pressures of formation of about 300 to 400 bars have been calculated for Bluebird aqueous fluids thru the Henry's law gas solubilities.

REFERENCES

Armstrong, R. L., 1975?, The Geochronometry of Idaho: Bunker Hill files, Univ. of British Columbia.

Arnold, R. G., Coleman, R. G., and Fryklund, V. C., 1962, Temperature of Crystallization of Pyrrhotite and Sphalerite from the Highland-Surprise Mine, Coeur d'Alene District, Idaho: Econ. Geol., v. 57, p. 1163-1174.

Barnes, H. L., 1979, Geochemistry of Hydrothermal Ore Deposits: QE390.B37 1969 553'.19 79-354, John Wiley and Sons.

Beck, J. W., 1980, Sulfide Ores within the Quill Ore Body, Bunker Hill Mine, Kellogg, Idaho: Unpub. M.S. thesis, Washington State Univ., 129 p.

Bennett, E. H. and Venkatakrishnan, R., 1982, A Palinspastic Reconstruction of the Coeur d'Alene Mining District based on ore deposits and structural data: Econ. Geol., v. 77, p. 1851-1866.

Bodnar, R. J. and Bethke, P. M., 1984, Systematics of Stretching of Fluid Inclusions 1: Fluorite and Sphalerite at 1 Atmosphere Confining Pressure: Econ. Geol., v. 79, p. 141-161.

Collins, P. F., 1979, Gas Hydrates in CO2-Bearing Fluid Inclusions and the Use of Freezing Data for Estimation of Salinity: Econ. Geol., v. 74, p. 1435-1444.

Cramer, S. D., 1982, The Solubility of Methane, Carbon Dioxide, and Oxygen in Brines from 0 to 300°C: U. S. Dept. of the Interior, Bureau of Mines, Report of Investigations 8706, 17 p.

Fournier, R. O. and Truesdell, A. H., 1973, An empirical Na-K-Ca geothermometer for natural waters: Geochimica et Cosmochimica Acta, v. 37, p. 1255-1275.

Harrison, J. E., 1972, Precambrian Belt Basin of Northwestern United States: Its Geometry, Sedimentation, and Copper Occurrences: Geol. Soc. America Bull. v. 83, p. 1215-1240.

Harrison, J. E., Griggs, A. B. and Wells, J. D., 1974, Tectonic Features of the Precambrian Belt Basin and their Influence on Post-Belt Structures: U. S. Geol. Survey Prof. Paper 866, 15 p.

Hershey, O. H., 1912, Genesis of the Silver-Lead Ores in the Wardner District, Idaho: Mining and Scientific Press, Bunker Hill files, 32 p.

Hershey, O. H., 1913, Origin of Lead, Zinc, and Silver in the Coeur d'Alene-1: Mining and Scientific Press, Bunker Hill files, p. 489-493. Origin of Lead, Zinc, and Silver in the Coeur d'Alene-2: Same source, p. 529-532.

Hershey, O. H., 1916, Origin and Distribution of Ore in the Coeur d'Alene: Private report to the Hecla Mining Company, Bunker Hill files, 31 p.

Hobbs, S. W. and Fryklund, V. C., 1968, The Coeur d'Alene District, Idaho: Ore Deposits of the United States, 1933-1967: Ridge, J. D., ed.: New York, Am. Inst. Mining Metall. Petroleum Eng., Inc., p. 1417-1435.

Hobbs, S. W., Griggs, A. B., Wallace, R. E., and Campbell, A. B., 1965, Geology of the Coeur d'Alene District, Shoshone County, Idaho, U.S. Geol. Survey Prof. Paper 478, 139 p.

Hollister, L. S. and Crawford, M. L., 1981, Mineralogical Association of Canada, Short Course in Fluid Inclusions: Applications to Petrology: Mineralogical Assoc. of Canada, Short Course Handbook, Vol. 6, May 1981, 304 p.

Juras, D., 1977, Structural Geology of the Bunker Hill Mine: Private report to the Bunker Hill Co., 111 p.

Kozlovsky, Y. A., 1984, The World's Deepest Well: Scientific American, Vol 251, Number 6.

Landis, G. P. and Leach, D. L., 1983, Silver-Base Metal Mineralization as a Product of Metamorphism: Coeur d'Alene District, Shoshone County Idaho: GSA Abstracts with Programs 1983, Vol 15, Number 5.

Landis, G. P., Leach, D. L. and Hofstra, A. H., 1984, Silver-Base Metal Mineralization as a Product of Metamorphism- Coeur d'Alene District, Shoshone County, Idaho: Concepts of Genesis: MBMG Belt Symposium 2, 1983, Special Publication 90- "The Belt", Warren Hobbs, Ed.

Leach, D. L. and Hofstra, A. H., 1983, Fluid Inclusion Studies in the Coeur d'Alene District, Idaho: GSA Abstracts with Programs 1983, Vol 15, Number 5.

Long, A., Silverman, A. J. and Kulp, J. L., 1960, Isotopic Composition of Lead and Precambrian Mineralization of the Coeur d'Alene District, Idaho: Econ. Geol., v. 55,

p. 645-658.

Meyer, R. L., 1977, Geology of the Bunker Hill Mine: S.E.G. Coeur d'Alene Field Conference Notes, Nov. 3-5, 1977, 5p.

Mills, J., 1980, Correspondance to Bob Meyer, Bunker Hill files, 2p.

Naumov, G. B., Ryzhenko, B. N. and Khodakovsky, I. L., 1974, Handbook of Thermodynamic Data: NTIS report PB 226 722, (328 p.) p. 246-7.

Nehring, N. L. and D'Amore, F., 1981, Gas Chemistry and Thermometry of the Cerro Prieto Geothermal Field: Preprint: Proceedings of the Third Symposium on the Cerro Prieto Geothermal Field, Baja Cal., Mexico, March 1981. To be published by LBL, 6 p.

Pichavant, M., Ramboz, C. and Weisbrod, A., 1982, Fluid Immiscibility in Natural Processes: Use and Misuse of Fluid Inclusion Data 1. Phase Equilibria Analysis- A Theoretical and Geometrical Approach: Chemical Geology, v. 37, p. 1-28.

Putnam III, B. R., 1980, Fluid Inclusion and Microchemical Analysis of the Hansonburg Mississippi Valley-Type Ore Deposits in Central New Mexico: Unpub. M.S. thesis, New Mexico Institute of Mining and Technology, 126 p.

Radford, N. A., 1973, Geology of the Crescent Mine and its Relationships to the Coeur d'Alene Silver Belt: Paper presented at the 1973 Pacific NW Metals and Minerals Conf., Bunker Hill files, 13 p.

Ramalingaswany, V. M., 1975, Stratiform Mineralization and Origin of Vein Deposits, Bunker Hill Mine, Coeur d'Alenes, Idaho: Unpub. M.S. thesis, Univ. of Washington, 46 p.

Ramalingaswany, V. M. and Cheney, E. S., 1982, Stratiform Mineralization and Origin of some of the Vein Deposits, Bunker Hill Mine, Coeur d'Alene District, Idaho: in SEG Coeur d'Alene Field Conference, Idaho- 1977: Idaho Bureau of Mines and Geology, Bulletin 24, May 1982, edited by Reid, R. R. and Williams, G. A.

Ramboz, C., Pichavent, M. and Weisbrod, A., 1982, Fluid Immiscibility in Natural Processes: Use and Misuse of Fluid Inclusion Data 2. Interpretation of Fluid Inclusion Data in terms of Immiscibility: Chemical Geology, v. 37, p. 29-48.

Ransome, F. L. and Calkins, F. C., 1908, Geology and Ore Deposits of the Coeur d'Alene District, Idaho: U.S. Geol. Survey Prof. Paper 62, 203 p.

Roedder, E., 1972, Composition of Fluid Inclusions: U.S. Geol. Survey Prof. Paper 440 JJ, 164 p.

Roedder, E. and Franck, E. U., in Rickard, D. T. and Wickman, F. E., 1979, Chemistry and Geochemistry of Solutions at High Temperatures and Pressures: Natural Occurrence and Significance of Fluids Indicating High Pressure and Temperature: QE 501 .P53 v. 13-14, Pergamon Press, p. 9-87.

Sisson, V. B., Crawford, M. L. and Thompson, P. H., 1981, CO2-Brine Immiscibility at High Temperatures, Evidence from Calcareous Metasedimentary Rocks: Contrib. Mineral. Petrol., v. 78, p. 371-378.

Sorensen, A. E., 1969, Geological Research Progress 1966-1967: Private report to Hecla Mining Co., Wallace, Idaho, 104 p.

Shmulovich, K. I. and Kotova, P. P., 1982, Mineral Equilibria in a Hot H_2O-CO_2-Electrolyte Fluid: Geochemistry International, v. 19, No. 5, p. 146-160.

Walker, W., 1977, Discussion- Metallogenesis in the Coeur d'Alene: Unpub. Correspondence, 7 p., Bunker Hill files.

White, B. G. and Winston, D., 1977, The Revett/St. Regis "Transition Zone" near the Bunker Hill Mine, Coeur d'Alene Mining District, Idaho: Unpub. manuscript, Bunker Hill Co. files, 7 p.

Windley, B. F., 1977, The Evolving Continents: QE511.5.W56, John Wiley Sons Ltd. 385 p.

APPENDIX TABLE OF CONTENTS:

GAS ANALYSES

Table 1 in the appendix lists the results for gas analyses of fluid inclusions by the method of thermal decrepitation.

Samples were selected which contained at least 5 or 10 grams of homogeneous crystal, if possible. Some samples were smaller in size, such as the Crescent quartz, due to the small amount of material availiable. Each sample was crushed to less than 0.5 cm pieces and the fine dust screened out. Samples were then inspected for impurities under a low power microscope and chemically cleaned as follows; a wash with distilled H_2O, soaking for three hours in alcohol to remove organic impurities, a wash with distilled H_2O, boiled overnight in HNO_3, washed 10 times with distilled-deionized H_2O, boiled overnight in d.d. H_2O, given a final washing and dried out at 85^oC.

Samples were then placed in a quartz furnace and evacuated to below 2×10^{-5} atm. Helium tests were made to determine if air leaks were present. When ready to run, a background reading was taken on the mass spectrometer and the sample heated to the desired temperature. A liquid N_2 trap was placed on the line to the mass spectrometer to separate the fluid inclusion gases into condensable and non-condensable fractions. A dry ice and alcohol trap was placed before this to help freeze out H_2O. An effort was

made to heat the samples at similar temperatures and lengths of time- usually 550°C for 20 minutes. The samples were left open to the gas freezing traps for a while- until the P_{cm} (capacitance monometer) stabilized and only non-condensable gases were left to indicate their pressure, which was recorded. The non-condensable gases were then run thru the mass spectrometer and a visual check of the spectra made on a cathode ray tube display. At this point air leaks could be detected by the presence of He and major gas spectra. After recording the sample and background readings on magnetic tape the line was evacuated of residual non-condensable gases. The liquid N_2 trap was removed- allowing the condensed gases to vaporize with any H_2O freezing out in a dry ice-alcohol trap after about 30 minutes equilibration. The condensable gases were then run thru the mass spectrometer, a visual check of gases made and data stored on magnetic tape.

Two methods were used to measure the H_2O content. When the H_2O content was large enough to be weighed, it was frozen in a capillary tube of pre-determined weight. If not, the only recourse was to measure the pressure of the H_2O gas- via the capacitance monometer. The relation; Grams $H_2O = KP_{cm}$, was used to calculate the amount of H_2O in samples marked with an asterisk(*) in Table 1 (K is a function of the curve relating the pressure on the capacitance monometer to the amount of water present in the

confined volume). This is based on a calibration curve made by thermally decrepitating different known weights of biotite having a known H_2O content. The calculated wt.% H_2O values in Table 1 seem generally reasonable or slightly low. Runs 365-366 should probably have a value of about 95 wt.% H_2O, as in runs 337-338, instead of only 57.1 wt.% H_2O as calculated. Regardless of a possible undercalculation of about 30 %, the P_{cm} H_2O values do show the anomalously high gas wt.% inclusion types well. These are mainly the higher thermal decrepitation temperature, stepwise heated runs. H_2O weights were immeasurable in these run types when the capillary method was used (runs 330-1 and 326-7). Measurements made by the capillary method are reproducible, and probably accurate- especially when more than 1 mg of H_2O was present. Runs 306-7 and 320-1 show close agreement and are an example of the excellent reproducibility obtained by this method.

Gas contents were calculated using the "CALC.3" program which utilizes a matrix calculated from the run data to derive mass spectral 'line' values and residuals for the given gases present. The fractionation factors used were modified for H_2S, SO_2, CH_4, C_2H_n and C_3H_n to eliminate interference from peaks shared with major gases (fig.70). The sulfur gases and organics were calculated on the basis of their most distinctive peaks.

Figure 70. Modifications to the "CALC.3" program:

		<---- gas fraction, less H_2O - ---------->								
SAMPLE NUMBER	H_2O	N_2	CO_2	CH_4	C_2H_n	C_3H_n	H_2S	SO_2	Ar	Notes:
Runs 328-329	79.6	06.9	89.3	0.23	1.75	1.49	0.07	0.21	0.04 wt.%	T_d = 550°C, Hook
41-11-7E Qtz		10.3	84.9	0.61	2.44	1.42	0.09	0.14	0.04 mol%	vein, Crescent mine
330-331	????	23.6	71.8	0.51	2.32	1.47	0.05	0.18	0.07 wt.%	stepwise T_d = 750°C
		32.2	62.2	1.22	2.95	1.28	0.05	0.11	0.07 mol%	same sample
Runs 345-346	12.1	0.90	98.0	.004	1.01	----	,015	0.02	.003 wt.%	T_d = 400°C, Hook
41-11-7E Sid		1.40	97.1	0.01	1.47	----	0.02	.015	.004 mol%	vein, Crescent mine
Runs 306-307	86.8	12.9	85.9	????	????	????	0.06	0.21	0.37 wt.%	T_d = 550°C
19'J' Qtz		18.8	79.6	????	????	????	0.08	0.13	0.37 mol%	pre-existing xl
Runs 320-321	88.3	12.5	82.5	0.41	2.03	1.97	0.05	0.50	0.05 wt.%	T_d = 490°C, part of
19'J' Qtz		18.0	76.0	1.03	2.73	1.81	0.06	0.32	0.05 mol%	same crystal (xl)
326-327	????	17.3	32.6	2.71	8.88	3.95	0.95	33.6	0.11 wt.%	stepwise T_d = 750°C
		25.0	30.0	6.85	12.0	3.64	1.14	21.3	0.11 mol%	same sample
Runs 351-352	96.7	14.7	68.1	0.19	3.36	4.31	0.72	8.27	0.16 wt.%	T_d = 400°C
25 Francis Sph		21.4	63.0	0.50	4.83	4.00	0.87	5.26	0.17 mol%	
Runs 359-360	81.2*	17.5	52.5	0.68	8.85	19.9	0.03	0.39	0.22 wt.%	T_d = 550°C,
9 Jersey Milky Qtz		23.9	45.5	1.63	11.3	17.2	0.03	0.24	0.21 mol%	pre-mineralization(?)
361-362	15.3*	11.6	30.8	0.42	19.7	26.6	0.89	9.84	0.21 wt.%	stepwise T_d = 750°C,
		16.0	27.1	1.01	25.4	23.4	1.01	5.95	0.20 mol%	same sample

TABLE 1: GAS ANALYSES RESULTS

		<---- gas fraction, less H_2O ---------->								
SAMPLE NUMBER	H_2O	N_2	CO_2	CH_4	C_2H_n	C_3H_n	H_2S	SO_2	Ar	Notes:
Runs 335-336	88.8	21.4	55.3	3.36	8.91	6.89	0.88	3.12	0.12 wt.%	T_d = 550°C
110-35-21 Qtz		27.6	45.5	7.60	10.6	5.67	0.94	1.77	0.11 mol%	pre-existing xl
Runs 304-305	lost	19.9	51.0	1.29	3.90	7.55	0.21	15.1	.029 wt.%	(NO = 1.04 wt.%),
120-35-21 Qtz		28.0	45.8	3.20	5.14	6.80	0.25	9.36	.028 mol%	T_d = 550°C, smoky vein Qtz ass/w deconsolidation.
Runs 233-234	97.6	37.3	54.7	5.04	0.99	1.58	0.12	0.14	0.12 wt.%	T_d = 550°C, Main Stage
100-35-24 Qtz		44.9	41.9	10.6	1.11	1.21	0.12	.074	.098 mol%	Bluebird vein
Runs 363-364	27.9*	21.2	50.2	1.88	8.78	15.2	,169	2.42	0.14 wt.%	stepwise T_d = 750°C
100-35-24 Qtz		28.1	42.2	4.34	10.8	12.8	,184	1.40	.129 mol%	7-15-81B
Runs 347-348	lost	26.2	56.8	0.35	6.12	6.63	0.25	3.72	---- wt.%	T_d = 400°C
100-35-24 Sph C		35.0	48.4	0.82	7.65	5.65	0.28	2.18	---- mol%	
Runs 349-350	5.66*	0.39	75.6	.013	4.55	4.49	0.42	14.5	.002 wt.%	T_d = 400°C
100-35-24 Gal										P^d_{cm} = 0.000*
Runs 222-223	97.0	36.2	57.8	1.01	0.67	2.59	,145	1.21	0.42 wt.%	T_d = 500°C
110-35-24 Qtz		46.5	47.2	2.26	0.80	2.11	0.15	0.69	0.38 mol%	
Runs 230-231	????*	25.4	71.9	.072	0.33	1.30	0.37	0.27	0.32 wt.%	T_d = 550°C
110-35-24 Qtz										
Runs 256-257	lost									

		<---- gas fraction, less H_2O ---------->								
SAMPLE NUMBER	H_2O	N_2	CO_2	CH_4	C_2H_n	C_3H_n	H_2S	SO_2	Ar	Notes:
Runs 260-261 110-35-24 Qtz	95.0	33.6 43.0	42.5 34.6	0.84 1.89	5.22 6.23	15.8 12.9	0.44 0.47	1.30 0.73	0.31 wt.% 0.28 mol%	T_d = 550°C
Runs 353-354 110-35-24 GA Qtz	97.5	34.6 44.1	52.0 42.3	0.99 2.21	3.53 4.20	8.30 6.74	,031 ,033	0.18 0.10	0.36 wt.% 0.32 mol%	T_d = 300°C
355-356	67.4*	15.0 19.5	72.4 60.0	6.18 14.1	2.88 3.49	3.38 2.80	,020 ,021	0.10 .059	----- wt.% ----- mol%	stepwise T_d = 500°C (NC peaks off center), same sample.
357-358	8.17*	15.7 22.2	78.6 70.9	0.40 0.98	2.46 3.26	2.70 2.44	,027 ,031	0.11 .070	0.05 wt.% 0.05 mol%	stepwise T_d = 750°C, same sample.
Runs 336-337										
Runs 312-313 110-35-21	43.4	75.0 82.0	22.4 15.6	0.32 0.61	0.43 0.44	1.30 0.90	,018 ,016	.035 .017	0.19 wt.% 0.15 mol%	T_d = 540°C (NO = 0.33 wt.%), Milky Qtz.
Runs 341-342 110-35-21A	74.9	59.3 61.5	28.9 19.1	9.88 18.0	0.56 0.54	1.05 0.70	,013 ,011	0.16 .072	0.18 wt.% 0.13 mol%	T_d = 550°C, Milky Qtz, pre-reverse shear, pre-mineralization.
343-344	36.3*	49.7 54.8	24.5 17.2	6.36 12.3	7.36 7.58	9.42 6.62	,033 ,030	2.19 1.06	0.47 wt.% 0.37 mol%	stepwise T_d = 750°C, same sample
Runs 316-317 14 Brown Sph	lost	43.2 51.7	40.3 30.7	1.45 3.04	8.97 10.0	5.26 4.00	,075 ,074	0.56 0.30	0.21 wt.% 0.17 mol%	T_d = 380°C

		<---- gas fraction, less H_2O ---------->								
AMPLE NUMBER	H_2O	N_2	CO_2	CH_4	C_2H_n	C_3H_n	H_2S	SO_2	Ar	Notes:
ıns 238-239	lost	35.6	60.9	2.30	----	----	,038	.064	1.09 wt.%	T_d = 550°C
Brown Qtz		45.0	48.9	5.09	----	----	,040	.035	0.96 mol%	single crystal
ıns 337-338	95.0	18.5	77.2	0.72	1.40	2.03	,008	.060	.060 wt.%	T_d = 550°C
Brown Qtz B		25.8	68.7	1.77	1.82	1.80	,009	.037	.059 mol%	
339-340	39.3*	24.9	63.2	1.05	4.76	5.63	,032	0.17	0.21 wt.%	stepwise T_d = 750°C,
		33.1	53.5	2.43	5.90	4.76	,035	0.10	0.20 mol%	same sample
ıns 365-366	57.1*	17.7	71.0	0.28	3.91	6.08	,038	0.72	0.22 wt.%	T_d = 400°C
Brown Qtz		24.8	63.3	0.69	5.11	5.42	,044	0.44	0.21 mol%	
367-368	1.42*	6.41	89.3	0.31	1.45	2.44	----	0.11	---- wt.%	stepwise T_d = 550°C,
		9.61	85.2	0.81	2.02	2.33	----	0.07	---- mol%	same sample
369-370	30.8*	20.7	23.5	1.03	19.3	34.4	0.17	0.77	.094 wt.%	stepwise T_d = 750°C,
		26.6	19.2	2.32	23.1	28.1	0.18	0.43	.084 mol%	same sample

Sample Number	$\frac{CO_2}{N_2}$	$\frac{N_2}{C_2 + C_3H_n}$	$\frac{CH_4}{C_2 + C_3H_n}$	$\frac{H_2S}{C_2 + C_3H_n}$	$\frac{SO_2}{C_2 + C_3H_n}$	$\frac{N_2}{Ar}$
328-9	8.24	2.67	0.158	0.0226	0.0350	243.
330-1	1.93	7.61	0.288	0.0126	0.0252	472.
345-6	69.4	0.952	0.830	0.0127	0.0101	373.
306-7	4.23	-----	-----	------	------	50.
320-1	4.22	3.96	0.227	0.0126	0.0701	356.
326-7	1.20	1.60	0.438	0.0727	1.36	219.
351-2	2.94	2.42	0.0566	0.0983	0.597	91.
359-60	1.90	0.839	0.0572	0.00112	0.0083	114.
361-2	1.69	0.328	0.0207	0.0207	0.122	80.
335-6	1.65	1.70	0.467	0.0573	0.108	249.
304-5	1.64	2.34	0.268	0.0208	0.785	990.
233-4	0.933	19.4	4.57	0.0524	0.0318	455.
363-4	1.50	1.19	0.184	0.00779	0.0593	218.
347-8	1.38	2.63	0.0617	0.0208	0.164	----
349-50						
222-3	1.02	16.0	0.777	0.0524	0.233	123.
230-1						

Table 2. Ratios used in comparing the gas analyses, in mole %.

Sample number	$\frac{CO_2}{N_2}$	$\frac{N_2}{C_2 + C_3H_n}$	$\frac{CH_4}{C_2 + C_3H_n}$	$\frac{H_2S}{C_2 + C_3H_n}$	$\frac{SO_2}{C_2 + C_3H_n}$	$\frac{N_2}{Ar}$
256-7						
260-1	0.805	2.25	4.57	0.0244	0.0382	154.
353-4	0.959	4.03	0.202	0.00302	0.00931	137.
355-6	3.08	3.10	2.24	0.00337	0.00939	----
357-8	3.19	3.89	0.172	0.00552	0.0123	449.
336-7						
312-3	0.190	61.2	0.455	0.0121	0.0125	552.
343-4	0.314	3.86	0.866	0.00208	0.0746	149.
341-2	0.311	49.6	14.5	0.00909	0.0587	461.
316-7	0.594	3.69	0.217	0.00527	0.0211	300.
238-9	1.09	----	-----	-------	------	47.
337-8	2.66	7.13	0.489	0.00259	0.0102	439.
339-40	1.62	3.11	0.228	0.00331	0.00922	164.
365-6	2.55	2.36	0.0655	0.00417	0.0421	117.
367-8	8.87	2.21	0.186	-------	0.0161	----
369-70	0.722	0.520	0.0453	0.00356	0.00847	315.

Table 3. Organic compound line spectra ratios.

SAMPLE	C2::C3	C3::C4	C4::C5	C5::C6	C3::C5	C2::C4
328-9	0.764	29.6	17.6	------	530.	22.6
330-1	0.737	22.9	8.57	------	196.	16.9
345-6	1.10	37.4	------	------	------	41.
306-7	0.523	22.8	7.30	0.333	166.	12.
320-1	0.504	9.25	6.91	1.06	63.9	4.6
326-7	0.413	12.2	2.16	1.20	26.4	5.
351-2	0.474	10.1	5.23	1.88	52.8	4.8
359-60	0.260	27.9	4.78	0.668	133.	7.25
361-2	0.583	12.6	5.91	0.88	75.	7.34
335-6	0.38	9.6	7.1	1.2	68.	3.65
304-5	0.30	13.	3.2	1.7	41.	3.9
233-4	0.49	19.	5.3	0.53	101.	9.31
363-4	0.48	21.	6.1	0.62	127.	10.
347-8	1.86	14.	4.0	1.6	58.	26.
349-50	0.85	11.7	2.4	1.8	28.	9.9
222-3	0.14	11.	13.5	0.99	150.	1.54
230-1	0.13	7.7	6.5	1.0	50.	1.0
256-7	------	------	------	------	------	------
260-1	0.20	11.9	3.8	------	45.	2.4
260'	0.24	10.5	3.5	0.94	37.	2.5
353-4	0.23	16.	6.9	------	109.	3.7
355-6	0.66	16.	6.5	1.1	101.	10.6
357-8	0.75	16.	13.	0.17	212.	12.
236-7	0.75	36.	------	------	------	27.
312-3	0.20	29.	4.3	0.68	126.	5.7
343-4	0.76	10.	4.5	0.29	46.	7.6
341-2	0.50	13.	5.4	0.24	71.	6.5
316-7	1.7	13.	6.3	1.1	82.	22.1
238-9	0.52	23.	4.2	0.26	96.	12.
337-8	0.43	31.	4.5	0.54	137.	13.
339-40	0.71	20.	8.7	------	170.	14.
365-6	0.46	20.5	3.0	0.53	62.	9.4
367-8	0.49	9.4	7.1	0.62	67.	4.6
369-70	0.36	30.	4.2	1.07	126.	11.

SAMPLE	grams H_2O	H_2O mol%	Gases mol%	CO_2 mol%	N_2 mol%	CH_4 mol%	C_2+C_3 mol%	Ar mol%	H_2S mol%	T°C
328-9	.0008	88.95	11.05	9.38	1.14	.067	.43	.0044	.0099	550
306-7	.0012	93.3	6.71	5.34	1.26	nil	nil	.025	.0054	550
320-1	.0023	94.1	5.86	4.45	1.055	.060	.27	.0029	.0035	490
359-60	.0002	89.65	10.35	4.71	2.47	.169	2.95	.022	.0031	550
351-2	.0016	98.49	1.51	0.95	0.323	.0075	.133	.0026	.013	400
335-6	.0002	93.75	6.25	2.84	1.72	.475	1.02	.0069	.059	550
233-4	.0081	98.7	1.32	0.552	0.592	.140	.031	.0013	.0016	550
222-3	.0140	98.5	1.47	0.692	0.682	.033	.043	.0056	.0022	500
353-4	.0012	98.7	1.27	0.537	0.560	.028	.139	.0041	.00042	300
260-1	.0016	97.6	2.37	0.821	1.02	.045	.435	.0066	.011	550
337-8	.0037	97.6	2.43	1.67	0.627	.043	.088	.0014	.00022	550
341-2	.0010	79.3	20.7	3.95	12.7	3.73	.257	.027	.0023	550

TABLE 4. Gas Analyses including water.

SAMPLE DESCRIPTIONS:

1) GAS ANALYSES SAMPLES:

Runs 222-3; 110-35-24 quartz, euhedral clear crystals from vugs in en echelon shears. Location 'A' about floor 12 (fig. 9, p 25).

Runs 230-1; 110-35-24 quartz, euhedral clear crystals from vugs in en echelon shears. Location 'A' about floor 12 (fig. 9).

Runs 233-4; 100-35-24 quartz, euhedral clear crystals from vugs in milky quartz shear which is within a main stage Bluebird vein. Sample location is the same as the photo in figure 22, at about W3650, N280 floor 5 (fig. 9, 'B'). Sphalerite and galena crystals were present in these vugs, including those of figure 22. Fluid inclusion samples are from the same location. A quartz crystal group with hydrothermal sericite was given to Mike Palin for possible study.

Runs 238-9; 14 Brown quartz, euhedral clear crystals within a shear zone. The shear zone consisted of crushed wall rock and abundant quartz shears- both milky and clear crystal quartz. Abundant, euhedral sphalerite crystals were present to 4 cm in size. Much of this euhedral sphalerite was light in color (honey colored) indicating a

low Fe content. This shear zone was bordered by main stage Bluebird mineralization which contained abundant pyrite. This run consisted of a single crystal.

Runs 260-1; 110-35-24 quartz, euheral clear crystals from vugs in en echelon shears. Location 'A', floor 12 (fig. 9).

Runs 304-5; 120-35-21 smoky vein quartz, associated with deconsolidation of wall rock (Revett quartzite). This smoky vein quartz showed no fluid inclusions large enough to study. Abundant parallel replacement intervals of sub-microscopic inclusions (unidentified) are believed to be responsible for the smoky color. This type of quartz was only observed to border (within about 100 feet) regions of deconsolidated wall rock and is probably a product of the deconsolidation process. The deconsolidation is post-main stage Bluebird mineralization.

Runs 306-7; 19 'J' quartz (20-16-31 floor 14), pre-existing crystal within a steel-galena vein. The 19 'J' is a E-W trending, highly sheared Link vein. This pre-existing crystal contained abundant, euhedral galena inclusions indicating contemporaneity with Pb deposition. The crystal was subhedral due to rolling within

the vein during shearing. Size 2cm.

Runs 312-3; 110-35-21 milky quartz, pre-mineralization, pre-reverse shear. Sample is from quartz in figure 18. This quartz was offset by later Bluebird sphalerite veins. Fractures within hand specimens showed late siderite, sphalerite and galena relative to the milky quartz. The orientation of the milky quartz vein is S75E 40N, bedding is S40E 55S.

Runs 316-7; 14 Brown sphalerite, euhedral crystals to 4 cm, color- honey yellow to "beer-bottle" brown in thin section. Contain euhedral solid quartz inclusions as well as fluid types. Unzoned. See 238-9 for more information.

Runs 320-1; same as 306-7.

Runs 328-9; 41-11-7E quartz, Crescent mine, Hook vein. Euhedral, clear quartz crystal in a vug in a siderite-tetrahedrite-quartz replacement vein. This vug contained euhedral siderite to 2mm, euhedral tetrahedrite to 4 mm and a single euhedral quartz crystal about 1 cm in length. Same as figure . This quartz showed parallel replacement intervals as indicated by fluid inclusion rows. Inclusions of solids were mostly of replaced siderite with possible ruby silvers. The exception is a sphalerite inclusion (fig. 33).

Collected by Rudy Kluiber with Dave Dalton.

Runs 330-1; same sample as 328-9.

Runs 335-6; 110-35-21 quartz, pre-existing subhedral crystal within a steel-galena vein. Contained abundant, euhedral galena inclusions. Located about N750 W4300 (fig. 9).

Runs 337-8; 14 Brown quartz, same as 238-9 but the sample consists of more than one crystal from the same vug.

Runs 339-40; same sample as 337-8.

Runs 341-2; same information as 312-13, but another sample.

Runs 343-4; same sample as 341-2.

Runs 345-6; 41-11-7E siderite, Crescent mine, Hook vein. This siderite showed parallel replacement intervals consisting of sub-microscopic unidentified inclusions in thin section. In hand specimen this siderite appeared to be of the replacement vein type. This hand specimen contained the vug from which runs 328-9 were made. Tetrahedrite veinlets were present in the hand specimen.

Runs 347-8; 100-35-24 sphalerite, euhedral, dark reddish-brown but transparent in thin section. Size to 1cm. Same location and information as runs 233-4.

Runs 349-50; 100-35-24 galena, euhedral- size to 1cm. Same location and information as runs 233-4.

Crystal form-octahedral.

Runs 351-2; 25 Francis sphalerite, boudined (?). This sphalerite was part of a slurry injection ("toothpaste-tube-injection"). The sphalerite was pre-existing and moderately sheared within a steel galena matrix. The sphalerite size was up to 3 cm in diameter, but fractured. This sample contained possible re-healed secondary inclusions- which may have formed during "slurry-injection". 25-Level of a steel-galena vein system, associated with Link (?) mineralization.

Runs 353-4; 110-35-24 quartz, euhedral, over 200 grams of clear crystals to 3 cm in length. The vug was in a near horizontal tension gash connecting a south dipping shear (The apparent dip about 45 degrees). The euhedral quartz crystals lined the bottom of the cavity and the top of the cavity was lined with equally large, clear to yellow calcite crystals. A euhedral galena crystal, 2 cm across, was present at the upper contact with the wall rock and was encased by the later calcite. A late sericitic gouge was also present. The wall rock contained psuedo-stratiform Pb mineralization leading from the contact with the galena crystal and

was of similar width. No depletion zone was present. Only minor sphalerite was found in this vug. Fluid inclusion study specimen 110-35-24 QSG was from this vug. Location 'A', floor 12 (fig. 9).

Runs 355-6; same sample as 353-4.

Runs 357-8; same sample as 353-4.

Runs 359-60; 9 Jersey, milky white quartz. This quartz is non-mineralization. The Jersey vein is a Link vein with steel galena mineralization.

Runs 361-2; same as 359-60.

Runs 363-4; 100-35-24 quartz. It is uncertain whether or not this quartz is the same sample as run 233-4 or another crystal from the same sample with the 550^|o\|C stepwise thermally decrepitated gases vaccumed off (Human error in procedure and notes). Other information is the same as 233-4. Location 'B' at 10 level (fig. 9).

Runs 365-6; 14 Brown Qtz, euhedral,clear crystals. Other information is the same as 238-9.

Runs 367-8; same sample as 365-6.

Runs 369-80; same sample as 365-6.

FLUID INCLUSION LEACHATES- Procedure

Eight samples were selected from the Bunker Hill mine for crush-tube leachate analyses (six quartz, two spalerite). Sample selection was limited to those containing a sufficient amount of homogeneous material (about 40 grams per run). Only samples from Bluebird type vein mineralization met this requirement and the results specifically concern this stage. The samples were broken to the size of the crush tube diameter- less than 2 cm and cleaned. Cleaning procedure consisted of washing the sample crystals, quartz rod blanks and steel crush tubes with H_2O, alcohol for 3 hours, a rinse with H_2O, boiling overnight in conc. HNO_3, 10 rinses with H_2O, boiling overnight in H_2O and a final rinse with H_2O. The samples and some of the quartz rod blanks were placed in electrolytic cells until the cell current was negligible. All of the water used was distilled and deionized.

The samples were placed on a vacuum line and taken down to about 2×10^{-5} torr to eliminate all atmospheric gases and check for air leaks. The metal tube was then crushed and opened to a closed volume of vacuum line with a liquid N_2 trap. The system was then left to equilibrate for about 3 hrs, during which time all the water and condensable gases would freeze out. The pressure of non-condensable gases could be measured at this point and the gases could also be

run through the mass spectrometer (if the sample was previously taken down to a greater vacuum). This was not done with these samples because they had already been analyzed by the thermal decrepitation method and the mass spectrometer was "down" during the leachate runs. The H_2O from the fluid inclusions was then frozen-out into capillary tubes of known weight and sealed off. The weight of H_2O evolved from the crushed inclusions was then measured by re-weighing the capillary tubes.

The crushed samples were then poured out of the crush-tubes into pre-cleaned teflon beakers and leached with 1/2 % ultra-pure HNO_3 for 20 minutes, 3 times, for a total leachate volume of 50 ml. One sphalerite run was leached with H_2O only. Sample leachates were passed thru disposable "Nalgene" filter units which had been pre-rinsed 10 times with 0.5 % ultra-pure HNO_3.

Various blanks were run first to determine and eliminate possible sources of contamination.

APPENDIX Table 5: Fluid Inclusion Leachate Data

The columns in Table 5 list the trace element concentrations in terms of ppm/50 ml and ppm/d.f., an abbreviation for parts per million per 50 milli-liters multiplied by a dilution factor. The dilution factor is the amount of water obtained during crushing divided by 50 ml, which is the volume all runs were diluted to before analysis. Since many of the runs were blanks which yielded no water upon crushing, no dilution factor is involved and no entry appears in the ppm/d.f. column alongside the run. The concentrations listed in the ppm/d.f. column are the minimum concentrations present in the fluid inclusion waters less background.

SAMPLE	DILUTION FACTOR
15	7812.5
17	3623.
18	3788.
19	3496.5
21	19231.
22	2427.
23	2525.
24	12195.

Several abbreviations appear in Table 5:

'-' concentration is below the detection limit

'+' concentration is above the range of linearity

'nd' no data, not analyzed for

'tr' trace, below range of linearity (1.00 over a value of 2.00) lower value of 1.00, upper value of 2.00

Sample descriptions:

Appendix Table 5- Sample descriptions

1) Qtz rod blank
2) Qtz rod blank
3) Qtz rod blank + 20.4 mg Solution A in capillary tube
4) 1 % UTX (ultra-pure HNO_3)
5) 1 % Solution A, 1 % UTX, 98 % DD.H_2O (distilled, deionized)
6) 1:1000 Solution A + 0.1 ml UTX (diluted with DD.H_2O)
7) 1 % Solution B, 1 % UTX, 98 % DD.H_2O
8) DD.H_2O
9) Qtz rod blank + 57.1 mg Solution B in capillary tube
10) 1:1000 Solution B + 0.1 ml UTX (diluted with DD.H_2O)
11) 1 % UTX beaker wash (contamination test)
12) Qtz rod blank, uncrushed, not on electrolytic cell, soaked in 1 % UTX (contamination test)
13) DD.H_2O from first rinse thru Nalgene filter
14) DD.H_2O from 4th rinse thru Nalgene filter
15) 14 Brown Sph, rinsed with DD.H_2O only
16) Qtz rod blank, filter was washed 10 times to eliminate contamination
17) 110-35-24 clear Qtz xls
18) 14 Brown Qtz
19) 110-35-24 Qtz xls, slightly cloudy
20) Qtz rod blank, filter was washed 10 times
21) pre-reverse shear, pre-mineralization Milky Qtz, 110-35-21
22) 100-35-24 Qtz
23) 110-35-24 Qtz
24) 14 Brown Sph, one wash with 1 % UTX

TABLE 5. Fluid Inclusion Leachate Data.

SAMPLE	Na		Ca		K	
	ppm 50ml	ppm d.f.	ppm 50ml	ppm d.f.	ppm 50ml	ppm d.f.
1	0.94		1.74		tr	
2	1.94		2.32		0.84	
3	23.0		5.16		2.65	
4	-		-		nd	
5	nd		nd		nd	
6	39.2		4.89		5.08	
7	nd		nd		nd	
8	-		-		-	
9	27.2		12.8		6.34	
10	44.2		12.8		10.4	
11	-		-		-	
12	-		nd		-	
13	0.1		3.10		-	
14	-		-		-	
15	0.63	4922	(0.586 / 0.88)	(4578 / 6875)	0.47	3670
16	-		(0.255 / 0.46)		-	
17	1.5	5435	(2.18 / 2.84)	(7898 / 10289)	0.93	3370
18	1.35	5114	(1.13 / 1.55)	(4280 / 5871)	1.21	4580
19	2.95	10350	8.4	29370	1.24	4340
20	-		(0.16 / 0.35)		-	
21	0.44	8269	(1.07 / 1.47)	(20600 / 28300)	1.12	21500
22	3.4	8228	(1.46 / 1.95)	(3540 / 4733)	1.60	3880
23	3.6	9091	(4.41 / 5.57)	(11100 / 14100)	1.16	2930
24	-	-	(1.08 / 1.49)	(13200 / 18200)	tr	

SAMPLE	Mg		Mn		Fe	
	ppm 50ml	ppm d.f.	ppm 50ml	ppm d.f.	ppm 50ml	ppm d.f.
1	0.41		-		-	
2	0.48		-		-	
3	0.96		-		1.1	
4	tr		nd		-	
5	nd		tr		17.2	
6	2.1		nd		0.5	
7	nd		tr		18.0	
8	tr		nd		-	
9	1.7		tr		2.0	
10	2.2		-		0.9	
11	-		nd		-	
12	tr		nd		nd	
13	0.67		nd		nd	
14	nd		nd		nd	
15	0.15	1172	1.8	14060	-	
16	tr(.05)		-		-	
17	tr		0.06	217	tr	
18	0.1	379	tr		tr	
19	0.24	839	0.34	1190	2.9	10140
20	tr(.03)		tr(.01)		tr	
21	0.1	1920	tr		tr	
22	0.1	240	tr		tr	
23	0.11	280	0.23	580	2.1	5300
24	0.11	1340	7.0	85000	0.9	11000

SAMPLE	Zn ppm 50ml	Ag ppm 50ml	Cu ppm 50ml	Pb ppm 50ml	Pb ppm d.f.	Cd ppm 50ml	Cd ppm d.f.
1	0.14	nd	0.23	0.004		-	
2	0.41	nd	0.54	0.067		-	
3	1.2	-	2.1	0.12		-	
4	-	nd	0.008	-		nd	
5	nd	-	1.2	0.033		nd	
6	1.9	-	nd	tr		0.003	
7	nd	0.002	nd	0.053		nd	
8	-	nd	0.003	0.045		nd	
9	1.5	-	nd	0.13		0.0003	
10	2.0	-	1.07	-		0.0014	
11	-	nd	-	0.031		-	
12	-	nd	0.002	-		nd	
13	-	nd	0.008	0.01		nd	
14	-	nd	0.094	-		nd	
15	0.61	-	-	-		0.0008	6.
16	1.1	-	1.56	0.010		0.0008	
17	0.54	-	nd	0.46	1663	0.0008	3.
18	0.25	-	0.47	0.054	205	-	
19	0.24	-	nd	0.48	1675	-	
20	0.70	-	0.86	0.070		-	
21	0.38	-	nd	0.025	481	-	
22	0.12	-	0.05	0.22	541	-	
23	0.19	-	0.45	0.062	157	-	
24	7.0	-	-	-		0.0006	7.

SAMPLE	As		SO_4		Cl	
	ppm 50ml	ppm d.f.	ppm 50ml	ppm d.f.	ppm 50ml	ppm d.f.
1	tr		0.0026		6.	
2	-		0.0067		20.	
3	tr		0.0044		115.	
4	-		-		9.	
5	-		nd		nd	
6	-		+		70.	
7	tr		nd		nd	
8	-		-		-	
9	-		+		250.	
10	-		nd		110.	
11	nd		nd		1.	
12	nd		nd		2.	
13	nd		0.0027		nd	
14	nd		-		nd	
15	0.0032	(25.)	+	+	2.	(15600)
16	0.0028		0.0017		7.	
17	0.029	105.	0.0015	(5.4)	22.	79700
18	0.0051	(19.)	0.0010	(4.0)	22.	83000
19	0.0036	(13.)	0.0093	33.	22.	77000
20	0.0025		0.0005		4.	
21	0.0051	98.	0.0012	23.	22.	423000
22	0.0027	(6.5)	0.0009	(2.)	45.	109000
23	0.0074	19.	-	-	38.	96000
24	0.0027	(33.)	nd	nd	7.	85000

FLUID INCLUSION MICROTHERMOMETRY DATA:

A). Minimum temperatures of first-melting:

110-35-24 quartz; <-26.2°C, -28.2°C, -35°C,
-28.5°C, -30°C, -27°C, and
-25.5°C.

100-35-24 quartz; <-31°C and -27°C.

100-35-24 sphalerite; <-31°C.

19'J' quartz; <-34°C and -30°C.

B). Data- Decomposition temperatures for gas-hydrates.
Sample designation refers to level-orebody-stope.
All 35 orebody designations refer to the Quill orebody.

SAMPLE	of inclusions	Temerature °C
1) 110-35-24 quartz QSG	15	+3.9 to +6.4
2) 110-35-24 quartz	1	+6.1 to +6.3
3) 110-35-24 quartz	5	+6.3 to +6.6
4) 110-35-24 quartz	6	+6.0 to +6.2
5) 110-35-24 quartz	2	+6.1 to +6.2
6) 110-35-24 quartz	1	+5.7 to +6.5
7) 110-35-24 quartz	4	+4.0 to +5.2
8) 110-35-24 quartz GA	3	+3.1 to +3.2
9) 110-35-24 quartz GA	1	+3.7 to +4.9
10) 14 Brown quartz	5	+10.2 to +10.7
11) 14 Brown sphalerite	2	+3.6 to +4.8
12) 130-35-23 sphalerite	2	+4.2 minimum
13) 100-35-24 sphalerite	1	+3.4 to +4.1
14) 110-35-23 calcite, (late)	1	+9.5 minimum
15) 110-35-21 pre-existing quartz "proto-Link"	9	+11.1 to +13.2
16) 19'J' quartz	6	+11.0 to +11.4
17) Crescent quartz	2	+9.4 to +10.4

Alternative method of graphing the preceding data (to histogram fig. 39, p.55).

Gas-hydrate decomposition temperatures. Sample numbers are placed near horizontal-range bars.

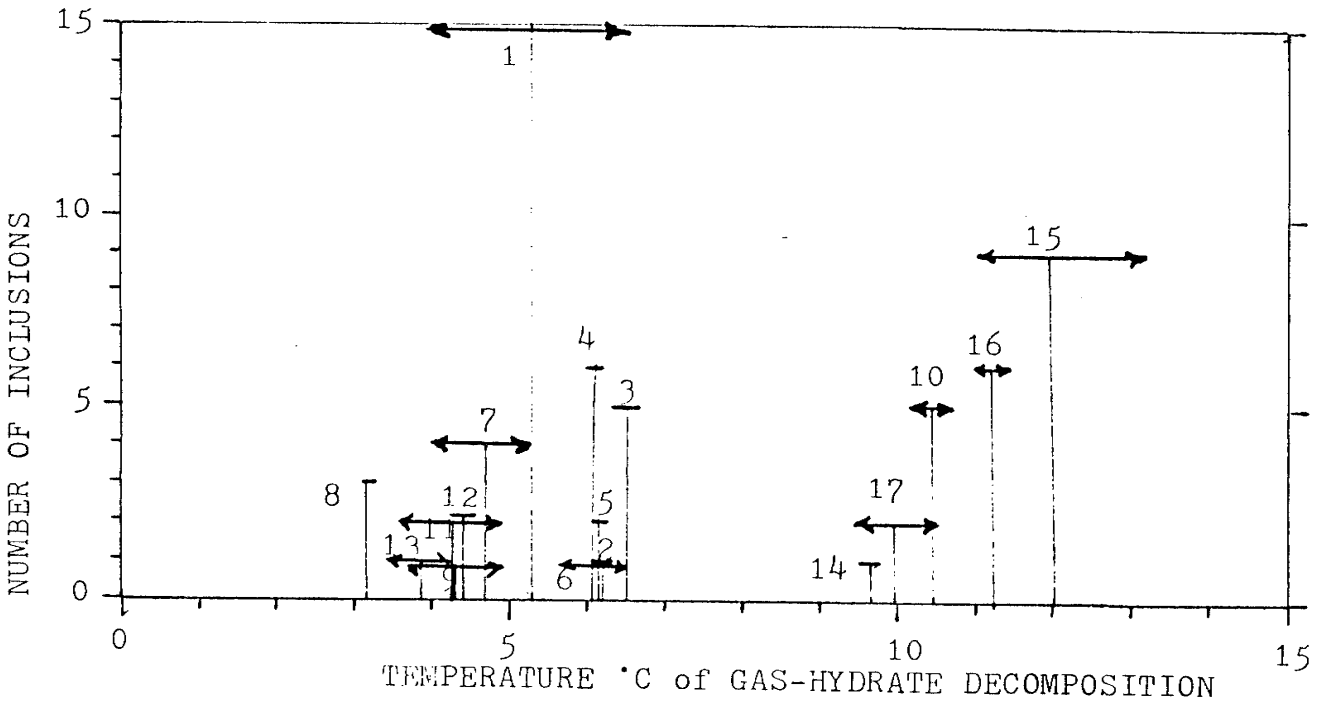

```
                    RANGE IN HOMOGENIZATION TEMPERATURE
SAMPLE              100        200        300        400 C
(And Data Type)      |    |     |    |     |    |     |
110-35-21 quartz:      ss   pppppp
  16 data; 2s,14p
120-35-24 quartz:   s s s                 p
  15 data; 7s,8p
19'J' quartz:         s  s     s     pp
  8 data; 4s,4p
14 Brown sphalerite:        s s s    ?  ? ?  p
  12 data; 3s,3?,6p
14 Brown quartz:          g        pp
  21 data; 2g,19p
120-35-21 quartz:                p
  3 data; 3p
--------------------|    |     |    |     |    |     |
110-35-24 quartz:           s sss   pp
  QSG
  16 data; 9s,7p
130-35-23             s
  sphalerite
  2 data; 2s
110-35-23                 pp
  calcite
  2 data; 2p
110-35-24 quartz:                   bp
  GA
  11 data; 11p
  b; bubble min
Crescent quartz:                      p
  7 data; 7p
110-35-24 quartz:                   gbbp g   gp
  steve
  b; bubble min.
  6 data; 3p,3g
--------------------|    |     |    |     |    |     |
```

C). Sample descriptions with miscellaneous notes:

100-35-23 quartz; fluid inclusions oriented parallel to crystallographic directions. Decrepitation problems.

100-35-23 "Mega"-crackle breccia; Although fluid inclusions were visible in sphalerite, they were too small to study. The sample contains early quartz with later sphalerite, galena and pyrite(?). Numerous solid inclusions were present in the sphalerite, probably galena (early relative to sphalerite). Sericite (fig. 25, p. 40). Location 'F' at 10 level (fig. 9).

100-35-24 quartz; crystal group with later sphalerite, galena and chalcopyrite. Most fluid inclusions were Type-1A but some Type-1C inclusions were present.

100-35-24 sphalerite; dark variety,numerous planar inclusions, possibly secondary. Sample location is the same as figure 22 (p. 39), and the same as the previous quartz. The minimum T_h is greater than 172°C. Decrepitation problems. Embaying grain boundry with galena (fig. 32, p. 48). Location 'B' (fig. 9).

110-35-24 quartz SN 14; from vugs within the en echelon shears (fig. 11). A doubly polished section was made of the replacement veinlet in figure 11 (photo 2) which indicates that the sphalerite contains abundant earlier chalcopyrite. Galena is latest paragenetically. No euhedral crystals from within the en echelon shears in this immediate are contained chalcopyrite or siderite.

Location 'A', 12 level (fig. 9).

110-35-24 quartz; euhedral, cloudy core with numerous fluid inclusions, clear terminations, complex crystal group forming a "single crystal" 3 cm in length. Collected by Steve Levine.

110-35-24 quartz GA; parallel planes of fluid inclusions. Type-2 liquid immiscibility was observed in non-homogenizeable inclusions. Gas analyses runs 222-3, 230-1, and 353-4 etc. Location 'A' (fig. 9).

110-35-24 quartz QSG; with replacement intervals as indicated by sphalerite inclusions (figs. 34, 35). The co-planar rows-type relation between fluid inclusions are transitional to "cloud"-type textural relationships. Type-1 liquid immiscibilty was observed (fig. 55) as well as Type-2 liquid immiscibility (fig. 56). Location 'A' (fig. 9).

110-35-23 calcite; from collapse breccia, the calcite is clear and formed in open space after the collapse of mineralized bedding. The calcite is later than sphalerite and pyrite. Location 'E' (fig. 9).

110-35-21 quartz; negative quartz crystal fluid inclusions. Crystal group; euhedral galena is included within an outer

quartz crystal. Type-2 liquid immiscibility observed. A sample from 110-35-21 f1 15, N465 W4060, collected by Steve Levine... "Rounded quartz crystal from PbS veinlet,

2-5 mm PbS crystal mush" may be from the same location. A polished plate was also made from this sample.

120-35-21 quartz; euhedral, clear. Growth zoned inclusions parallel to crystallographic directions. This sample is later than main stage Bluebird mineralization and was found in a pocket of deconsolidated wall-rock with euhedral chalcopyrite crystals. The minimum T_h is greater than 175°C but the inclusions couldn't be seen well enough at higher temperatures for a true T_h. A T_m = -9.3°C was obtained for ice in 5 inclusions.

120-35-24 quartz; single euhedral crystal. Most inclusions are Type-1A (non-boiling?).

130-35-23 quartz; fluid inclusions were too small or unsuitable for study.

130-35-23 sphalerite, floor 4; crystal group with inclusions oriented subparalel to the individual "crystal outlines". Fluid inclusions within this sample were impossible to homogenize due to decrepitation problems, but the T_h is probably greater than 183°C, the maximum pre-decrepitation temperature observed. Type-1 immiscibility was frequently observed.

Figure 45 (page 84) is from this sample.

14 Brown quartz (140-18-22) floor 9 (approximately N2250 W5130 floor 8 location for a similar area); The plate was made from a crystal group. The basal zone of one crystal contains a "cloud" of Type-1A inclusions with

15-25 % vapor, probably non-boiling. At least some of the quartz is earlier than, or contemporaneous with sphalerite as indicated by sphalerite grown in inclusion crystal interfaces. The gaseous inclusion of figure 54 which developed a liquid phase upon heating is from this sample. Gas analyses 238-9 and 365-6 etc., were from the same set of vugs within the same shear zone of the sample.

14 Brown sphalerite (140-18-22) same location as the previous sample; Type-1 liquid immiscibility observed in secondary(?) inclusions. Large primary inclusions had T_h's to 352°C., and showed very unusual phase behaviour about 10 degrees before homogenization (The liquid phase appearred to change state).

Crescent quartz; The basal zone of the crystal has inclusions of siderite cleavage rhombs. The basal zone also contains abundant fluid inclusions with a highly variable percentage of the vapor phase (boiling?). A liquid- CO_2(?) phase usually forms within the inclusions upon cooling, but before freezing. Often a possible sulfide "speck" is present in the inclusion. Type-1 liquid immiscibility is generally present at 175°C. Most fluid inclusions become very difficult to observe at higher temperatures.

Crescent siderite; numerous inclusions, too small to identify. Some euhedral later tetrahedrite. Late

quartz replacement veinlets, reltion to tetrahedrite is uncertain.

19'J' quartz; same as gas analyses runs 306-7, 320-1. Numerous fluid inclusions, "cloud"-type growth appearance under low magnification. 5-10 % of the inclusins are of the dry-gas type at room temperature. About 30 % contain about 60 % vapor. About 60 % contain less than 60 % to 15 % vapor. This proportion of inclusion types varies within different sections of the crystal, with parts of it containing over 70 % of the dry-gaseous type, having irregular negative crystal outlines formed by the meeting of separate small quartz crystals. Chalcopyrite is present in a sheared border of the pre-existing crystal.

This thesis is accepted on behalf of the faculty of the Institute by the following committee:

David L. Norman
Advisor

Clay T. Smith

Carl Hoppe

16 October 1985
Date